Zeitschrift: IABSE reports = Rapports AIPC = IVBH Berichte

Band: 54 (1987)

Rubrik: Session 3: Non-stationary processes and serviceability (advances and applications)

SESSION 3

August 27, 1987 (morning)

Non-Stationary Processes and Serviceability

(Advances and Applications)

Procédés non-stationnaires et aptitude au service

(progrès et applications)

Nicht-stationäre Prozesse und Gebrauchszustände

(Fortschritte und Anwendungen)

Chairman: H.W. Reinhardt, The Netherlands

Invited Lecturers:

F.H. Wittmann, P.E. Roelfstra, Switzerland
Constitutive Relations for Transient Conditions

Z.P. Bazant, USA
Non-Stationary Long-Time Processes Causing Loss of Serviceability

Leere Seite
Blank page
Page vide

Constitutive Relations for Transient Conditions

Lois constitutives pour des conditions transitoires

Werkstoffgesetze unter nichtstationären Bedingungen

Folker H. WITTMANN
Professor
Swiss Fed. Inst. of Techn.
Lausanne, Switzerland

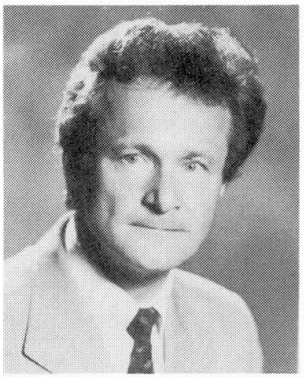

Folker H. Wittmann, born 1936, habilitated in Physics of Building Materials at Munich Institute of Technology. For 4 years he was professor for Building Materials at Delft University of Technology, The Netherlands. He is now professor and director of the Laboratory for Building Materials at the Swiss Federal Institute of Technology, Lausanne.

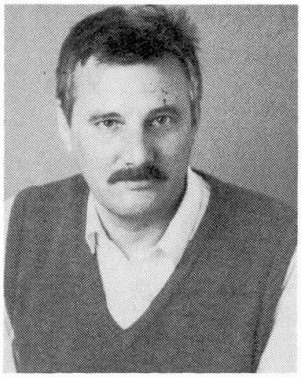

Pieter E. Roelfstra, born 1946, got his civil engineering degree at Delft University of Technology, The Netherlands. For 12 years he was involved in structural engineering at the Ministry of Public Works. Actually he is head of the group Modelling and Numerical Analysis of the Laboratory for Building Materials at the Swiss Federal Institute of Technology, Lausanne.

Pieter E. ROELFSTRA
Civil Engineer
Swiss Fed. Inst. of Techn.
Lausanne, Switzerland

SUMMARY

In order to link material properties with their structure, three structural levels are introduced. First of all, the ageing of the cement-based matrix under transient conditions is modeled. Then the time-dependent deformations of a composite material are determined by applying the concept of numerical concrete. A quasi-homogeneous material with statistically distributed properties is used to elucidate the influence of strain softening and crack formation on total deformation. Thermal incompatibility of the composite structure is taken into consideration.

RÉSUMÉ

Dans le but de lier les propriétés du matériau à sa structure, trois niveaux structuraux ont été introduits. Le vieillissement de la matrice de pâte de ciment a été introduit dans le modèle sous des conditions non stationnaires. Puis, l'application du concept du béton numérique permet de déterminer les déformations en fonction du temps d'une structure composite. Un matériau quasi-homogène avec une distribution statistique des propriétés a été utilisé pour élucider l'influence du radoucissement et de la formation de fissures sur la déformation totale. L'incompatibilité thermique de la structure composite a été prise en compte.

ZUSAMMENFASSUNG

Drei Gefügeniveaus werden definiert und eingeführt. Dann wird zunächst die Alterung der Zementsteinmatrix unter nichtstationären Bedingungen simuliert. Unter Anwendung des Konzepts 'der numerische Beton' werden die zeitabhängigen Verformungen eines zusammengesetzten Werkstoffes beschrieben. Ein quasi-homogenes Material mit statistisch verteilten Eigenschaften wurde generiert, um den Einfluss der Verformungserweichung und der Rissbildung auf die Gesamtverformung unter Beweis zu stellen. Die thermische Inkompatibilität eines zusammengesetzten Werkstoffes wird berücksichtigt.

1. INTRODUCTION

Basic creep of concrete that means creep without moisture exchange can be predicted within a reasonable confidence interval. Based on experimental results basic creep can be predicted for a wide range of different concrete compositions. A power function describes the time-dependence of basic creep sufficiently well. It is also known for a long time that creep under sealed conditions is high compared to creep of dry concrete. Many authors have even stated that creep of dry concrete can be neglected.

It is somewhat more difficult to describe shrinkage of concrete correctly. Nevertheless there are again sufficient experimental data which allow us to predict the time-dependence, the final value, and the influence of geometry reasonably well if the concrete composition and the environmental conditions are given (see for instance [1].

Controversal views still exist, however, on the most common type of time dependent deformation, i.e. simultaneous creep and shrinkage [2]. Some authors believe that creep under these conditions is magnified while others prefer to attribute the observed increase of the total deformation to an increased shrinkage. In these discussions it has not always been fully realised that simultaneous creep and shrinkage have to be considered to be a transient hygral deformation.

In most codes creep under drying conditions is indicated to be considerably bigger for all durations of load than basic creep under sealed conditions. If it is true that this time-dependent deformation is a transient process creep of a drying specimen must become negligibly small once a structural element is dried, than on the long run basic creep may become bigger.

One reason for the fact that this important aspect of concrete behaviour is still under discussion is that the different and interrelated processes are so complex that most experimental data cannot be interpreted straight away. So far numerical simulation methods are the only means to come to a better understanding. It has been outlined elsewhere in which way the concept of numerical concrete can be applied to simulate elastic deformations of a composite material and drying of a composite material with a porous matrix [3]. In this paper it is also shown that the interfacial zones have an important influence on the time-dependence of drying and on the moisture distribution within a drying specimen.

Results described in [3] will be used here as a basis for further investigations.

The major aim of this contribution is to point out that the concept of numerical concrete [4,5] can be applied to describe transient hygral deformations of a composite material such as concrete. Special emphasis will be placed on the significance of strain softening and crack formation for hygral deformations. Finally it will be shown that thermal transient conditions can be dealt with in a similar way.

2. CONSTANT AND TIME DEPENDENT STATE PARAMETERS IN THE 3L-APPROACH

2.1 General remarks

Concrete is a composite material with a porous matrix. During the hardening of the cement based matrix and before a load is applied a complex state of stresses is created in the structure due to thermal and chemical shrinkage [6]. When the formwork is removed drying of a concrete element begins. As a consequence two types of additional stresses are created : (a) tensile stresses in zones near the surface and compressive stresses in the humid center caused by the time-dependent moisture gradient, and (b) tensile stresses in the drying matrix and compressive stresses in the inert aggregates. In reality the situation is further complicated by the fact that the properties of the cement based matrix change (aging effect) as the hydration continues. In the dried outer zones, however, hydration is soon stopped. This leads to an inhomogeneous porous matrix.

It has been pointed out earlier that the structure of concrete can be subdivided at least in three different hierarchic structural levels [2]. The basic ideas of this concept, which is now called 3L- Approach, are outlined in detail elsewhere [3].

The microlevel serves to describe the processes in and the properties of the porous matrix. Advanced numerical simulation methods can be applied to introduce realistic state parameters such as degree of hydration, moisture content, moisture capacity and permeability. The mesolevel has been introduced to take the composite structure of the material into consideration. If the composite structure of concrete is simulated in a realistic way and if the point properties are sufficiently well known the response of structural elements can be predicted under arbitrary conditions.

This systematic study can be considered to be a rational way to develop material laws. The macrolevel of the 3L-Approach is finally used to formulate these relations in such a way that they can be directly applied in computerized structural analysis.

2.2 Modelling of the microstructure

2.2.1 Formation of the structure and aging

In this chapter we describe briefly new developments of modelling the formation of the microstructure of hardened cement paste with the help of numerical methods. All mechanical and physical properties of hardened cement paste are linked directly with its microstructure. Thus, if we are able to simulate the formation of the microstructure and build in real micro-mechanisms, then it is possible in principle at least to deduce constitutive relations which describe mechanical and physical behaviour of hcp under simple and very complex conditions. The first step in this direction has been done at NBS [24]. They simulated the formation of the microstructure in 3D of cement compound C_3S with a shrinkage core model and obtained in this way useful information on the pore size distribution and the contact zones between C_3S particles.

Extension of this model for different types of cement (cements having a different clinker composition) is possible if we can describe the different hydration rates of each compound and their mutual interaction in realistic way. Research on this level has therefore to be focused on reaction kinetics [7,8,9].

Terms like aging may probably be replaced in the futur by for instance contact surface between hydrating particles or time-dependent bond density [10].

For the mechanical analysis of such a simulated structure, which we might call numerical HCP, we have to investigate whether continuum or discrete mechanics is most appropriate. We should mention here also an earlier developed model from which some basic concepts can possibly be implemented [11].

2.2.2 Degree of hydration in a drying sample

The hydration process under transient conditions can be described in principle by three differential equations [25].

$$
\begin{aligned}
C_H \dot{h} + p\dot{\alpha} &= \nabla \cdot (\lambda_{HH} \nabla h + \lambda_{HT} \nabla T) \\
C_T \dot{T} - q\dot{\alpha} &= \nabla \cdot (\lambda_{TH} \nabla h + \lambda_{TT} \nabla T) \qquad (1) \\
\dot{\alpha} &= F_1(\alpha) \cdot F_2(T) \cdot F_3(h)
\end{aligned}
$$

where C_H and C_T are hygral and thermal capacities respectively, h is the relative humidity, T is the temperature, λ_{HH} and λ_{HT} are cross permeabilities and α is the degree of hydration. Coefficients p and q depend on the type of cement. This system of differential equations is highly nonlinear, because all materials properties depend strongly on actual temperature, humidity and degree of hydration. Functions $F_1(\alpha)$, $F_2(T)$ and $F_3(h)$ have to be determined from experimental results. A relatively small computer code has been developed to solve this system of equations under constant or variable boundary conditions [4]. Two typical results are shown in Figs. 1 and 2.

In Fig. 1 we can see that the degree of hydration remains low in the region near the surface which is exposed to drying. This means that mechanical properties such as modulus of elasticity, which are linked directly with the degree of hydration, vary also under these conditions as function of the distance to the surface. At the same time permeability is higher in the surface region.

Fig. 2 shows that due to self dessiccation moisture content in the center part decreases and hence moisture gradients are built up with respect to the wet boundary. These gradients cause the observed water uptake of specimen stored under these conditions.

With this model the evolution of state parameters such as temperature, humidity and degree of hydration as function of time and space can be described. This is an essential step in the so-called point property approach.

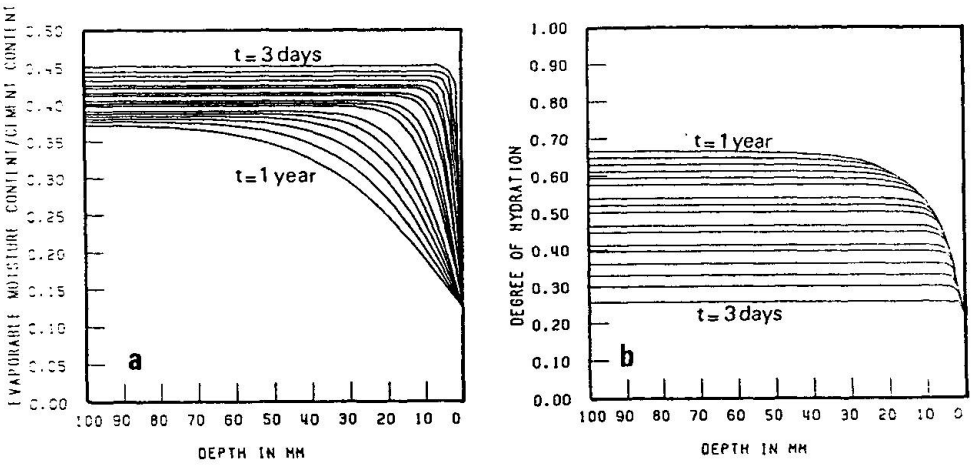

Fig. 1 Evolution of evaporable water content (a) and degree of hydration (b) as function of time and distance from the surface of a wall with a thickness of 200 mm exposed to a relative humidity of 50 %.

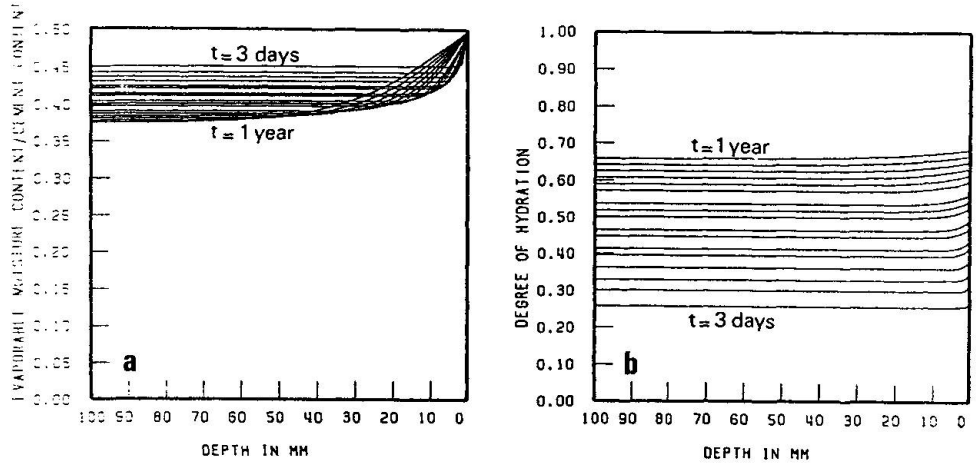

Fig. 2 Evolution of the evaporable water content (a) and degree of hydration (b) as function of time and distance from the surface of a wall with a thickness of 200 mm stored under water.

2.3 Modelling of the composite structure

Composite structures with arbitrarely shaped aggregates grains can be simulated with a computer [12]. Aggregate volume content and particle size distribution can be taken into consideration [5,13]. A typical example is shown in Fig. 3a. For the analysis the generated structure has to be idealized by a finite element mesh. It has turned out that the interface between matrix and aggregate grains with its characteristic properties has to be taken into account separately. In this contribution we used for simplicity a composite structure with 27 circular aggregate grains as shown in Fig. 3b.

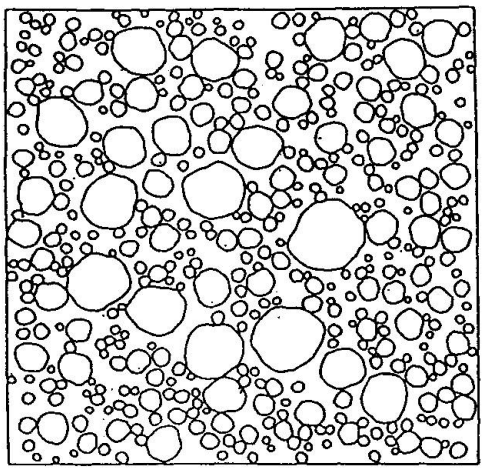

Fig. 3a Computer simulated composite structure of normal concrete.

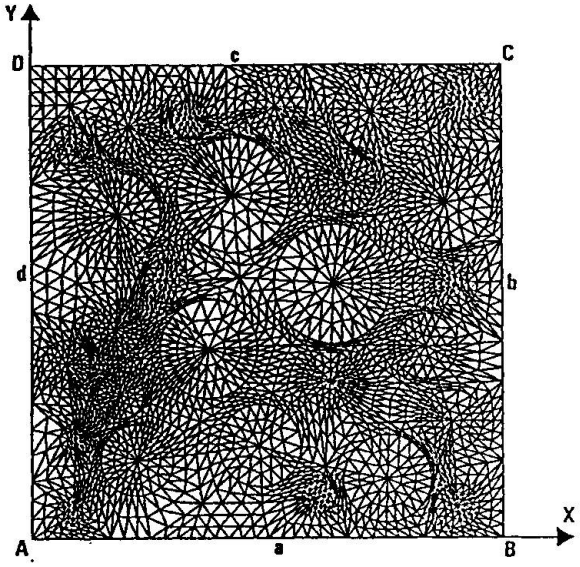

Fig. 3b Finite element idealization of the composite structure used in the analysis.

3 BASIC CREEP AND DRYING OF A COMPOSITE MATERIAL

3.1 Basic creep of a composite material

The complex state of stress in the simulated structure of concrete (see Fig. 3b) under loading conditions is shown in [3]. This structure is used here to study the time-dependent behaviour under sustained load and under isohygral conditions (basic creep). It is assumed that the aggregate grains in the structure behave perfectly linear elastic and that the small contributions of creep of the interfaces to the global (macroscopical) creep may be neglected. Due to creep the complex stress distribution in the material will change in time. The non linear rate type creep law we used for this situation is given in eq. (2) :

$$\dot{\varepsilon} = \frac{1}{m\tau_D} \frac{a_1 a_2 \sinh b\sigma}{bE}^{m} \frac{1}{\left[\int_t^t |\dot{\varepsilon}| d\tau\right]^{m-1}} \qquad (2)$$

where σ is the actual stress, $b = 1.8/fc'$ is a measure for nonlinear creep, fc' is the compressive strength, $a_1 = \exp[Q/R(1/F_0 - 1/T)]$ is Arrhenius's equation to take the influence of the actual temperature T into consideration, Q is the activation energy, R is the universal gas constant, T_0 is the reference temperature (usually $T_0 = 293^0K$), $a_2 = (12h-5)/7$ is the expression to take the influence of the actual pore humidity h into consideration (in case of basic creep a_2 is a constant), E is Young's modulus and τ_D is the time in days after loading at which the creep strain is equal to the elastic strain for $a_1 a_2 = 1$ and σ is constant. m is a positive number representing a material constant and $\left[\int_t^t |\dot{\varepsilon}| d\tau\right]$ is the actual path length of the creep strain (intrinsic time). For a constant stress, temperature and pore humidity this equation can be integrated analytically and one will find a power law according to eq. (3) :

$$\varepsilon(t-t') = \frac{t-t'}{\tau_D}^{\frac{1}{m}} \frac{a_1 a_2 \sinh(b\sigma)}{bE} \qquad (3)$$

It should be noted that eq. (2) does not take into account aging and creep recovery. Aging effects on mechanical and physical properties can be modelled by means of the concept described in chapter 2. Creep recovery needs, however, not to be modelled as a separate phenomena. The origin for creep recovery is caused by the residual potential energies in the elastic components of the composite structure after unloading and is the logic result of an appropriate analysis and application of numerical concrete.

In the example given here we used the same distribution of Young's modulus of the mortar matrix elements as described in [3]. In addition time τ_D of eq. (2) was varied according to a Gaussian distribution (τ_D = 31 days, p = 10 days, cut off at 1 and 61 days). The positive materials coefficient m has been chosen to be 3 and the product $a_1 \cdot a_2$ was fixed to be 1. The composite structure was submitted to an external compressive load of σ_y = -10 N/mm^2. Fig. 4 shows the total strain as function of duration of load (t-t'). The macro-creep strain as function of the duration (t-t') is plotted on a log-log scale in Fig. 5.

In Fig. 5 it can be seen that the "effective" basic creep strain of the composite structure describes almost perfectly a power law. The effective compliance function is given in eq. (4) :

$$\varepsilon_T(t-t') = \frac{\sigma}{E}\left[1 + \left(\frac{t-t'}{109}\right)^{0.324}\right] \qquad (4)$$

where E = 29874 N/mm^2 is the effective modulus of elasticity as calculated in [3].

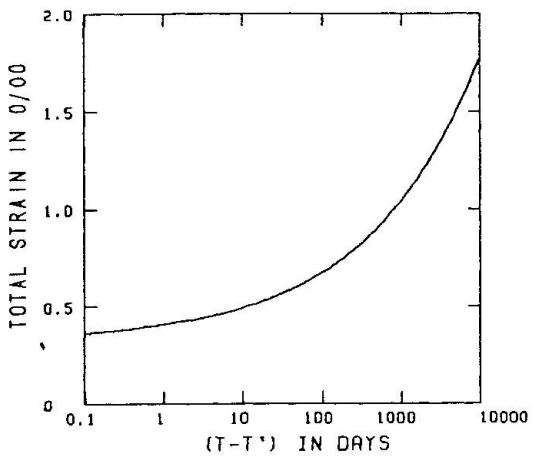

Fig. 4 Calculated total strain as function of duration of load (linear ordinate).

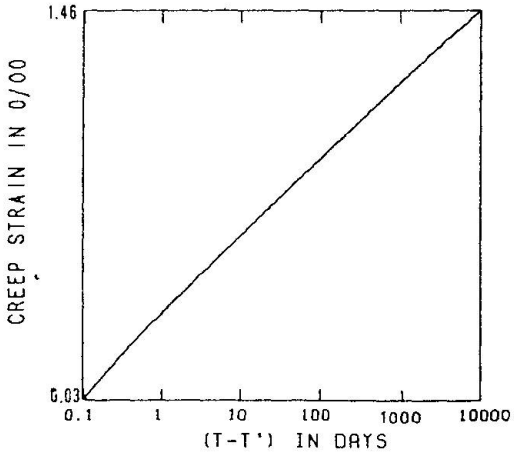

Fig. 5 Calculated basic macrocreep as function of duration of load (t-t') (logarithmic ordinate).

Fig. 6 shows the redistribution of potential energies in the different components of the composite material as function of the duration of load (t-t´).

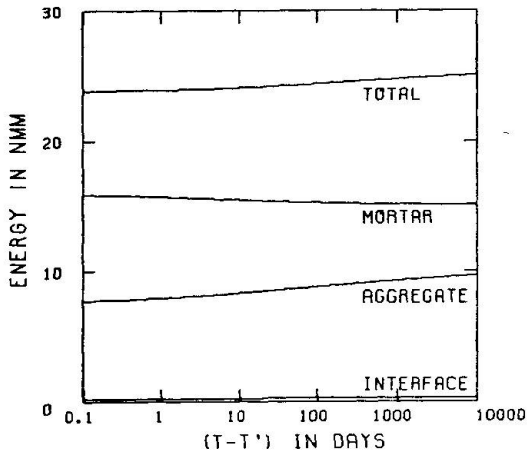

Fig. 6 Distribution of potential energies stored in the different components and the total value as function of duration of load (t-t´).

As can be seen in Fig. 6 there is a transfer from potential energy of the mortar matrix to the aggregate grains. After unloading this energy is freed again an thus this internal redistribution of energy can be considered as the driving force for partial creep recovery. The model has still to be extended with elastic components in the mortar matrix and even in HCP. From analysis performed with the extended model a generalized macro-creep law or algorithm will be deduced. It is doubtfull whether such a creep law on the macro-level can be expressed in one simple compliance function. We should mention here a mathematical expression for macro-creep strain which gives qualitatively correct deviations from the linear superposition principle [14].

3.2 Drying and hygral shrinkage of a composite material

In the point property approach we can state that hygral shrinkage depends linearly on pore humidity h. The real mechanisms of hygral shrinkage such as change of surface energy and disjoining pressure with changing pore humidity are explained elsewhere [15]. This implies that in principle the overall shrinkage of a composite structure can be determined if the evolution of the distribution of the pore humidity as function of time can be calculated. Simulation of the drying process of a composite material is carried out in [3].

In Fig. 7 the calculated moisture distribution of a composite material, 3 days after exposing to drying, is shown.

Assuming that the unrestrained hygral shrinkage of the mortar matrix is linked to pore humidity h linearly as indicated by eq. (5) and using the initial strain concept in the numerical analysis, the overall (macro) shrinkage can be determined.

$$\varepsilon_{us} = -0.002 + 0.00002\ h \quad (h \text{ in } \%) \tag{5}$$

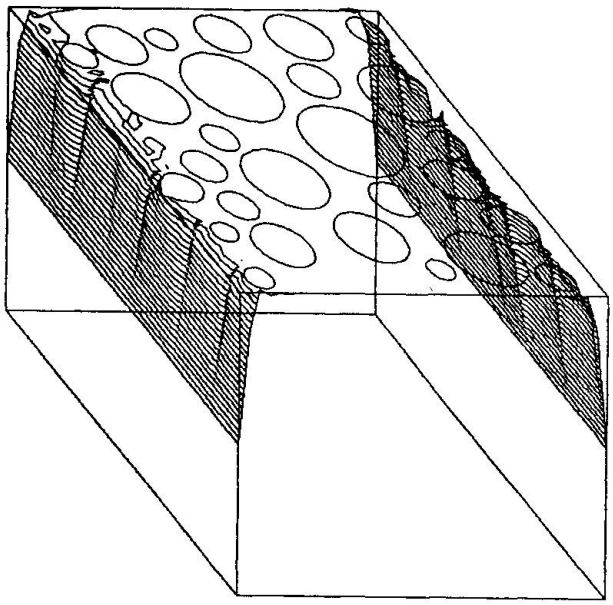

Fig. 7 Calculated moisture distribution of a composite material 3 days after exposing to drying (see [3].)

The deformations of the composite structure calculated in this way are shown in Fig. 8.

In Fig. 9 the corresponding major stress distribution in the mortar matrix is shown. In this figure the length of the lines is a measure for the major stress level. From the analysis of the tensile major stresses (max. ~14 N/mm^2) it becomes obvious that without taking crack formation into consideration no realistic result could be obtained. In earlier codes of numerical concrete we had already introduced crack formation with a tensile strain softening concept [5,16]. In these codes the direction of the softening behaviour was fixed in the elements at the moment the major stress exceeded the tensile strength. The direction of the major stress in the next loading steps, however, did not always coincide with the fixed direction of softening. This is caused by redistributions in the very complex state of stresses of the composite material. Consequently, some elements kept a certain rigidity in the major stress direction and were "locked". This problem can possibly be overcome by using a multiple crack model. In this context we should mention here a very attractive mathematical framework which can handle multiple crack formation without violation material frame indifference [17]. The implementation of such a model in the numerical concrete codes will, however, increases computer time considerably because one needs to keep track of the state of every crack. Another solution is the use of an isotropic strain softening model which can be justified on grounds of the relative small mesh sizes which are used in the numerical concrete structures [4].

A concept which is certainly more satisfying from a materials science point of view is the prediction of multiaxial softening relations by simulating crack formation and propagation in mortar structures with LEFM [18,19]. It is essential that these models take care of friction. Further studies are needed to find out which solution is the most realistic and convenient one. Therefore, the influence of crack formation on shrinkage is first studied by means of a simplified model which will be discussed in the next paragraph.

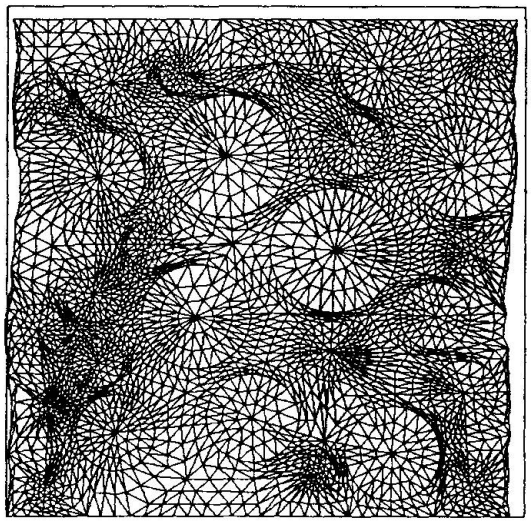

Fig. 8 Calculated deformations corresponding to the stage of drying shown in Fig. 7.

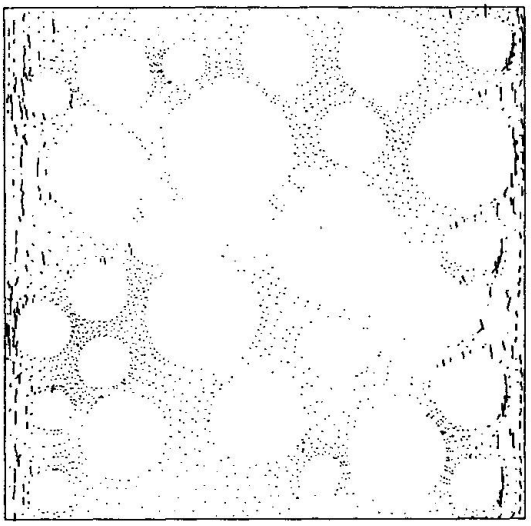

Fig. 9 Calculated major stress distribution in the mortar matrix corresponding to the stage of drying shown in Fig.7.

4 DEFORMATION UNDER TRANSIENT HYGRAL CONDITIONS

4.1 Numerical model of a quasi homogeneous material

It has been shown in the preceeding chapter how the drying of a composite structure can be predicted numerically. We have seen that the resulting stresses in the material overcome tensile strength of the matrix. As has been pointed out finally crack formation in the composite structure will be taken into consideration. For the moment being we will use a numerical model of a quasi homogeneous material to investigate the effect of crack formation on the total deformation under transient hygral conditions.

A computer code has been developed to predict the time dependent behaviour of concrete slabs [4]. The length and the thickness of the slab can be introduced. For the analysis a regular mesh with simple triangular finite elements is generated automatically. Coarser and finer meshes can be chosen by the user.

It is assumed that the drying process takes place perpendicular to the two parallel and opposite surfaces of the slab. The nonlinear drying process can therefore be calculated uniaxially, and all nodes with the same distance to the surface have the same time dependent humidity.

Creep and shrinkage have been introduced in a similar way as described in the preceeding paragraphs. In addition a strain-hardening and softening model has been introduced. To simulate the localization processes in regions with high tensile stresses a statistical distribution of the tensile strength has been assumed. Details of this model are described elsewhere [4,26]. The strain-hardening and softening model used in the following two examples is shown in Fig. 10.

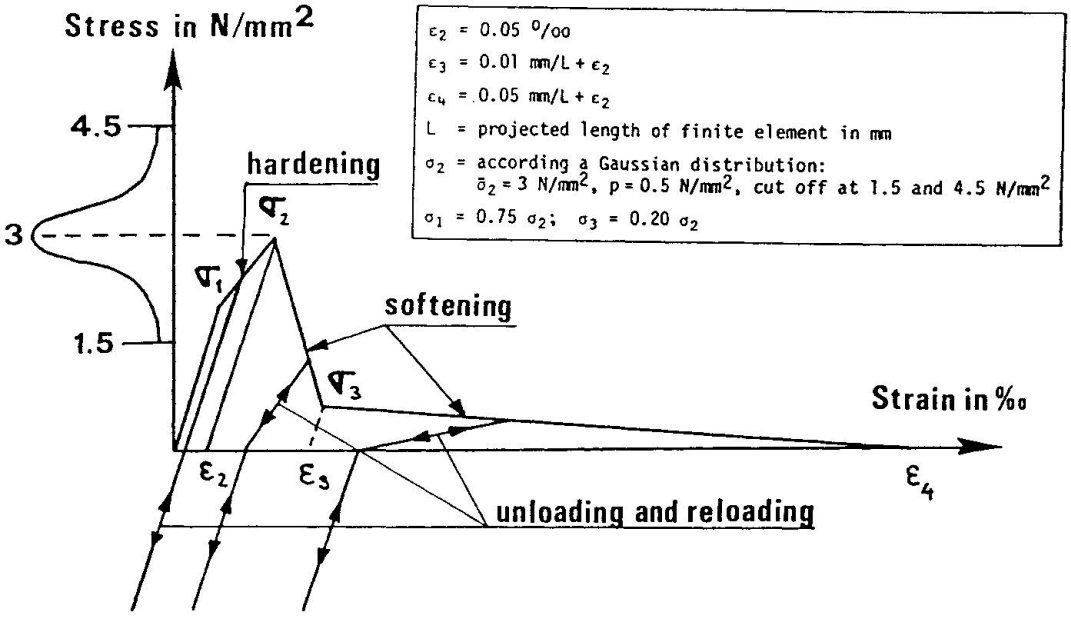

Fig. 10 Strain-hardening and softening model applied in the analyses.

4.2 Influence of crack formation on total deformation under hygral transient conditions

As an example we will simulate shrinkage of a slab of a thickness of 120 mm and a height of 240 mm. The slab is supposed to be exposed at both sides to air with a relative humidity of 50 %. The unrestrained shrinkage is supposed to be :

$$\varepsilon_{us} = -0.0018 + 0.000018\ h \quad (h \text{ in } \%) \qquad (6)$$

At 50 % RH this corresponds to a final shrinkage deformation of -0.9 o/oo.

First the uniaxial distribution of humidity as function of time was calculated with the nonlinear diffusion equation described elsewhere [20].

In Fig. 11 the calculated deformations, the distribution of damage energy and the zones where strain softening occurs (localization process) after three different durations of drying are shown.

In this model we call damage energy the amount of energy which is consumed in the tensile strain hardening branch of the diagram shown in Fig. 10. It should be noted that in this analysis tensile strain hardening and softening behaviour was fixed in advance in the longitudinal direction of the slab to gain CPU time. As can be seen in Fig. 11 localization of strain softening has taken place in 3 regions, but a complete stress-free crack was not created. This is due to tensile creep behaviour and the assumed distribution of the tensile strength. In this model the influence of tensile creep on strain softening is not yet taken into account explicitely. This is a subject which needs to be developed further in order to simulate realistically subcritical loading conditions.

The calculated shrinkage curve (a) of the slab is shown in Fig. 12.

As can be seen the final shrinkage of curve a is lower than the assumed unrestrained shrinkage of -0.9 o/oo corresponding to a relative humidity of 50 %. This is caused by the residual strain in the softening regions after unloading (see fig. 10 and fig. 11). Curve b in Fig. 12 represents the calculated shrinkage curve for which hardening and softening behaviour was suppressed by increasing the tensile strength. This curve can be considered to be the shrinkage curve under compressive loading conditions. The final shrinkage of this curve is higher than the unrestrained shrinkage at 50 % RH. This is caused by the influence of humidity on the creep rate. During the drying process tensile creep takes place in the dry regions, while compressive creep takes place in the wetter core. Thus, although the internal stress field (caused by drying) is in equilibrium, the overall (macroscopic) creep is not zero and increases shrinkage without crack formation. In Fig. 13 the ratio between curve (b) and curve (a) as function of duration of drying ($t-t'$) is shown. From this analysis it can be concluded that there is a marked difference between shrinkage under load and free shrinkage reduced by crack formation (which is the shrinkage we generally measure in our experiments). This difference will probably still be increased if we take the heterogeneous structure of concrete into consideration.

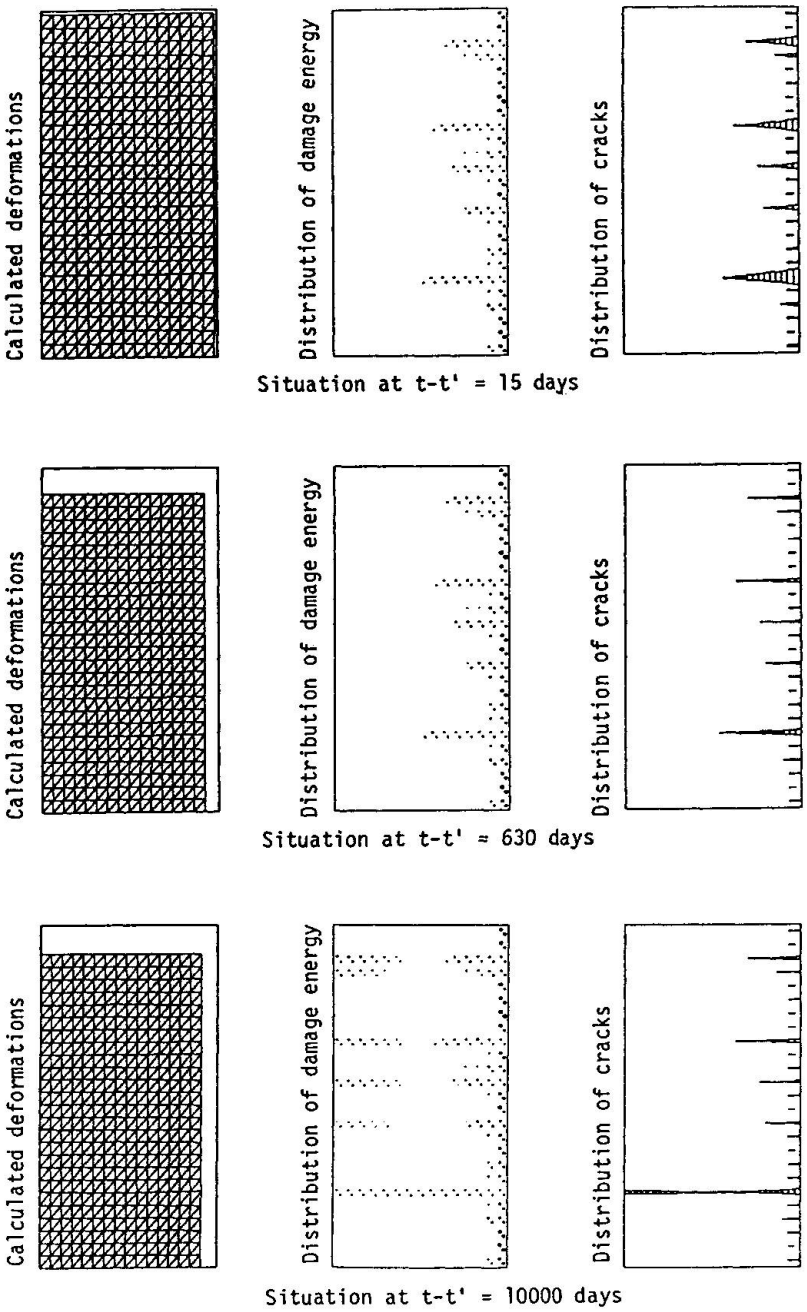

Fig. 11 Calculated deformations, distributions of damage energy and strain softening at three different durations of drying.

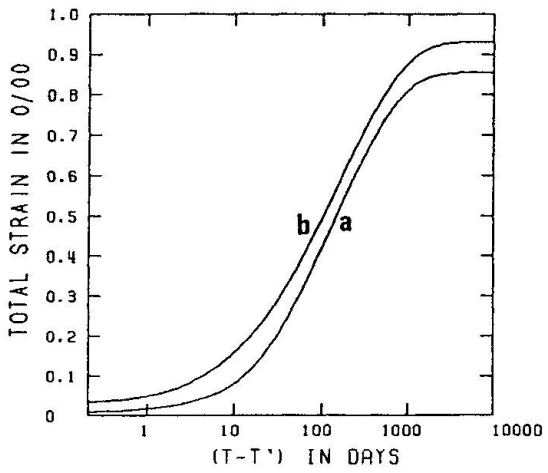

Fig. 12 Calculated shrinkage curves with (a) and without (b) crack formation as function of duration of drying.

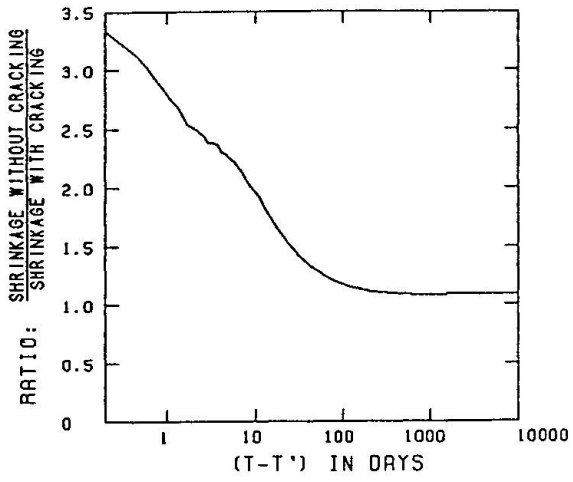

Fig. 13 Ratio of shrinkage without and shrinkage with crack formation as function of duration of drying.

In Fig. 14 experimental results of creep and shrinkage tests on sealed and drying cylinders of HCP are shown [21]. When we determine again the ratio between the shrinkage under load ε_s and the free shrinkage ε_s^o we obtain the curves shown in Fig. 15. The applied load is indicated as parameter.

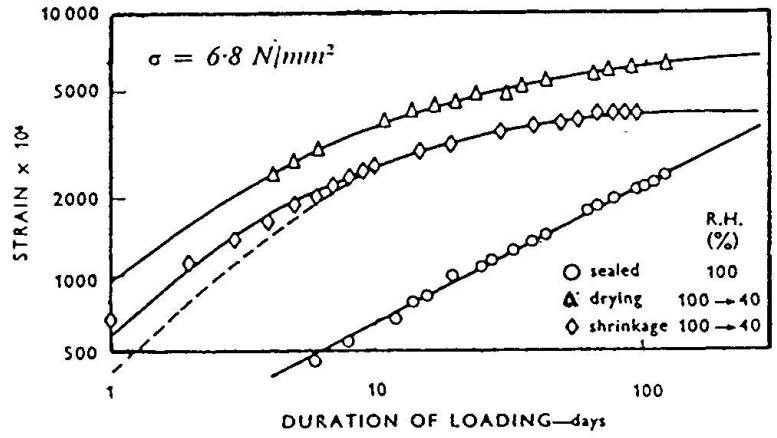

Fig. 14 Creep of hollow cylinders of HCP. Results of tests carried out under sealed conditions (at 100 % RH) and under drying conditions (from 100 % to 40 % RH). Pure shrinkage is also shown [21].

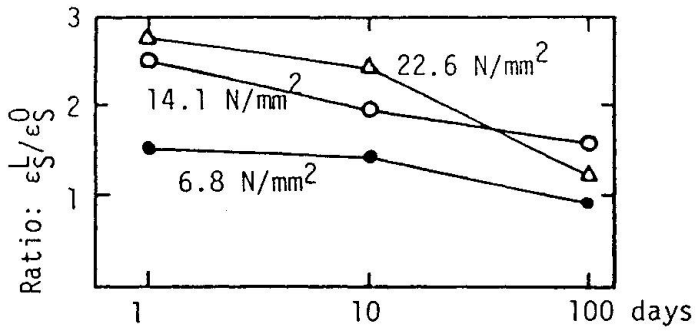

Fig. 15 Ratio between shrinkage under loading ε_s^L and free shrinkage ε_s^0 as function of duration of drying. Applied external stress is the parameter. (Data after [21]).

A number of results of similar test series has been evaluated in the same way. At the beginning always a factor of about 2 or slightly bigger has been found and as drying proceeds this factor decreases and approaches finally 1. The relation shown in Fig. 15 agrees qualitatively well with the numerical prediction shown in Fig. 13. This relation can be considered to be characteristic for transient hygral deformation. For longer periods of drying the remaining creep function corresponds to the lower creep of dried concrete. The result of this analysis may still be modified once the circumferential stresses around the aggregates are taken into consideration.

The model has further been used to study geometrical effects on shrinkage. In our laboratory very accurate shrinkage measurements have been carried out on cylinders with different diameters [1]. These cylinders were exposed to a relative humidity of the surrounding air of 65 %. In Fig. 16 the measured shrinkage strains at different durations of drying are indicated.

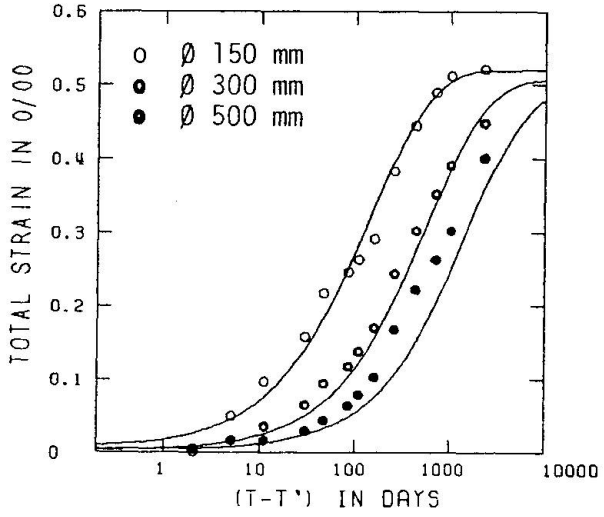

Fig. 16 Comparison between measured shrinkage strains of cylinders with Ø 150 mm 300 mm and 500 mm, exposed to RH 65 %, and calculated shrinkage curves based on a nonlinear diffusion equation and a tensile strain-hardening and softening model with residual strains. Measurements by [1].

In the model moisture capacities, permeabilities and unrestrained shrinkage were adopted to get a close fit with the shrinkage measurements of the cylinder with a diameter of 150 mm. Next the same materials data were used to predict the shrinkage curves of the cylinders with diameters 300 mm and 500 mm. Results are shown also in Fig. 16. It should be noted that we used "equivalent" thickness of the slabs calculated with the model in order to be able to compare with the results obtained experimentally with cylinders. As can be seen in Fig. 16, the predicted final shrinkage with the model becomes less as the geometry increases. This corresponds well with the results just mentioned [1] as well as with other experimental findings [22].

Although generally a reasonable agreement between experimental results shown in Fig. 16 and the numerical prediction can be observed there remains a systematic deviation. The shrinkage prediction based on diffusion theory underestimates the hygral deformation at longer durations of drying and for bigger specimens. This discrepancy can be explained by the fact that aging of the material is not represented adequately in the model. Aging can have different effects on shrinkage. The diffusion coefficient decreases, the final value of shrinkage can even increase due to the presence of more hydration products and finally the increased tensile strength leads to an accelerated shrinkage due to reduced crack formation.

5 DEFORMATION UNDER TRANSIENT THERMAL CONDITIONS

5.1 Influence of a sudden change of temperature on basic creep of a composite material

It has been shown above that drying creates a complex state of stress in a composite material (see Fig. 9). In case the coefficients of thermal dilatation of the matrix and the aggregates are not identical any temperature change necessarely must create internal stresses. In Fig. 17 a typical example of a numerical simulation of this situation is shown [13]. In this case α_M for the matrix has been chosen to be $12 \cdot 10^{-6}$ K^{-1} and α_A for the aggregates has been chosen to be $7 \cdot 10^{-6}$ K^{-1}. The tensile stresses in the aggregates and the compressive stresses in the matrix are indicated by means of their major stresses.

Now let us suppose that the composite structure shown in Fig. 3b is loaded at room temperature and the creep is measured until $t-t' = 15$ days. Then the temperature is linearly increased to 70^0C in 12 hours and the resulting deformations are further followed.

This situation has been simulated numerically and results are shown in Fig. 18. During the initial period modest basic creep is observed. When the temperature is changed first of all a thermal expansion is noticed and later the thermally increased basic creep follows. In the left part of Fig. 18 the elastic energy of the different components is plotted. The aggregates are temporarely partly unloaded while the surrounding matrix has to take over the corresponding compressive stresses. Due to the increased creep at elevated temperatures these stresses are quickly reduced.

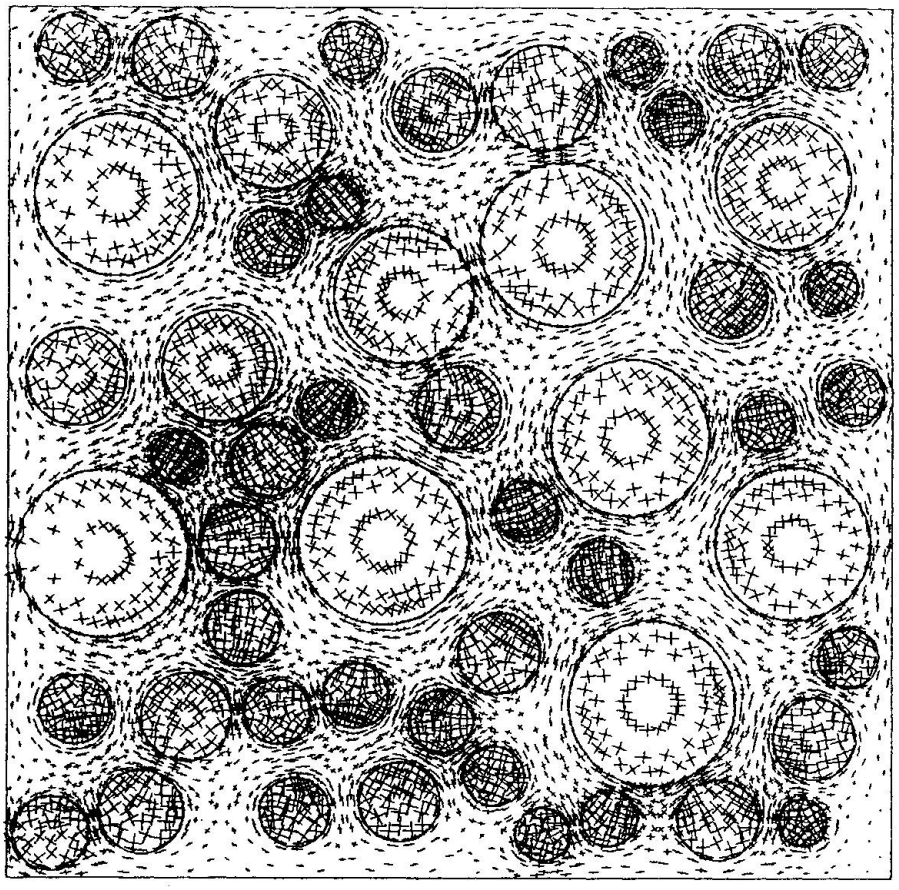

Fig. 17 Calculated major stress distribution in a composite structure due to a thermal shock.

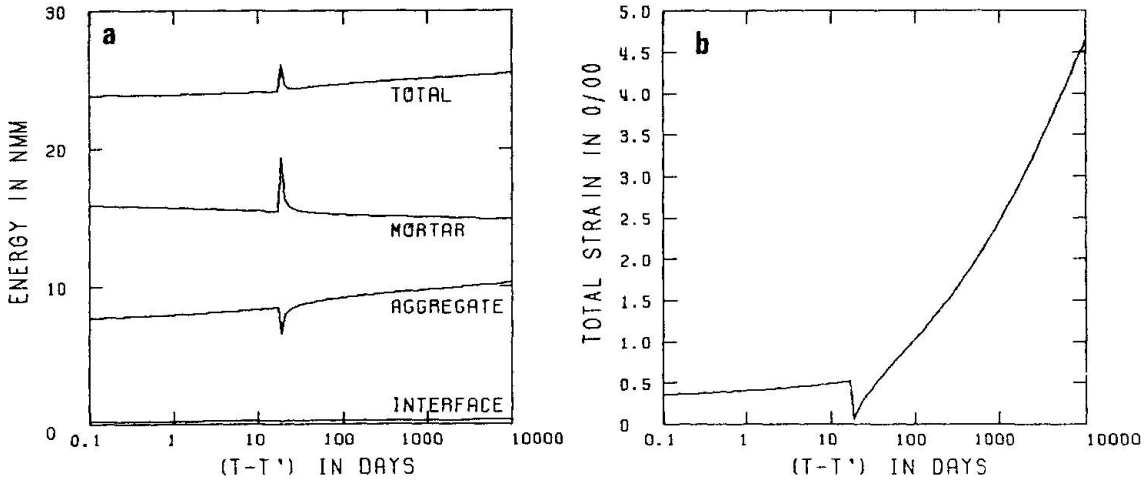

Fig. 18 (a) Distribution of potential energies stored in the components and total stored potential energy as functionof duration of loading.
(b) Total deformation as function of duration of loading.
The temperature is kept constant at 20^0C up to (t-t´) = 15 days; then the temperature is linearly increased in 12 hours to 70^0C and further kept constant.

5.2 Influence of sudden change of temperature on drying and total deformation

In the preceeding section we have supposed that the specimen was tested under sealed conditions. Let us now repeat the theoretical experiment of 5.1 but this time under drying condition, i.e. in 50 % RH.

In Fig. 19 the loss of evaporable water is plotted as function of time. For comparison the drying under isothermal conditions (20^0C) are shown too. For further details of this calculation we refer to [3,23]. In this same publication the influence of temperature on the water capacity and the permeability are given. At $t-t' = 15$ days the drying rate increases noticebly.

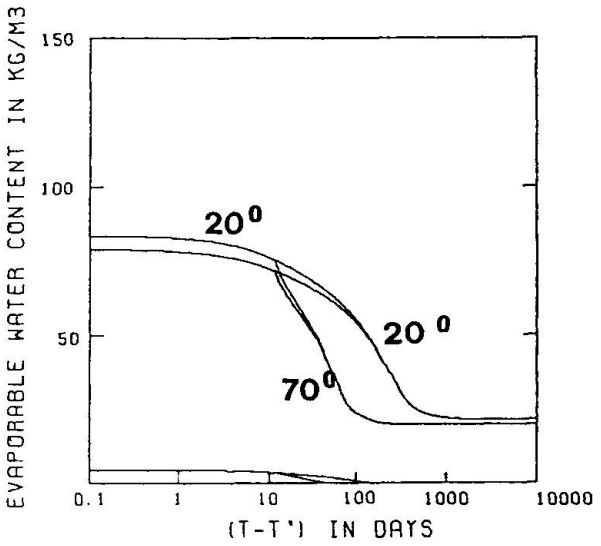

Fig. 19 Loss of evaporable water as function of duration of drying for two different temperature histories (see also [20,23]).

The corresponding total deformation is shown in Fig. 20. Initially the time-dependent deformation is bigger because the specimen is stored in a drying environment. The change of temperature cause first of all again thermal expansion. Then the creep at elevated temperatures sets in at an increased rate. The drying process and hence shrinkage comes to an end at about 200 days. Then creep rate must be expected to be considerably slowed down.

For comparison the total time-dependent deformations shown in Figs 19 and 20 are replotted in Fig. 21. The initial increase of deformation under drying conditions can clearly be seen. While the sealed sample continues to creep at a high rate after the temperature change the drying sample undergoes a transition which leads to a significantly reduced total deformation.

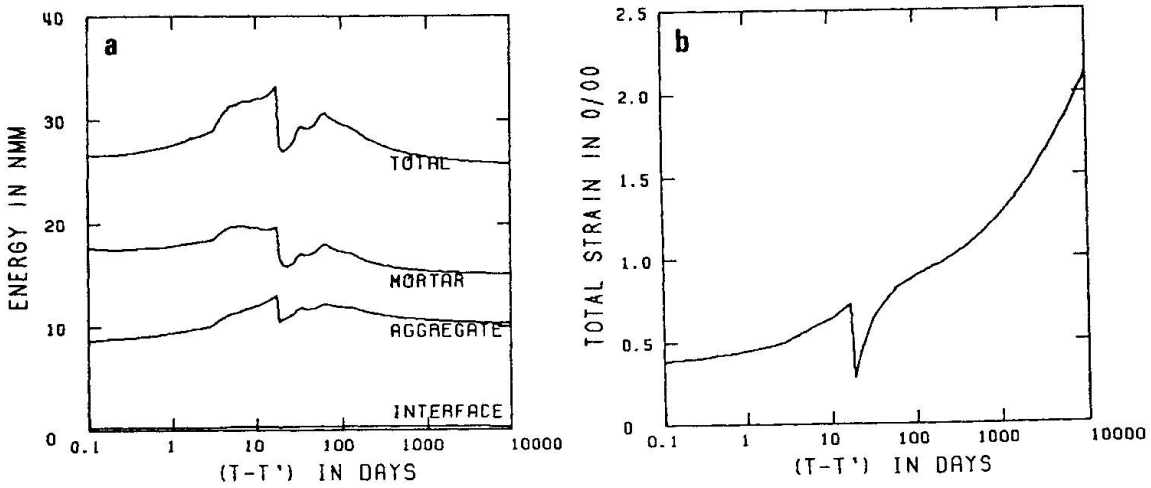

Fig. 20 (a) Distribution of potential energies stored in the components and total stored potential energy as function of duration of loading.
(b) Total deformation as function of duration of loading.
The drying process starts at the moment the load is applied.
The temperature is kept constant at 20^0C up to (t-t') = 15 days; then the temperature is linearly increased in 12 hours to 70^0C and further kept constant.

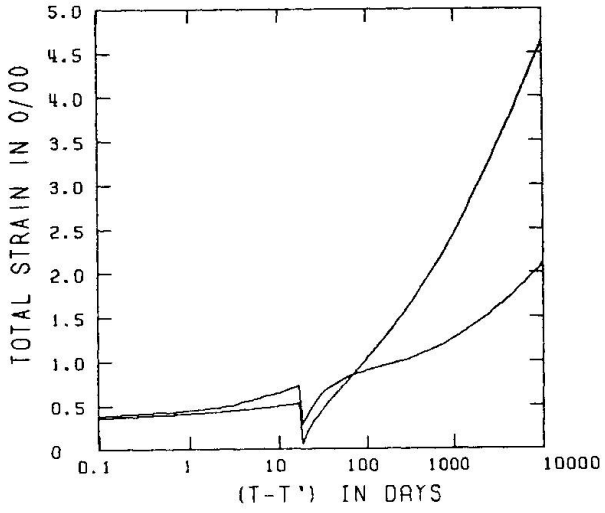

Fig. 21 Comparison between the calculated total deformations shown in Fig. 18b and Fig. 20b.

It should be noted here that the increased temperature only accelerates the transition. Under normal temperatures the same behaviour will be observed at much longer times. Further the attention is drawn to the fact that any temperature change immediately causes an increased rate of deformation due to the internal stress concentration.

6. CONCLUSIONS

- Some basic concepts of numerical simulation of the formation of the microstructure of HCP are outlined. The aim of this approach is to replace arbitrary terms like aging by more realistic terms like bond density in the xerogel and bonds between hydrating particles of HCP.
- Actual state parameters such as temperature, humidity and degree of hydration can be determined under transient hygral and thermal conditions by solving numerically a series of appropriate coupled differential equations with given boundary conditions.
- Shrinkage of a composite structure without crack formation, based on calculated moisture distributions, has been determined with numerical concrete codes.
- The influence of crack formation, tensile strain-hardening and softening on the total deformation of a quasi-homogeneous drying material has been studied by means of model based on FEM. With this model the difference between shrinkage without crack formation and shrinkage with crack formation can be quantified.
- As has been shown already earlier drying shrinkage and creep of concrete cannot be separated. The total deformation depends on thesuperimposed stress fields.
- Transient hygral deformation can be realistically predicted if the concept of point properties is applied rigorously.
- Transient thermal deformation has to be dealt with in the same way.

REFERENCES

1. ALOU F., FERRARIS C.F. and WITTMANN F.H., Etude expérimentale du retrait du béton, Mat. et Constr. RILEM (to be published 1987).
2. WITTMANN F.H., Structure and mechanical properties of concrete, The Architectural Reports of the Tohoku University, 22 (1983) pp. 93-112.
3. WITTMANN F.H. and ROELFSTRA P.E., Numerical concrete applied to predict constitutive laws of porous composite materials, SMIRT-9, Lausanne, H 2/1, (to be published 1987).
4. ROELFSTRA P.E., Numerical concrete, Ph.D. Thesis, Swiss Federal Institute of Technology, Lausanne, (to be published 1987).
5. SADOUKI H., Simulation et analyse numérique du comportement mécanique de structures composites, Ph.D. Thesis, Swiss Federal Institute of Technology, Lausanne (to be published 1987).
6. ACKER P., BOULAY C. and ROSSI P., On the importance of initial stresses in concrete and of the resulting mechanical effects, Cem. Concr. Res. (to be published 1987).
7. KNUDSEN T., On particle size distribution in cement hydration, Proc. 7th Int. Congr. Chem. Cement, Paris, Vol. II, I, (1980) pp. 170-175.
8. BEZJAK A., JELENIC I., MIAKAR V. and PANOVIC A., A kinetic study of alite hydration, Proc. 7th Int. Congr. Chem. Cement, Paris, Vol. II, I, (1980) pp. 111-116.

9. JAWED I., SKALNY J. and YOUNG J.F., Hydration of portland cement, Chapter 6 in Structure and Performance of Cements, ed. P. Barnes, Applied Science Publishers Ltd, Barking, Essex, England (1983).

10. DOUGILL J.W., Comment in Recorders Report of session 2 of the fourth RILEM International Symposium on Creep and Shrinkage of Concrete : Mathematical Modeling, held at Northwestern University, Evanston, Illinois, August 1986 (to be published 1987).

11. BAZANT Z.P., Viscoelasticity of solidifying porous material concrete, J. Eng. Mech. Div., ASCE, Vol. 103, No EM6 (1977) pp. 1049-1067.

12. WITTMANN F.H., ROELFSTRA P.E. and SADOUKI H., Simulation and analysis of composite structures, Mat. Sci. and Eng. 68 (1984-1985) pp. 239-248.

13. ROELFSTRA P.E., SADOUKI H. and WITTMANN F.H., Le béton numérique, Mat. et Constr. 107 (1985).

14. BAZANT Z.P. and TSUBAKI T., Weakly singular integral for creep rate of concrete, Mech. Res. Commun. 7 (1980) pp. 335-340.

15. WITTMANN F.H., Creep and shrinkage mechanisms, Chapter 6 in Creep and Shrinkage in Concrete Structures, Ed. by Z.P. Bazant and F.H. Wittmann, John Wiley & Sons Ltd (1982).

16. ROELFSTRA P.E. and SADOUKI H., Total fracture energy in composite materials, SVMT/DVM, Basel (1986).

17. DE-BORST, Nonlinear analysis of frictional materials, Ph.D. Thesis, Delft University of Technology, The Netherlands (1986).

18. ZAITSEV Y.U. and WITTMANN F.H., Crack propagation in a two-phase material such as concrete, Proc. 4th Int. Conf. on Fracture (ICF-4), Waterloo, Canada, Vol. 3 (1977) pp. 1197-1204.

19. HU X.Z., COTTERELL B. and MAI Y.M., Computer simulation models of fracture in concrete, In Fracture Toughness and Fracture Energy of Concrete, ed. by F.H. Wittmann, Elsevier Science Publishers, Amsterdam, The Netherlands (1986).

20. KAMP C.L., ROELFSTRA P.E. and WITTMANN F.H., Mechanisms of moisture transfer through porous materials, SMIRT-9, Lausanne (to be published 1987).

21. WITTMANN F.H. and LUKAS J., The application of rate theory to time-dependent deformation of concrete, Mag. of Concr. Res. Vol. 26, 89 (1974) pp.191-197.

22. HANSEN T.C. and MATTOCK A.H., Influence of size and shape of member on the shrinkage and creep of concrete, J. Am. Concr. Inst. 63 (1966) pp. 267-290.

23. KAMP C.L., ROELFSTRA P.E., MIHASHI H. and WITTMANN F.H., Diffusion mechanisms and drying of concrete at elevated temperatures, SMIRT-9, Lausanne (to be published 1987).

24. JENNINGS H.M. and JOHNSON S.K., Simulation of microstructural development during the hydration of a cement compound, J. Am. Ceram. Soc., 69 (1986) pp. 790-795.

25. JONASSON J.E., Moisture fixation and moisture transfer in concrete, SMIRT-8, Brussels, H5/11 (1985) pp. 235-242.

26. ROELFSTRA P.E. and WITTMANN F.H., Numerical modelling of fracture of concrete, SMIRT-9, Lausanne (to be published 1987).

Leere Seite
Blank page
Page vide

Nonstationary Long-Time Processes Causing Loss of Serviceability

Processus évolutif à long terme provoquant la diminution de l'aptitude au service

Nicht-Stationäre Langzeitprozesse und reduzierte Gebrauchstauglichkeit

Zdenek P. BAZANT
Prof. of Civil Eng.
Northwestern University
Evanston, IL, U.S.A.

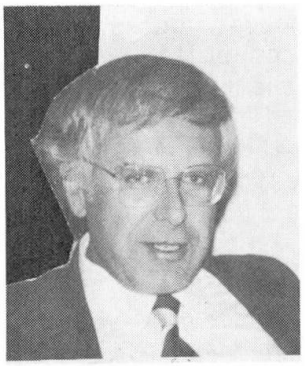

Born and educated in Prague, Dr. Bažant joined the faculty of Northwestern University in 1969 where he has been Professor since 1973 and served as Structural Engineering Coordinator and as Director of the Center for Concrete and Geomaterials.

SUMMARY

The article presents a broad but nonexhaustive overview of the state-of-the-art and modern research directions in mathematical modeling of long-time processes engendering loss of serviceability of concrete structures, and to highlight some selected recent advances. Particular attention is given to creep and the effects of moisture and temperature, the fracture aspects of long-time damage, physically based models for freeze-thaw durability and for corrosion of steel, and probabilistic modeling – an essential ingredient of serviceability analysis.

RÉSUMÉ

L'article présente une revue, large mais non exhaustive, des directions de la recherche moderne dans la modélisation mathématique de processus à long terme provoquant la diminution de l'aptitude au service de structures en béton armé. Quelques progrès récents sont présentés. Une attention particulière est donnée au fluage et aux effets de l'humidité et de la température, aux aspects de rupture suite à des dommages anciens, à des modèles physiques pour l'étude de la durabilité sous l'effet de cycles gel-dégel et pour la corrosion de l'acier ainsi que des modèles probabilistes – un élément essentiel pour l'étude de l'aptitude au service.

ZUSAMMENFASSUNG

Der Vortrag gibt einen breiten, jedoch nicht umfassenden Überblick über den Kenntnisstand und die modernen Entwicklungen in der mathematischen Beschreibung langdauernder Prozesse, die den Gebrauchszustand von Massivbauten beeinträchtigen können; weiter beleuchtet er einige ausgewählte Neuentwicklungen. Besonders werden Kriechen, Wirkungen von Feuchte und Temperatur, die Brucherscheinungen bei Langzeitschädigung, physikalisch begründete Frost-Tau-Beständigkeit, Stahlkorrosion und Wahrscheinlichkeitsmodelle behandelt, die wesentliche Bestandteile einer Gebrauchsfähigkeitsberechnung sind.

1. INTRODUCTION

Concrete construction, an over-quarter-billion-dollar industry in the United States, is often plagued by long-time serviceability problems. All too often, slender prestressed concrete bridges, pavements, ocean structures, dams, containments, tanks, building structures, etc. suffer excessive deflections, cracking, corrosion or other serviceability impairments and have to be either closed or repaired well before the end of their initially projected design life. The cost to the society is tremendous, and in fact greatly exceeds in strictly economic terms the cost of catastrophic failures due to mispredicted safety margin. These economic costs are not only reflected in the actual damages but also in wrong economic decisions in the selection of design alternatives. For example, in competitive bidding one type of structure may appear to cost 20% less than another type of structure but should not be selected if its design life should turn out to be 30% shorter than that of the other alternative. Concrete structures of excellent serviceability, of course, can be and have been designed, but at the present we are still far from being able to achieve in structural design the optimum balance between the conflicting requirements of serviceability, economy of construction and maintenance, high performance and safety against catastrophic collapse.

The salient aspect of the problem is that serviceability depends on many physical-chemical processes, each of which is influenced by numerous factors. It is impossible to make close predictions and decide which processes and factors dominate in a given case unless a mathematical model which takes all these processes and factors into account is developed and computationally implemented. The processes which affect long-time serviceability or durability are in general nonstationary in time and involve:

1. Chemical aging, i.e., a change of material properties by long-time chemical processes such as cement hydration;

2. Creep, both viscoelastic and viscoplastic;

3. Effects of variable moisture content and water diffusion through the pores;

4. Effects of temperature variations;

5. Fracture processes, which involve development of cracking and other progressive damage as well as the bond deterioration;

6. Fatigue, which affects primarily interface bond;

7. Freeze-thaw durability;

8. Corrosion of steel and concrete; and

9. Chemical attack, such as alkali-cement reaction, penetration of chloride ions, sea water attack, carbonation, etc.

The intent of this lecture is to present a broad apercu of the current state-of-the-art and research directions in computational mechanics of concrete creep and other serviceability problems and then focus on some selected recent advances in mathematical models of several physical processes which determine long-term serviceability and have been investigated at the author's institution. Some basic probabilistic methods which need to be incorporated in such analyses will be also reviewed.

2. STATE-OF-THE-ART AND RESEARCH DIRECTIONS IN CREEP AND SHRINKAGE

The literature on concrete creep and shrinkage is vast and continues growing at an increasing pace; see Fig. 1 which shows the plot of the annual numbers of publications on material behavior models and on probabilistic models which

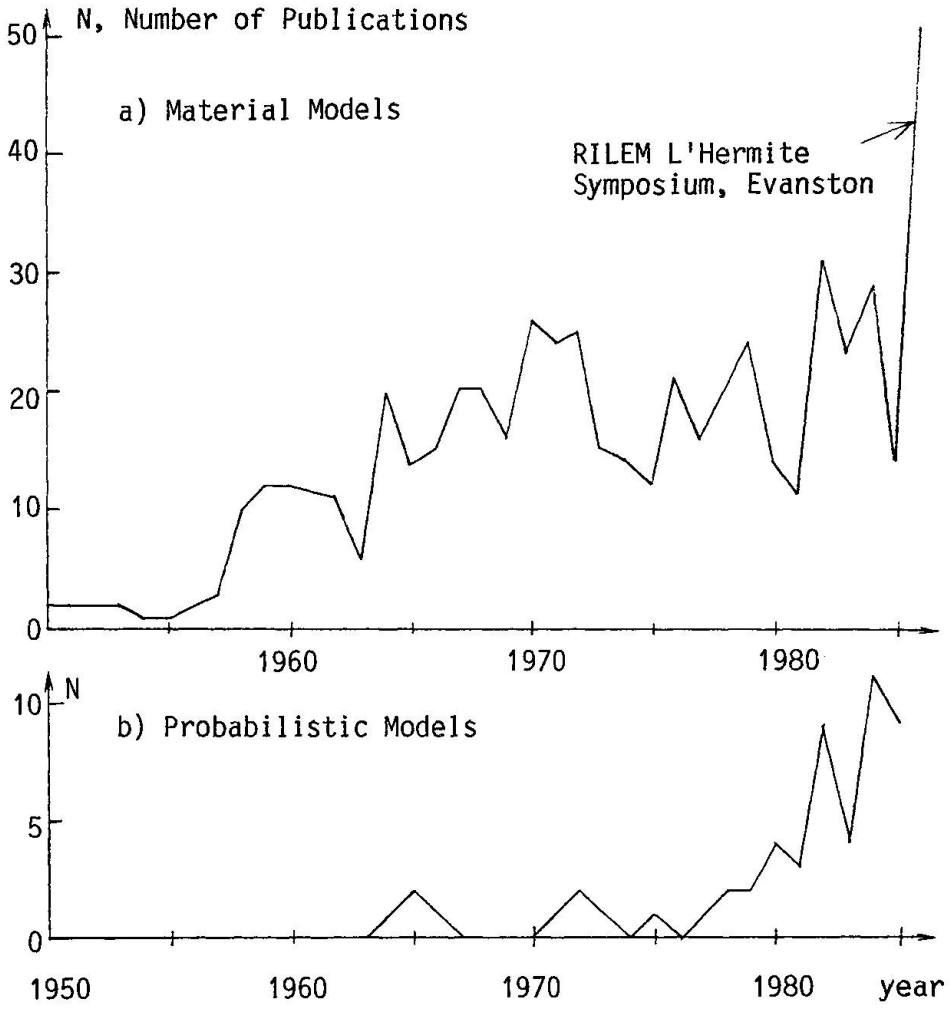

Fig. 1 - Plot of the annual number of publications on mathematical modeling of creep and shrinkage and their effect in structures, extracted from RILEM State-of-the-Art Report [1].

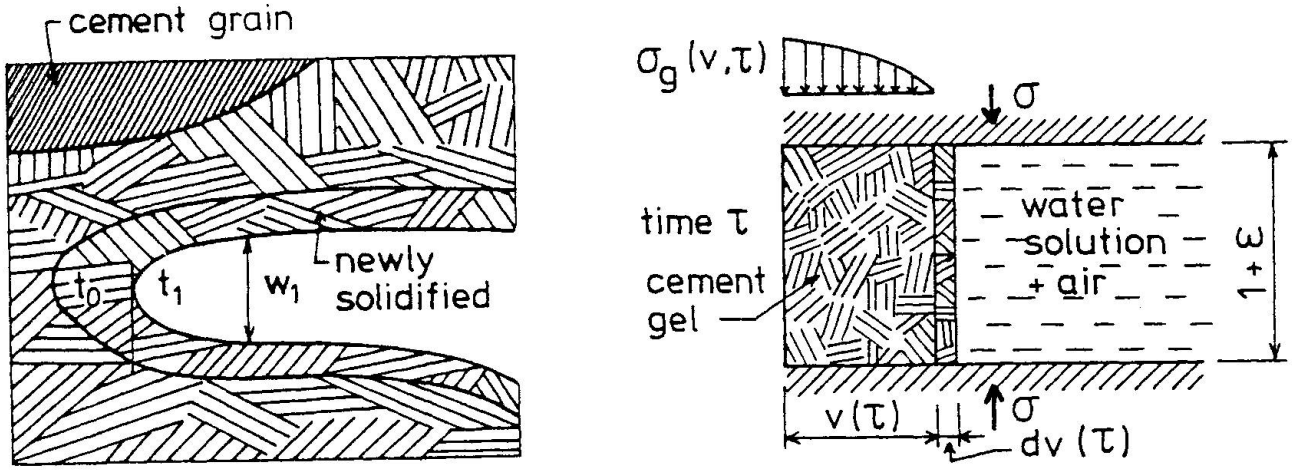

Fig. 2 - Model of Solidification of Portland Cement from Ref. 22.

were referenced in a recent state-of-art report (1986) in which a total of 1036 works were cited. As seen from today's perspective, the evolution of creep and shrinkage theory can be subdivided into three phases:

In Phase I, which ended roughly fifteen years ago, elementary phenomenologic data have been acquired and simplified linear models, realistic for only a limited range of time and environmental conditions, were developed. In Phase II, which might be regarded as nearly complete by now, the experimental base was greatly extended and systematically compiled, especially with regard to the effects of temperature and humidity, and a comprehensive theory of linear analysis with aging has been formulated. In Phase III, which we are now entering, a coherent and realistic general theory must be developed if we should be able to derive significant benefits from the availability of powerful computers. This theory no doubt (1) needs to be nonlinear, (2) needs to be based on physical processes on the microstructural level, and (3) must cover not only deterministic but also probabilistic aspects of long-time predictions.

The theory needs to be also extended to some challenging new problems, for example the problem of radioactive waste disposal. In this regard, questions are being raised as to what is the creep at variable elevated temperatures for periods spanning into thousands of years. The empirical formulas still in use in the current code recommendations are, of course, useless for such long times, and the only hope is a consistent rational theory based on the knowledge of physical mechanisms.

The fact that the prediction of creep and shrinkage in structures involves great uncertainty and random variability has been thought to negate the need for an accurate, sophisticated theory. The contrary conclusion, however, is justified. The random variability can, and must, be taken into account by a probabilistic design approach. The probabilistic design, however, makes sense only if the deterministic theory which corresponds to the mean behavior is sound, for otherwise the probabilistic analysis does not deal with truly random errors but with systematic errors disguised as random ones. Improvement of the constitutive relations for creep appears to be a prerequisite for significantly reducing the statistical error of the predictions of creep effects in structures, which is often enormous for the present models but can in fact be rather low in the laboratory.

With the linear theory of concrete creep we have probably arrived almost as far as we can go. The current state-of-the-art [1] may be briefly described as follows:

1. The structural analysis can be carried out for a general compliance function as measured, including the aging effect. The latest formulas for the compliance function, such as the log-double power law and the triple power law [1] can approximate the measured compliance data almost as closely as the scatter of data permits one to discern. Although the theoretical basis of the linear analysis is the principle of superposition for arbitrary variable stress and strain histories, it is most effective for computer solutions to convert the compliance function within the computer program into a rate-type model which may be interpreted by a spring-dashpot rheologic model with age-dependent viscosities and elastic moduli. The humidity and temperature effects may be most realistically incorporated in this rate-type form as influences on the viscosities of the spring-dashpot model [1].

2. In many applications, especially for simple structures and for simple humidity and temperature histories, sufficiently accurate linear solutions can be obtained by the age-adjusted effective modulus method [2,3,1,10,6]. Its error with regard to the exact solutions of linear integral equations is insignificant in comparison to the error of the linearity assumption itself.

On the other hand, the classical effective modulus method, which is not appreciably simpler than the age-adjusted one, is sufficient only for those cases where the stresses are nearly constant in time.

3. The linearity assumption fails not only above the service load range but also when moisture effects and cracking dominate and when the stress history includes large changes of stress after a long period of creep. When the linear creep law is converted to the rate-type form to make numerical computations more efficient, the conversion algorithm yields viscosities and elastic moduli which may violate thermodynamic restrictions, having negative values for some (short) time periods [1,3]. After long studies it appears that this theoretical difficulty cannot be overcome within the realm of a linear theory and is probably caused by the fact that we are trying to use a linear theory for what is inherently a nonlinear phenomenon. Another dubious consequence of the linearity assumption is that the creep recovery curves may be obtained as nonmonotonic, due to the fact that the measured creep curves for different ages at loading may diverge. Most likely, this phenomenon is a manifestation of a deviation from linearity. The most important deviation of creep from linearity is caused by simultaneous drying or wetting and, as recently transpired, also by simultaneous temperature changes.

4. In the current code recommendations [6,7] as well as many computational studies, the creep and shrinkage in the entire cross section of a beam or plate is characterized by a single mean compliance function and mean shrinkage function. This is a source or large error as well as complexity. The mean cross section compliance function for a drying environment in reality depends on the cross section shape as well as the type of loading (e.g., bending, compression, tension, torsion). With this practice, the coefficient of variation of the errors of the long-time prediction of the compliance function and shrinkage function apparently cannot be reduced below about 18% even if the most sophisticated formulation is used, and about 40% if the simple formulations of the type of code recommendatons are used [8,1]. The formulation of the true material creep and shrinkage properties applicable to a point rather than the entire cross section is much simpler and can also be made with a much smaller error. The cross section must then, of course, be subdivided into layers or finite elements, and the creep and shrinkage of each such layer or element must then be based on the calculated humidity and temperature for the same element rather than on the mean environmental humidity and temperature.

With regard to the characterization of the creep and shrinkage properties for structural analysis, the current thinking [1] might be characterized as follows:

1. The standard recommendation should specify the compliance function rather than the creep coefficient or specific creep defining only the creep part of strain. The reason is that, due to significant short-time creep, the definition of the elastic modulus is ambiguous, depending strongly on the duration of measurement. The elastic modulus values recommended in the codes are suitable only for elastic analysis and are rather different from the elastic modulus vaues which correctly correspond to the recommended values of the creep coefficients.

2. If the entire cross section of a beam or plate is characterized by one mean compliance function, this function should be formulated as the sum of the basic creep compliance and the additional compliance due to drying. The reason is that the shapes of the curves of these two compliance functions are rather different; the drying compliance has a final asymptotic value while the basic one apparently does not, and the shape and values of the drying compliance curves depend on the cross section size and shape while those of

the basic compliance do not.

3. For physical reasons, as well as for reasons of convergence of numerical solutions, the constitutive equation or compliance function must satisfy the principle of continuity. This principle dictates that the strain responses for any two stress histories that are infinitely close to each other must be also infinitely close. E.g., if one strain history is caused by constant stress σ_1 applied from time t_1 to time t_2, and another strain history by a constant stress σ_0 applied from t_0 to t_1 and constant stress σ_1 applied from t_1 to t_2, the in the limit $\sigma_0 \to 0$ the second strain history must approach the first stress history.

4. Although a separation of creep into a reversible (delayed) component and an irreversible (flow) component can be introduced if desired, it is neither required nor justified by thermodynamics [1,10]. The reason is that in aging materials the reversible creep component cannot be characterized as a unique function of the thermodynamic state variables. Rather, it depends stronly on the age at unloading, the age at first loading, the recovery duration, the moisture history, etc.

5. The existing test data do not reveal the existence of any final asymptotic value for basic creep [1]. The question of its existance would be moot if a slope decrease (in log-time) were assumed to begin after the end of the lifetime of the structure, but this is not the case for various formulas in use, or given in standard recommendations. Therefore, it is desirable to change these formulas, especially since no particular simplification of structural computations is achieved by specifying the compliance function that has a final asymptotic value.

6. Among the simplest formulas for the basic creep compliance function, a power function of the load duration, with an exponent about 1/8, appears to be the best. However, measurements indicate a transition from the power law for short load durations to a logarithmic law for long load durations. The time of this transition increases as the age at loading increases while the strain value at the transition seems to be roughly the same for all ages at loading. The classical Ross' hyperbola as well as Dischinger's exponential are adequate only for creep durations of approximately one year, as originally derived, and their use for long-time extrapolations is incorrect, experimentally unjustified. The dependence of the basic creep strain at constant stress duration on the age at loading approximately follows an inverse power function [1].

7. Unlike thermorheologically simple materials, the compliance function of concrete unfortunately cannot be expressed as a function of a single time variable, the reduced time. Numerous attempts in this regard were unconvincing since they considered only very limited test data. Among other simplifications of the constitutive relation for creep, the strain hardening and time hardening (concepts in which the creep rate decline is expressed as a function of the current creep strain or the time elapsed from the first loading) are alone insufficient to describe the behavior of concrete under variable stress [1].

8. The constitutive relation for creep and shrinkage should be based to the maximum possible extent on mathematical formulations for the various physical processes involved in creep and shrinkage. The physical considerations and mechanism theories which have so far yielded information on the compliance function and the constitutive relation include [1]:

a) The activation energy theory, which governs the creep rate, as well as the rate of aging (hydration), and moisture diffusivity.

b) Diffusion theory for moisture and temperature effects.

c) Theories of capilarity, surface adsorption (free and hindered) and diffusion between the small and large pores in cement paste.

d) Thermodynamic restrictions.

e) Aging interpreted as time variability of the composition of a mixture of nonaging components.

f) Fracture mechanics and cracking models.

g) Basic restrictions of continuum mechanics, including the principles of objectivity, tensorial invariance, form invariance, continuity, etc.; and

h) Stochastic process modeling.

Since proposals for physical mechanisms whose consequences for the stress-strain relation or compliance function are not (or cannot) be formulated mathematically are of little use as they can be neither proved nor disproved. It is essential to require that proposals for new mechanism models be described in mathematical terms.

9. The diffusion theory of moisture transport, whose relevance is confirmed by experimental evidence, indicates that: (1) the half-time of shrinkage as well as drying creep is proportional to the square of the cross section size, to the drying diffusivity, and to the shape factor that results from weight loss measurements [8,1], and (2) the shrinkage function as well as the drying creep term should initially evolve as the square root of drying duration [35,8]. For better accuracy, however, corrections need to be introduced due to the spoiling effects of aging, cracking or strain-softening, and creep due to residual stresses. Calculations of the distributions of water content in structures at various times require the use of a diffusion equation which is strongly nonlinear, principally due to a strong decrease in diffusivity as the specific water content decreases [1].

10. The effect of temperature on creep is two-fold: The effect on creep rate, modeled through the dependence of the viscosity coefficients in a rate-type model on temperature, and the effect on the aging rate (hydration) [1,10]. These two effects counteract each other and have to be described by separate activation energy expressions. Sometimes one effect dominates, sometimes the other. Activation energy also governs the dependence of moisture diffusivity on temperature, which in turn determines the effect of temperature on shrinkage as well as drying creep.

11. Creep and shrinkage measurements provide strong experimental evidence that the increase of creep due to simultaneous drying, called also the Pickett effect, is the result of two physical phenomena: (1) Cracking or strain-softening due to residual stresses, which causes that the shrinkage observed on a companion load free specimen is much less than the true material shrinkage which takes place in a compressed creep specimen [12,13], and (2) a cross effect between creep rate and pore humidity rate, which can be described either as stress induced shrinkage or as a dependence of creep viscosities on pore humidity rates [13,1]. Explanation of the latter cross effect can be provided in terms of an effect of the diffusion of water between small and large pores in hardened cement paste on the rate of bond ruptures which cause creep. This diffusion must be caused by differences in chemical potentials of water in the small and large pores, which further indicate that there should also be a cross effect between the creep rate and the rate of temperature. Such a cross effect provides an explanation for the transitional thermal creep, i.e., an acceleration of creep due to simultaneous change of temperature [1].

12. Since thermodynamics deals only with substances invariable in time, the aging (hydration) should be mathematically described as a consequence of a

varying composition of a mixture of reacting constituents which are themselves time invariant (nonaging).

After this succint review of the current state of creep modeling and computational approach, we will now focus attention on the mathematical modeling of several physical phenomena which are important for creep as well as serviceability in general.

3. SOME RECENT ADVANCES

3.1 Basic Creep Model Based on Solidification Process

As already mentioned, a physically based model for the role of aging in concrete creep should be based on some suitably idealized formulation for the solidification process of portland cement in which the volume growth of the hydrated volume fraction of cement is the basic variable [22,10,1]. The hydration process is imagined to gradually deposit layers of tricalcium silicate hydrates and other chemical products of hydration on the surfaces of the pores filled with water (Fig. 2). From the mechanics viewpoint, the essential aspect of this process is that at the time when each infinitesimal layer of hydrated material is attached to the existing solid microstructure, it must be essentially stress free, and stress is introduced into it only by the subsequent deformation. Under the assumption that the hydrated material as deposited has time invariant properties, the aforementioned property led [22] to the following form of the uniaxial stress-strain relation for basic creep:

$$\dot{\varepsilon}(t) = \frac{\dot{\sigma}(t)}{E} + \frac{1}{v(t)} \int_0^t \dot{J}_g(t - t')\, dt' \qquad (1)$$

in which ε, σ = strain and stress, t = time = current age of concrete, superimposed dots denote derivatives with respect to time, E = time-independent elastic modulus, $v(t)$ = volume fraction of the hydrated cement, and $J_g(t - t')$ = rate of the compliance function for the hydrated material, which was originally considered to be free of any aging effect, and thus to be a function of a single variable, the time lag $t - t'$. This function has led to the triple power law which was found capable to describe very well the basic creep curves for concrete but still to have some shortcomings due to its neglect of nonlinearities and deviations from the principle superposition in time.

In recent studies (Bažant and Prasannan, in preparation), it transpires that this original creep model based on solidification (Eq. 1) should be extended in two respects: (1) the creep rate should be made to depend nonlinearly on stress in the same form as generally used in viscoplasticity, and (2) the compliance function of the material should depend on the time lag $\theta - \theta'$ of some reduced time θ rather than of the actual time t. The latter modification is indicated by taking into account the recently established fact that, in addition to volume growth, the hydrated material undergoes progressive polymerization. The polymerization stiffens the microstructure and thus causes increasing resistance to creep. These two physical aspects lead to the following modification of Eq. 1:

$$\dot{\varepsilon}(t) = \frac{\dot{\sigma}(t)}{E} + \frac{F[\sigma(t)]}{v(t)} \int_0^t \Phi[\theta(t) - \theta(t')]dt' \qquad (2)$$

in which F and Φ = positive smooth continuous monotonic functions, Φ representing the rate of compliance with regard to the reduced time θ, which can be

defined as $\theta(t) = t^s$, typically $s \approx 2/3$. For the growth of volume fraction one may approximately use the function:

$$v(t) = (t^{-m} + \alpha)^{-1},$$

with m, α = positive constants. Aproximately, $\Phi = (\theta - \theta')^{n-1}$, with $n \sim 0.1$.

According to the numerical studies of Prasannan, Eq. 2 not only describes very well the available test data on concrete creep curves at various ages at loading, but also describes approximately correctly the nonlinear dependence of creep on stress, the deviations from the superposition principle observed in creep recovery tests as well as in step-wise increasing step histories. Furthermore, the recovery curves are not obtained as nonmonotonic, and the creep curves at various ages at loading do not exhibit divergence.

The principal advantage of Eq. 2, however, is that the rate-type approximation, which can be obtained by expanding function Φ into Dirichlet series, corresponds to a spring-dashpot model in which only the viscosities are age-dependent while the elastic moduli are independent of reduced time θ (although they depend on the actual age t). This brings about a considerable simplification of creep structural analysis. Furthermore, based on the expansion of function Φ in Dirichlet series, one can give explicit expressions for the elastic moduli of the spring-dashpot model. These moduli are always positive, which removes the problem that in the existig models with age-dependent elastic moduli the values of these moduli can be obtained as negative for some short periods of time, as already mentioned. Moreover, due to the constancy of the elastic moduli for the spring-dashpot model, there is no numerical advantage in preferring the Maxwell chain model to the Kelvin chain model, and one may use the latter spring-dashpot model which has a more direct correspondence to creep data.

3.2 Stress-Induced Shrinkage and Thermal Expansion

Another formulation for creep which is based on a physical concept for the creep process and appears to greatly improve the description of the existing data for creep at simultaneous drying, is the idea of stress-induced shrinkage and thermal expansion. It is hypothesized that the viscosities in a spring-dashpot model, e.g., the Kelvin chain, depend on the rate of flow of water between small and large pores in the hydrated cement paste [13]. This idea has led for the μ-th unit of the Kelvin chain model to the stress-strain relation:

$$\frac{\dot{\sigma}}{E_\mu} + \frac{1}{\eta_\mu}(1 + k|\dot{h}|)\sigma = \dot{\varepsilon}_\mu + \kappa_\mu \dot{h} \qquad (3)$$

in which ε_μ = partial strain of the Kelvin chain unit, η_μ = viscosity for this unit, κ_μ = coefficient for the portion of the shrinkage rate attributable to this unit, and r = positive constant. In this equation, the term $r|h|$ may be considered as a term introducing a dependence of the overall viscosity on the pore humidity rate. It can be also shown that this dependence is a special case of a thermodynamic model based on the hypothesis of the movement of hindered adsorbed water proposed by Bažant in 1972 [11]. Algebraic rearrangement of Eq. 3 leads to an equivalent differential equation:

$$\frac{\dot{\sigma}}{E_\mu} + \frac{1}{\eta_\mu}\sigma = \dot{\varepsilon}_\mu + \kappa_\mu \dot{h} - \bar{\kappa}_\mu \dot{h}, \qquad \bar{\kappa}_\mu = \frac{k\sigma}{\eta_\mu} \operatorname{sign} \dot{h} \qquad (4)$$

in which $\kappa_\mu \dot{h}$ may be regarded as the stress induced shrinkage, representing an

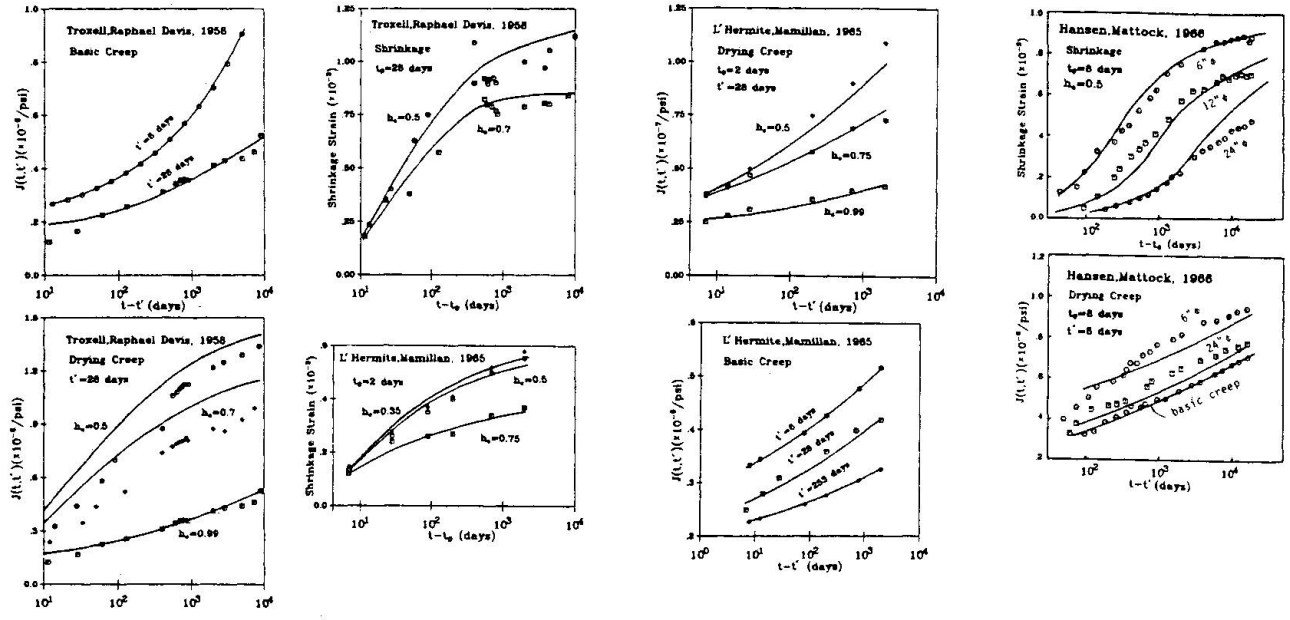

Fig. 3 - Stress-Induced Shrinkage Model with Cracking Compared with Previous Test Data (after Ref. 13).

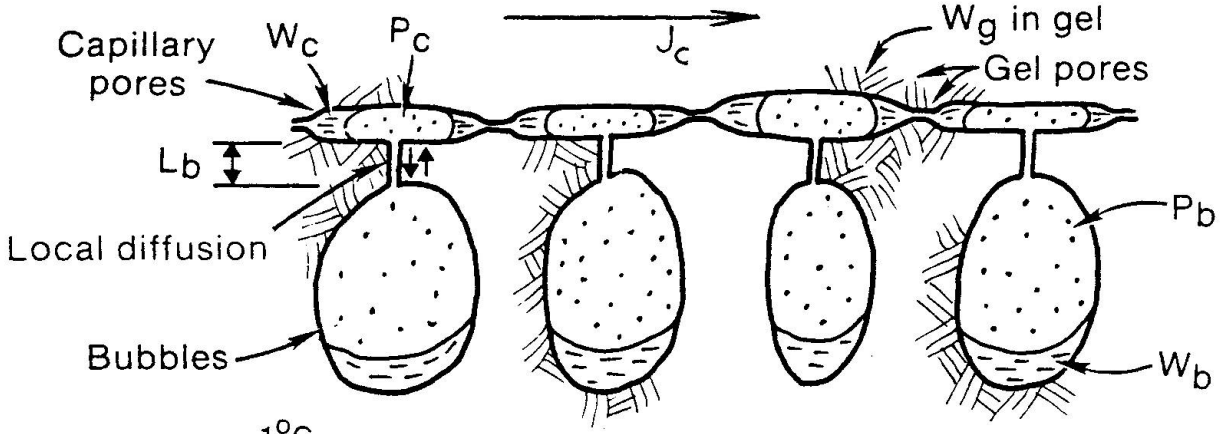

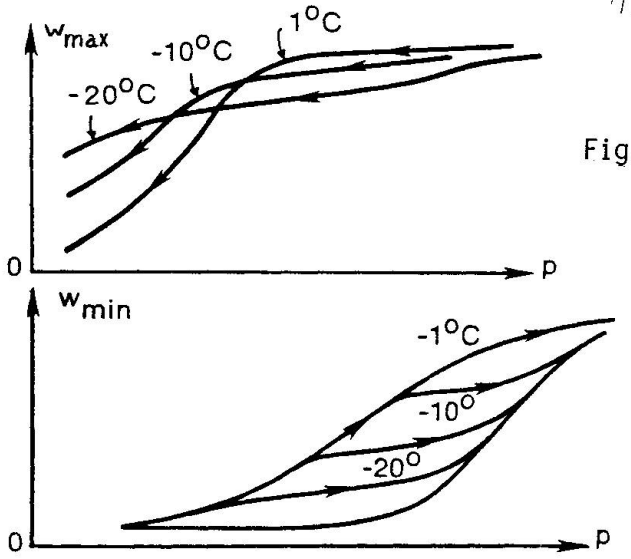

Fig. 4 - Example of calculated sorption-desorption isotherms for frozen concrete at various temperatures, used in a mathematical model for freeze-thaw damage, and a schematic picture of the macroscopic and local diffusion processes in the transfer of water in freezing concrete (after Ref. 37).

increased shrinkage when σ is compressive (negative) and $\dot{h}$ is negative (drying).

Based on thermodynamic arguments, a similar effect on viscosities is exerted by the rate of temperature T. As shown by Bažant, this leads to the phenomenon of stress-induced thermal expansion, a concept proposed by Thelandersson [14] by direct interpretation of test data and Bažant and Chern [13] as a special case of Bažant's 1972 aforementioned model [11].

In generalization to multiaxial stresses, the stress-induced shrinkage as well as the stress induced thermal expansion ceases to be isotropic, making possible for example stress-induced shrinkage shear or stress-induced thermal shear strain. It may be noted that variations of the pore humidity must also be reflected in a dependence of η_{μ} and of κ_{μ} on h. Furthermore, these quantities also depend on the equivalent age of concrete and on temperature. Finally, the solidification model in the form of Eq. 2 is more easily combined with the stress-induced shrinkage and thermal expansion than with previous models for the effect of humidity and temperature variations. For comparisons of the stress-induced shrinkage and thermal dilatation with numerous test results [13].

3.3 Fracture and Damage Phenomena Due to Nonuniform Shrinkage and Creep

As clearly demonstrated by Wittmann and Roelfstra [12] and also assumed in the modeling of Bažant and Wu [15] and others, the magnitude of creep at drying is strongly affected by cracking. The increase of creep in drying was explained by Wittmann and Roelfstra [12] as an apparent phenomenon, caused by the fact that the shrinkage observed on a shrinkage specimen is much less than the true shrinkage of the material, being strongly reduced by cracking, while the shrinkage which takes place in a compressed specimen is roughly equal to the true material shrinkage due to the fact that the compression stress prevents cracking. Subsequently, it has been concluded [13] that while this phenomenon is very important for explaining the drying creep effect (Pickett effect), it cannot explain it fully, and probably more than half of the drying creep effect must be attributed to a dependence of the creep viscosity on $\dot{h}$ as described above. In any case, though, cracking plays an essential role in any creep calculation at simultaneous drying as well as wetting, and by implication also at variable temperature.

Cracking is in creep calculations normally modeled as strain softening, i.e., as the decrease of stress at increasing strain (which is more correctly considered as a gradual decrease rather than an abrupt drop). The problem of strain softening has recently generated considerable discussions with regard to mesh sensitivity, convergence, and strain-localization instabilities. The problem is that the modeling must allow for the localization of cracking into distinct fractures, a problem which requires the use of fracture mechanics. The difficulties are due to the fact that neither the classical linear fracture mechanics, nor the stress-strain relation in the classical form, provides an adequate model for the distributed cracking phenomenon.

In recent studies of concrete fracture modeling [15] it has been found that the aforementioned problems can be circumvented if the concept of a nonlocal continuum is introduced into the model of cracking, or generally distributed damage. In a nonlocal continuum, in contrast to the classical, local continuum, one uses quantities which are obtained by averaging of some continuum variables over a characteristic volume, V_r, of the material centered around each given point of the structure. It has been also found that the classical nonlocal continuum, in which the strain is considered to be a nonlocal property, has certain theoretical defficiencies, and that the appropriate model for strain-softening should consist of a nonlocal continuum in which the strain is local. This implies that the elastic strain as well as

the stress have local definitions and the only state variables which are permitted to be nonlocal are those which govern distributed cracking (damage). The relation to fracture mechanics consists in the fact that the energy dissipated by cracking per unit volume of the cracked material gives the fracture energy when multiplied by the characteristic volume V_r. This approach, which was formulated by Bažant, Pijaudier-Cabot and Lin [17,18] was demonstrated to converge properly in various strain softening problems as the mesh is refined. It was proven to yield a finite energy dissipation due to cracking while the previous models for strain softening could yield in the limit of zero mesh size a vanishing energy dissipation, which was physically inadmissible.

Thus, computer analysis of creep and shrinkage with cracking may be carried out in the usual manner with the smeared cracking approach. However, the fracturing strain ε^{fr} which appears in the smeared cracking models (or the crack band model) must be processed through an averaging integral as follows:

$$\varepsilon^{fr} = \frac{1}{V_r} \int \alpha \, \varepsilon^{fr} \, dV \qquad (5)$$

in which ε^{fr} denotes the nonlocal fracturing strain which must be used in the constitutive equation instead of ε , V = volume, and α = a given function of space coordinates which represents a weighting function for the averaging. Based on the experience recently gained in studies of strain softening in general, it is likely that this approach should also provide a consistent model for strain-softening in the case of creep.

It may be noted that expansion of the integral in Eq. 5 into a Taylor series yields for the nonlocal fracturing strain an approximation which is roughly equivalent to considering the strength limit at the body surface to depend on the gradient of strain. This concept is in fact a classical idea which was proposed already by L'Hermite [16]. From his observations of shrinkage cracking in specimens of various sizes he concluded that realistic predictions can be obtained only if the strength limit is considered to be approximately inversely proportional to the gradient of shrinkage strain. Similar ideas also appeared in the modeling of ductility of reinforced concrete beams under seismic loading (e.g., Karsan and Jirsa, [20]. Recently, this approach has been developed much more rigorously for triaxial constitutive relations by Floegl and Mang [19] and Schreyer and Chen [21], although in no relation to concrete creep or shrinkage. It may be that these gradient formulations would provide another workable alternative to the nonlocal formulation indicated in Eq. 5.

3.4 Freeze-Thaw Durability

The serviceability of concrete structures exposed to freeze-thaw cycles is a theoretically rather complex problem where mathematical analysis can bring significant improvement in uderstanding. It might seem that the current state-of-the-art, which relies on the use of air entrainment to endow concrete with adequate freeze-thaw resistance, is satisfactory. However, the air entrainment reduces appreciably the strength of concrete, and in principle it would be preferable to achieve adequate freeze-thaw durability without having the large pores produced by air entrainment. Furthermore, as new types of cements and admixtures are being developed, it is important to understand how their different properties affect freeze-thaw durability.

As shown by Powers and others [38], the damage to concrete due to freezing is principally caused by the volume expansion of ice as it freezes. This volume expansion produces pressures in the pores, which can be relieved by water

diffusion to other pores that are not saturated, such as air bubbles created by air entrainment, or unsaturated larger capillary pores. This consideration indicates that a concrete whose degree of saturation is below a certain critical value should be resistant to freeze-thaw damage, as proposed by Fagerlund [39]. An important point is that water can freeze only in relatively large pores, while it never freezes in the cement gel pores of molecular dimensions which contain essentially absorbed water. Thus, control of porosity of concrete offers the possibility of providing adequate freeze-thaw resistence without creating air-entrained bubbles.

To gain better understanding, a mathematical model for freeze-thaw damage has been developed jointly at Northwestern University and W. R. Grace Co. [37]. This model is based on determination of the isotherms of specific water content versus pore pressure for various temperatures in the freezing range. These isotherms are theoretically predicted from the known isotherms at room temperature, taking into account the volume expansion of ice on freezing, as well as the depression of the freezing point as a function of the size of the pore, and the melting of ice as a result of pore pressure which exceeds the crystal pressure of ice for a given temperature. The formulation of the desorption-sorption isotherms for the freezing range is based on the pore size distribution function, and also takes into account the hysteresis due to possible partial saturation of pores with ice.

The equation of state of the pore water is then used in a diffusion model to calculate pore pressures. For this purpose, a double diffusion model is developed [37], which distinguishes between the macroscopic diffusion of water through concrete, and local diffusion between smaller and larger pores (the local diffusion provides an important mechanism for the relief of pressures due to freezing). A schematic idealization of the diffusion processes is depicted in Fig. 4.

A computer program which calculates the sorption isotherms in the freezing range and solves the diffusion problem with a time variation of the pore pressure distributions throughout a concrete specimen has been written by J. C. Chern and has been used in some limited analytical studies which indicate that the essential aspects of the problem as currently understood can be modeled mathematically. The use of this mathematical model reduces the problem of freeze-thaw durability to the problem of durability of concrete under stresses, normally of cyclic nature, which are produced by the pore pressures. A complete analysis should include the calculation of cracking and fracture produced by the pore pressures. The analysis requires coupling the aforementioned program with a computer program for cracking and fracture of a concrete structure.

While this mathematical model is still preliminary, it offers considerable promise for the understanding of the numerous factors which affect freee-thaw damage. Aside from the material properties, the freeze-thaw damage is also affected by various structural mechanics factors; e.g., a superimposed compressive stress can block the freeze-thaw damage, the size and shape of specimens must have considerable effect because it controls the rate of cooling of concrete in the interior as well as the rate of escape of water from the regions of high pore pressure, creep must have an effect since it reduces the self-stresses produced by freezing, etc. All these mechanics factors have so far been neglected in the estimates of freeze-thaw resistance of structures.

3.5 Corrosion of Reinforcement in Concrete

Although the physical processes involved in the corrosion of steel in concrete and their governing equations seem to be relatively well understood [40,41,46] at the present, the interaction of these processes is very complex and calls

for a comprehensive mathematical model which would make it possible to handle the numerous factors that affect the problem. Computer calculations based on such a mathematical model will probably be the best means for realistic predictions of corrosion resistance under a variety of circumstances and applications. An attempt for a comprehensive mathematical model of corrosion damage based on the known physical processes involved has already been made [43] and some elementary applications have been demonstrated, with the particular view of concrete structures exposed to sea water. This mathematical model describes interaction between the following physical processes:

1. Diffusions of oxygen, chloride ions and pore water through the concrete cover of reinforcement;

2. Chemical reaction producing ferrous hydroxide near the surface of the steel bar in concrete;

3. The depassivation of the steel bar caused by a critical concentration of chloride ions;

4. The cathodic and anodic electric potentials as functions of the concentrations of oxygen and of ferrous hydroxide, as described by Nernst's equation;

5. The polarization of electrodes due to changes in the concentration of oxygen and of ferrous hydroxide;

6. The flow of electric current through the electrolyte in pores of concrete;

7. The mass sinks or sources of oxygen, ferrous hydroxide and hydrated red rust at electrodes, based of Faraday law;

8. The rate of rust production, based on reaction kinetics.

Some of the processes involved are geometrically illustrated in Fig. 5. This figure also shows some typical idealized distributions of stresses which are caused by the volume expansion associated with conversion of iron into rust. The prediction of corrosion damage should ultimately be based on the calculation of the variations of stress distributions caused by rust formation, and the cracking or fracture which these stresses cause. To follow the corrosion process after the start of cracking, the model needs to further take into account the effect of cracks on the rate of transport of oxygen, chloride ions, water, and ferrous hydroxide.

Applicatility of the mathematical model for corroision has been demonstrated by various simplified examples [43], in which approximate estimates of the effective resistence of the corrosion cells have been made and the oxygen and chloride ion transports through concrete cover has been considered as quasi-stationary and one-dimensional, reducing the corrosion problem to an ordinary differential equation in time. For determination of the extent of cathodic and anodic areas and of the thickness of the rusting layer, a variational principle of maximum corrosion current (effectively equivalent to the principle of maximum entropy production) has been formulated. It was shown that the process can be controlled by various factors, e.g., by oxygen diffusion towards the cathode, by oxygen diffusion towards the anode, by limiting voltage, by chloride ion diffusion, by pH, by cover thickness, etc.

It was concluded that, without calculations, intuitive predictions of corrosion based on consideration of only one process involved in corrosion are in general inadequate. Further development of models of this kind, their experimental verification and calibration are an important problem for future research in computational methods for predicting long-time serviceability of concrete structures.

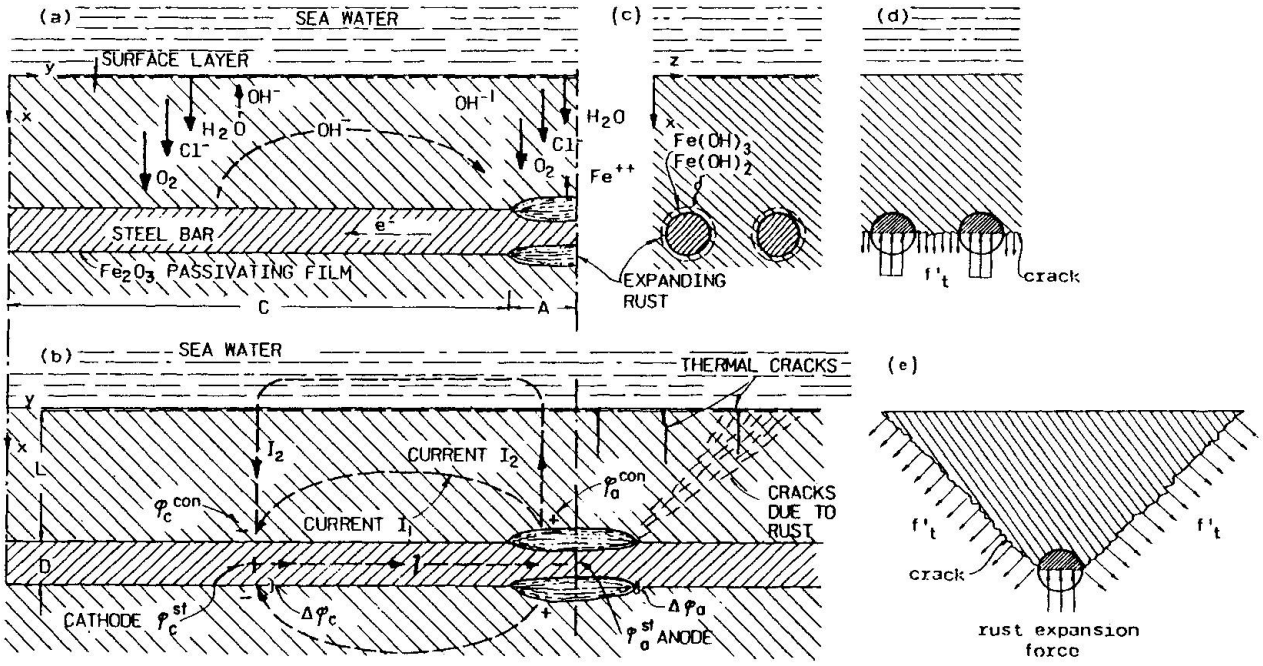

Fig. 5 - A simplified picture of the basic processes involved in steel corrosion and cracking of concrete cover (after Ref. 43).

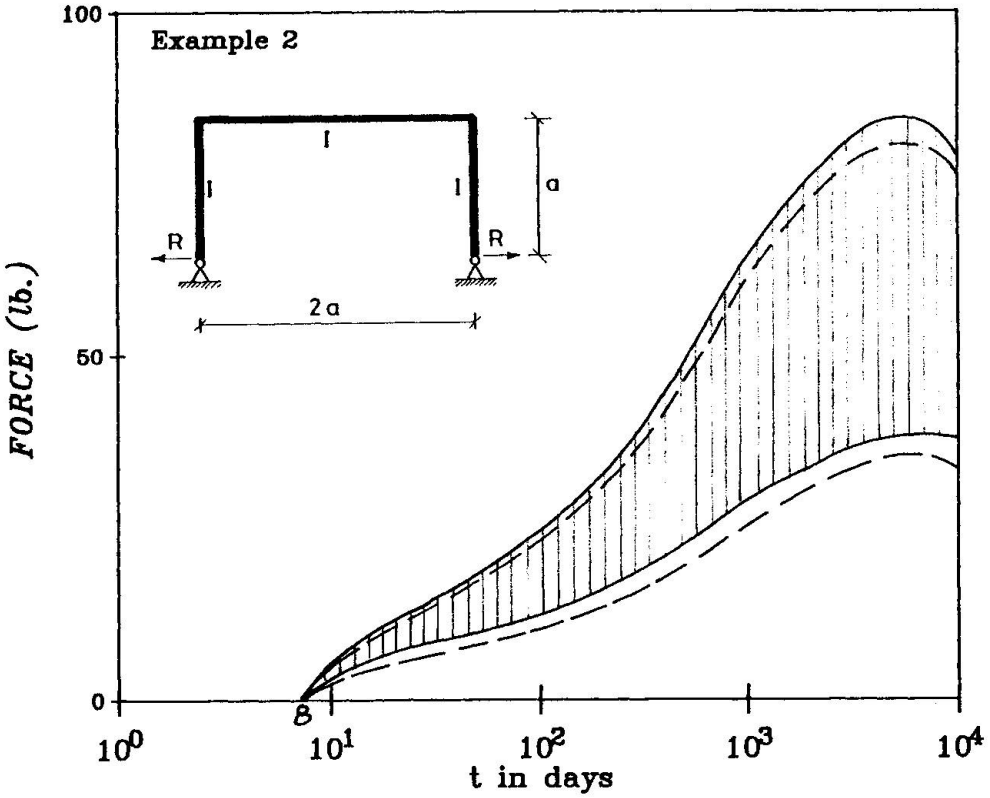

Fig. 6 - Example of a scatter band of mean ± standard deviation (68% probability limits) for shrinkage stresses in a concrete portal frame, obtained by latin hypercube sampling (after Ref. 33).

4. PROBABILISTIC ASPECTS OF SERVICEABILITY AND BAYESIAN UPDATING

Although prediction errors in the serviceability problems usually do not cause loss of human life (creep buckling excepted), they are important in economic terms, especially since the influencing factors and parameters are normally far more uncertain than the strength. This is certainly typical of creep and shrinkage prediction, for which it has been shown that the prediction errors (confidence limits) which are exceeded with a 10% probability are about ± 70% for the current code recommendations of ACI or CEB-FIP [1]. For these simple formulations, the major part of this error is due to the model error, i.e., the fact that the form of the creep and shrinkage law does not have a realistic form. However, even with the most sophisticated and comprehensive prediction model, the BP Model [8], these prediction errors are about ± 31% of the mean prediction. The major part of this error is due to the uncertainty of the effect of concrete composition and curing while the error of the creep and shrinkage law itself is small. In other serviceability problems such as freeze-thaw or corrosion cracking, the uncertainties are probably still larger. For example, regarding the permeabilities for chloride and ferrous oxides, or the shape of the sorption isotherms of frozen concretes and permeabilities for different pore fractions, we have at the present only order of magnitudes estimates. Nevertheless, even with this crude information, useful predictions which ensure adequate serviceability can be made if a probabilistic approach is used.

Even though the processes engendering serviceability loss are in principle always stochastic processes in time (as well as in space) [23,24], for many practical purposes the long-time structural response variables such as stress, strain or deflection can be considered to be functions of a certain set of random parameters $\theta_1,...\theta_n$. These parameters can in general be divided into intrinsic and extrinsic ones. The intrinsic ones are the material characteristics fixed at casting, such as the cement fraction, water cement ratio, aggregate cement ratio, or for corrosion problems the permeabilities for oxygen and chloride ions, etc. The extrinsic ones are the environmental variables such as the relative humidity, temperature, or concentration of chloride ions. Even if the method of structural analysis is linear, the dependence of structural response, such as deflection, on these random parameters is in general highly nonlinear. This makes exact explicit calculation of the standard deviation of the response difficult, and one should preferably use approximate numerical probabilistic methods.

As recently shown by Bažant and Liu [32.33] a very effective method is the latin hypercube sampling, which is considerably more efficient, for a large number of material prameters, than the method of point estimates previously used by Madsen and Bažant [27]. In this method, the assumed or known cumulative distribution of each random parameter is subdivided into layers of equal thickness, and the problem is solved many times deterministically for parameter values randomly chosen at the centers of the intervals corresponding to these layers. The selections of parameter values are done in random in such a way that the number of layers for each parameter and the number of runs of the deterministic program for the structural response be equal and that the value of each parameter from each layer is used in one and only one run of the program. The collection of the results from all the computer runs represents, for each response variable such as deflection, a set of responses with equal probabilities. So the statistics such as the mean response and its standard deviation can be calculated in the usual manner and, assuming normal distribution, its parameters can be easily determined. This then makes it possible to also estimate the confidence limits for the structural response.

As an example, Fig. 6 shows the results from Bažant and Liu for the maximum shrinkage stress in a portal frame, obtained according to the BP model using

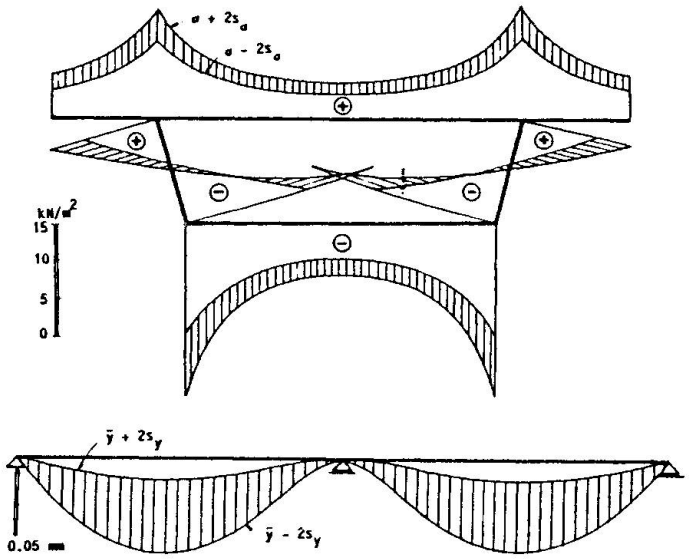

Fig. 7 - Example of the 95% confidence limits for longitudinal stresses at support cross section of a prestressed concrete box girder bridge (top) and deflections (bottom), obtained by latin hypercube sampling in Ref. 36.

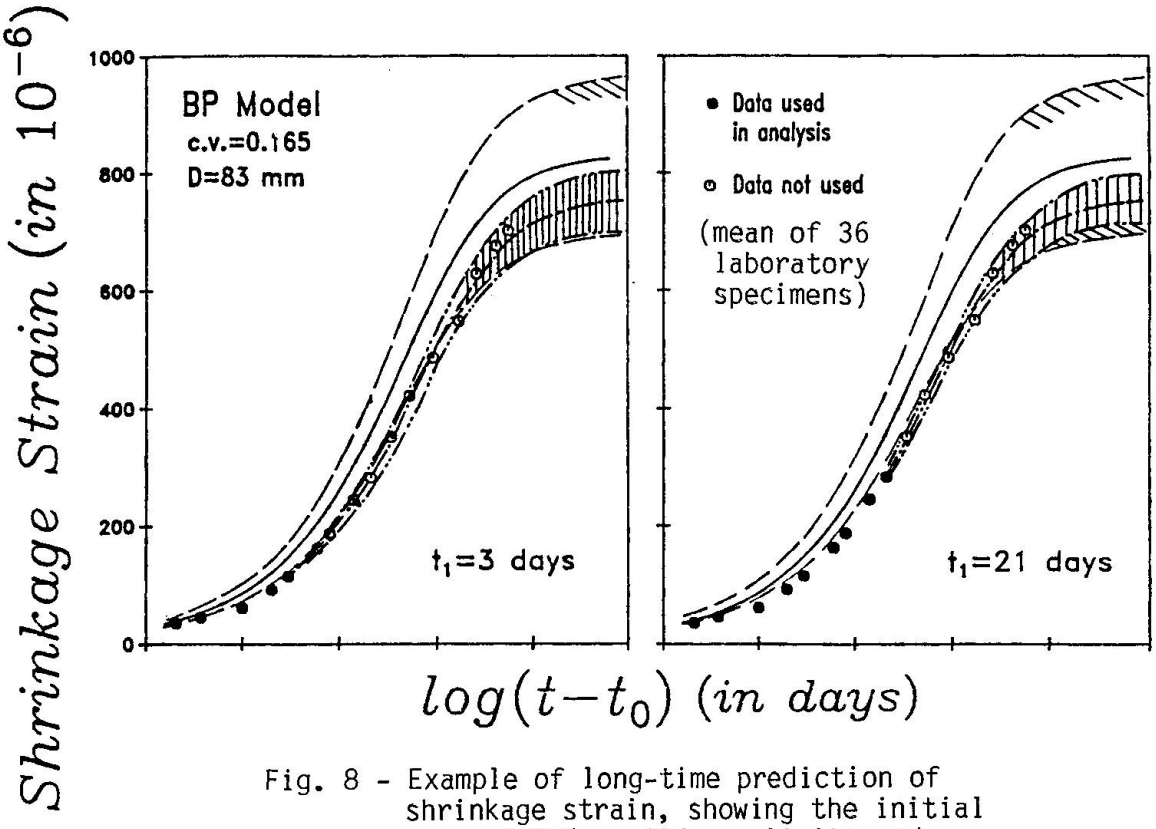

Fig. 8 - Example of long-time prediction of shrinkage strain, showing the initial band of 95% confidence limits and the posterior band after Bayesian updating, based on the solid data point only; after Ref. 35.

eight random parameters, each subdivided into thirty-two layers, while the number of computer program runs is also thirty-two. The solid lines in the figure represent the 90% confidence limits obtained by the latin hypecube sampling, while the dashed and dash-dot lines represent results of other approximate calculations. For the current code recommendatios of ACI or CEB-FIP, the scatter band would be appoximately twice as wide.

The method of latin hypercube sampling has been applied in calculations of creep effects of various structures such as prestressed concrte box girder bridges. Fig. 7, taken from the work of Křístek and Bažant [36], illustrates such an application for the calculation of the 95% confidence limits for the longitudinal stresses at the support cross section of a three span box girder bridge (top) and the corresponding deflections (bottom). These results, obtained from sixteen latin hypercube samples (i.e., sixteen layers, sixteen runs) and with eight random parameters, reveal that especially the deflections are rather sensitive to the uncertainties in the material properties and environmental influences. It should be noted that the width of the scatter band in Fig. 7 would approximately double if the current ACI or CEB-FIP models were used instead of the BP model.

The large uncertainties in long-time serviceability predictions apparent from the preceding examples can be drastically reduced by adopting a Bayesian approach [32,35]. In this approach, one needs additional information on the behavior of the material of the structure, such as some limited short-time measurements of creep and shrinkage of test cylinders or of the structure itself. As shown in Ref. 32 and practically illustrated in Ref. 35, the Bayesian approach can be combined very effectively with the method of latin hypercube sampling. For this purpose, one needs to calculate by latin hypercube sampling from the uncertainties of the model parameters the statistics of response for those short-time variables which are measured. The probabilities of the individual latin hypecube samples, which are normally equal, are then in this method adjusted according to Bayes probability theorem as follows:

$$P''(\underset{\sim}{X}_m^{(k)}) = P(\underset{\sim}{\theta}^{(k)} | \underset{\sim}{X}) = c_1 \, L(\underset{\sim}{X} | \underset{\sim}{\theta}^{(k)}) \, P'(\underset{\sim}{\theta}^{(k)}) \qquad (6)$$

in which P' = the prior probability of random parameter sample $\underset{\sim}{\theta}^{(k)}$, P'' is the posterior probability after Bayesian updating, $\underset{\sim}{X}_m^{(k)}$ is the column matrix of response values, c_1 is a normalizing factor ensuring that the sum of all posterior probabilities equals 1, and $L(\underset{\sim}{X} | \underset{\sim}{\theta}^{(k)})$ gives the likelihood function which implements the Bayesian updating; this function represents the prior probabilities of the measured values X given that the random parameter values are $\underset{\sim}{\theta}^{(k)}$. If all distributions are assumed to be normal and if all the short time measured values $\underset{\sim}{X}_m$ used for updating are assumed to be mutually independent, the likelihood function is easily calculated.

The results of Bayesian updating are illustrated in Fig. 8 (taken from [35]) for the problem of long-time shrinkage strains using the BP model. The wide scatter band gives the 95% confidence limits based on prior information, and the inner cross-hatched band gives the posterior, updated confidence limits based on the knowledge of the measurements up to either 3-days or 21-days (data shown by the solid points). The remaining measurements, shown by empty points, are not used for updating but are shown for comparison with the results, indicating that indeed the Bayesian updating contracts the predicted scatter band in a correct manner [35].

It must be emphasized that successful use of Bayesian updating requires the availability of a good and physically correct model. If the current ACI or

CEB-FIP prediction models are used in this type of Bayesian analysis [35], one finds that initial measurements do not lead to any improvement of predictions, principally because the basic trend of these models grossly deviates from the basic trend of measurements.

The Bayesian updating based on latin hypecube sampling is a general method [32] which can be applied to any structural problem of creep and shrinkage, as well as any long-time serviceability problem. The Bayesian approach offers the means of drastically reducing the uncertainties of long-time serviceability calculations and should be used in practice whenever possible, provided one deals with a creep-sensitive (or serviceability-sensitive) problem.

Treating the structural response as a mere function of random parameters is not quite realistic as far as the influence of environmental humidity and temperature is concerned. The environmental parameters represent stochastic processes in time, and the type of their fluctuation in time, as characterized by their autocorrelation function in time or its power spectrum, is important. Due to the nature of the diffusion equation, the humidty or temperature fluctuation components of low frequency (long period) penetrate their influence deep into the structure, while those of high frequency (short period) affect only a thin surface layer of the structure [28,30]. The attenuation of the amplitude of the fluctuations roughly follows the inverse square root of the depth below the surface, with the proportionality coefficient being larger for a longer fluctuation period.

The precise calculation of this behavior can be based on the spectral method for random processes, an approach similar to that used in stochastic dynamics. However, for concrete there is an additional important complication in that the material undergoes aging, which requires a nonstationary stochastic process analysis. Under certain assumptions about ergodicity, the power spectral method for random processes has been generalized to linear boundary value problems with aging properties in time [43]. The basic result of this generalization is that the spectral densities of input, S_f (e.g., environmental humidity process), and of response, S_g (e.g., the stress or deflection process), are related by an equation of the same form as for nonstationary processes, however with additional parameters, and the same is true for the associated standard deviations s_f and s_g:

$$S_g(\underset{\sim}{x}, t, t_0, \omega) = |\Phi(\underset{\sim}{x}, t, t_0, \omega|^2 \, S_f(\omega) \tag{7}$$

$$s_g = |\Phi(\underset{\sim}{x}, t, t_0, \omega| \, s_f \tag{8}$$

in which Φ = complex valued frequency response function of the structure obtained by linear analysis, ω = circular frequency of the component of the input process in time, t = age of concrete, t_0 = age at the time of exposure to random environment, and $\underset{\sim}{x}$ = coordinate vector. The response statistics based on Eqs. 7 and 8 have been calculated by finite element method (with complex valued nodal displacements) for some selected simple problems, such as the effect of humidity fluctuation on the wall of a reactor containment shell [28].

A simple form of the effect of the frequency of fluctuations of environmental humidity on creep as a function of the depth of the point below the surface or the thickness of the cross section has been given by Diamantidis, Madsen and Rackwitz [30] a formula which neglects the aging aspect of concrete but might be adequate for many practical purposes.

The current state-of-the-art [1] may perhaps be succinctly characterized by the following observations:

1. The prediction of the overall creep and shrinkage in a cross section from concrete composition and design parameters such as strength is at present highly uncertain, characterized by 95% confidence limits which are of the order ± 85% for the current code recommendations and about ± 37% for the most sophisticated model presently available (BP model).

2. The only presently available means of substantially reducing these uncertainties is to measure the short-time values of either structural response or test specimens, and then extrapolate in time. The simplest way to extrapolate is statistical regression. However, a better way is the Bayesian approach, in which the measured information is combined with the prior knowledge of all concretes. With the Bayesian approach, the 95% confidence limits for long-time predictions can be reduced to about ± 12%.

3. With the use of contemporary standard recommendations, the prediction errors are largely model errors rather than the actual randomness of creep and shrinkage.

4. The standard design recommendations of engineering societies should specify not only the recommended creep and shrinkage prediction model but also its coefficient of variation or confidence limits. Adoption of a more sophisticated model would then be rewarded with a smaller error, and the engineer would be able to choose a model of proper simplicity and sophistication, depending on the error which he deems to be acceptable for design. The acceptable value of the error will depend on whether the designed structure is creep sensitive or creep insensitive.

5. The errors of the current creep and shrinkage models in code recommendations are so large that finite element analysis, and even statically indeterminate frame analysis, of a creep sensitive structure hardly makes any sense unless statistics are calculated. The error due to the use of these models is in fact much larger than the error caused by replacing finite element analysis with simple back-of-the-envelope solutions for frames such as the portal method.

6. The probabilistic method of structural creep and shrinkage analysis is now available and ready for use in practice [1]. Its simplest version treats creep and shrinkage as a function of several random material parameters and calculates the statistics by a sampling method.

5. CONCLUSION

As is clear from the preceding exposition (despite the fact that it puts emphasis on the works carried out at the author's home institution), the progress in computational methods for long-time serviceability problems, particularly creep and shrinkage, has been significant during the recent years. Computational mechanics opens a new avenue which should be fully exploited in serviceability problems. All these problems are characterized by the presence of numerous influencing factors and simultaneous action of many physical processes which determine the long-time response. Although in a given problem only some of the influencing prameters and some of the processes dominate, computations are required to determine these parameters and processes and predict the long-time response.

Inevitally, all long-time serviceability problems have a strong random character, and structural calculations should be done in a probabilistic manner. Although the probabilistic treatment is rather complex where a detailed physical description is attempted, some simple methods are now available. The approach which is presently available for serviceability computations simplifies the response to be a function of a set of random model

parameters and the statistics are obtained by a sampling method, the latin hypercube sampling, which can be also combined with Bayesian updating and can be applied to finite element programs [44].

Structural calculations of damage which leads to serviceability loss must take into account various important physical phenomena such as the effects of simultaneous drying on creep, as manifested in the stress-induced shrinkage, and must involve calculations of cracking. Generally, diffusion calculations have to be coupled in these problems with stress and cracking analysis.

With the aforementioned ingredients, computational mechanics can greatly improve the serviceability design of concrete structures.

ACKNOWLEDGMENT

Financial support under U. S. National Foundation Grant No. MSM-8700830 to Northwestern University is gratefully acknowledged.

REFERENCES

1. State-of-the-Art-Report on Mathematical Modeling of Creep and Shrinkage of Concrete, by RILEM Committee TC69, chaired by Z. P. Bažant, in Preprints, 4th International Symposium on Creep and Shrinkage of Concrete: Mathematical Modeling, held at Northwestern University, Evanston, August 1986, pp. 39-456 (with 1036 literature references), (available from Northwestern University).

2. TROST, H., Auswirkungen des Superpositionsprinzips auf Kriech-und Relaxations-Probleme bei Beton und Spannbeton. Beton-und Stahlbetonbau, 62: No. 10, 230-8; No. 11, 261-9, 1967.

3. BAŽANT, Z. P., Prediction of Concrete Creep Effects Using Age-Adjusted Effective Modulus Method. Journal of the American Concrte Institute, 69, 212-217, 1972.

4. NEVILLE, A. M., and DILGER, W., Creep of Concrete, Plain, Reinforced, Prestressed. North-Holland, Amsterdam, 1970.

5. WITTMANN, F. H., Bestimmung physikalischer Eigenschaften des Zementsteins, Deutscher Ausschuss fur Stahlbeton, Heft 232, Wilhelm Ernst & Sohn, Berlin, 1-63, 1974.

6. ACI Committee 209 Report No. ACI 209 R-82, Prediction of Creep Shrinkage and Temperature Effects in Concrete Structures, prepared by D. J. Carreira, Z. P Bažant and D. E. Branson, ACI Spec. Publ. SP76, Am. Concrete Inst., Detroit, 193-300, 1982.

7. CEB-FIP Model Code for Concrete Structures, Commitée Eurointernational du Béton-Fédération Internationale de la Précontrainte, CEB Bulletin No. 124/125-E, Paris.

8. BAŽANT, Z. P., and PANULA, L., Practical Prediction of Time-Dependent Deformations of Concrete. Materials and Structures, Research and Testing (RILEM, Paris), 11, No. 65, 307-328; No. 66, 415-434; and 12, No. 69, 169-183, 1978-79.

9. ASCE Structural Division Task Committee on Finite Element Analysis of Reinforced Concrete, Finite Element Analysis of Reinforced Concrete (State-of-the-Art Report), Chapt. 6, ASCE, New York, 309-400, 1982.

10. BAŽANT, Z. P., Mathematical Models for Creep and Shrinkage of Concrete, Chapt. 7 in Creep and Shrinkage in Concrete Strucrtures, Z. P. Bažant and F. H. Wittmann, eds., John Wiley & Sons, London, 163-256, 1982.

11. BAŽANT, Z. P., Thermodynamics of Interacting Continua with Surfaces and Creep Analysis of Concrete Structures. Nucl. Eng. and Des., 20, 477-505; see also Cem. Concr. Res., 2, 1-16, 1972.

12. WITTMANN, F. H., and, ROELFSTRA, P., Total Deformation of Loaded Drying Concrete. Cem. Concr. Res., 10, 601-10, 1980.

13. BAŽANT, Z. P., and CHERN, J. C., Concrete Creep at Varible Humidity: Constitutive Law and Mechanism, Materials and Structures (RILEM, Paris), 18, 1-20, 1985; see also Stress-Induced Thermal Dilatation, J. of Engr. Mech. ASCE, in press.

14. THELANDERSSON, S., On the Multiaxial Behavior of Concrete Exposed to High Temperature. Nuclear Engr. and Design, 75, No. 2, 271-282, 1983.

15. BAŽANT, Z. P., Mechanics of Distributed Cracking. Applied Mechanics Reviews ASME, 39, No. 5, 1986.

16. L'HERMITE, R., and GRIEU, J. J., Etudes experimentales recentes sur le retrait des ciments et des betons. Annales I.T.B.T.P. (Paris), 5, No. 52-53, 494-514.

17. PIJAUDIER-CABOT, G., and BAŽANT, Z. P., Nonlocal Damage Theory. J. of Engng. Mech. ASCE, 113, 1987 - in press.

18. BAŽANT, Z. P., and PIJAUDIER-CABOT, G., Modeling of Distributed Damage by Nonlocal Continuum with Local Strain. Preprints, 4th Intern. Conf. on Numerical Methods in Fracture Mechanics, ed. by A. P. Luxmore, R. J. Owen (U. of Wales, Swansea, U.K.) and M.F. Kanninen (Southwest Research Institute), San Antonio,Texas, 411-432; see also Z. P. Bazant, F. B. Lin and G. Pijaudier-Cabot, Yield Limit Degradation: Nonlocal Continuum Model with Local Strain, in Computational Plasticity, Preprints of an Int. Conf. held in Barcelona, Spain in April 1987, ed. by D. R. Owen, Pineridge Press, Swansea, U.K., 1757-1779.

19. FLOEGL, H., and MANG. H. A., On Tension Stiffening in Cracked Reinforced Concrete Slabs and Shells Considering Geometric and Physical Nonlinearity. Ingenieur Archi 51, 215-242, 1981.

20. KARSAN, D., and JIRSA, J. O., Behavior of Concrete under Compression Loadings. J. of Structural Engineering Division ASCE, 95, (12), 2543-2563, 1969.

21. SCHREYER, H. L., and CHEN, Z., One Dimensional Softening with Localization. J. of Applied Mechanics ASME 53, 791-797, 1986.

22. BAŽANT, Z. P., Viscoelasticity of Porous Solidifying Material - Concrete. J. of Eng. Mech. Div., ASCE, 103, No. EM6, 1049-1067, 1977.

23. BENJAMIN, J. R., CORNELL, C. A., and GABRIELSEN, B. I., A Stochastic Model for the Creep Deflection of Reinforced Concrete Beams, Procedings, International Symposium on the Flexural Mechanics of Reinforced Concrete, American Concrete Institute, SP-12, Detroit, Mich., 557-580, 1965.

24. ÇINLAR, E., BAŽANT, Z. P., and OSMAN, E., Stochastic Process for Extrapolating Concrete Creep, Journal of the Engineering Mechanics Division, ASCE, 103, No. EM6, 1069-1088, 1977; (Discussion by I. J. Jordaan and Closure, 105, No. EM3, 485-489, 1979.

25. CORNELISSEN, H., Creep of Concrete - A Stochastic Quantity, Ph.D. Dissertation, Technical University, Eindhoven, The Netherlands, (in Dutch, with extended summary in English), 1979.

26. TURKSTRA, C. J., and REID, S. G., Structural Design for Serviceability, Proceedings of the Symposium on Probabilistic Methods in Structural

Engineering, St. Louis, Missouri, Ed. by M. Shinozuka and J. T. P. Yao, Published by American Society of Civil Engineers, New York, N.Y. 1981.

27. MADSEN, H. O., and BAŽANT, Z. P., Uncertainty Analysis of Creep and Shrinkage Effects in Concrete Structures, American Concrete Institute Journal, 80, 226-127, 1983.

28. BAŽANT, Z. P., and WANG, T. S., Spectral Finite Element Analysis of Random Shrinkage in Concrete, Journal of Structural Engineering, ASCE, 110, No. 9, 2196-2211, 1984.

29. TSUBAKI, T., Thermal Stresses in Concrete Subject to Periodic Temperature Change, Transactions of the Japan Concrete Institute, Japan Concrete Institute, 6, 347-354. 1984.

30. DIAMANTIDIS, D., MADSEN, H. O., and RACKWITZ, R., On the Variability of the Creep Coefficient of Structural Concrete. Materials and Structures, 17, No. 100, 321-328. 1984.

31. DITLEVSEN, O., Stochastic Visco-Elastic Strain Modeled as a Second Movement White Noise Process. International Journal of Solids and Structures, 18, No. 1, 23-35, 1982.

32. BAŽANT, Z. P., Probabilistic Analysis of Creep Effects in Concrete Structures, Proc. of the 4th Internatinal Conference on Structural Safety and Reliability (ICOSSAR '85), ed. by I. Konishi, A. H.-S. Ang, and M. Shinozuka, Kobe, Japan, 1, I-331-I-341, 1985.

33. BAŽANT, Z. P., and LIU, K.-L., Random Creep and Shrinkage in Structures: Sampling. Journal of Structural Engineering, ASCE, 111, 1113-1134, 1985.

34. WIUM, D. J. W., and BUYUKOZTURK, O., Variability in Long-Term Concrete Deformations. Journal of Engineering Mechanics, ASCE, 111, No. 8, 1792-1809, 1985.

35. BAŽANT, Z. P., KIM, J.-K., WITTMANN, F. H., and ALOU, F., Statistical Extrapolation of Shrinkage Data. ACI Materials Journal, 84, Part I, 20-34, Part II 83-91, 1987.

36. KŘÍSTEK, V., and BAŽANT, Z. P., Shear Lag Effect and Uncertainty in Concrete Box Girder Creep, J. of Structural Engng. ASCE, 113, (3) 557-574. 1987.

37. BAŽANT, Z. P., CHERN, J.-C., ROSENBERG, A. M. and GAIDIS, J. M. Mathematical Model for Freeze-Thaw Durability of Concrete. Report 86-11/694 in Center for Concrete and Geomatrials, Northwestern University, Evanston, Il., 1986.

38. POWERS, J. C., and HELMUTH, R. A., Theory of Volume Changes in Hardened Portland Cement Paste During Freezing. Proc. Highway Research Board 32, 285, 1953.

39. FAGERLUND, G., The Critical Degree of Saturation method of Assessing the Freeze/Thaw Resistance of Concrete. Materials and Structures (RILEM, Paris), 10, No. 58, 1977.

40. SPELLMAN, D. L., and STRATFULL, R. F., Concrete Variables and Corrosion Testing. Highway Research Record No. 423, 27-45, 1973.

41. TUUTI, K., Corrosion of Steel in Concrete. Report, CBI (Swedish Cement and Concrete Institute), Royal Institute of Technology,Stockholm, Sweden, 1977.

42. GJØRV, O.E., Concrete in the Oceans, Marine Science Communication, 1, No. 1, 51-74, 1975.

43. BAŽANT, Z. P., Physical Model for Steel Corrosion in Concrete Sea Structures. J. of the Structural Division ASCE, 105, No. ST9, Part 1 -1137-1153, Part II-1155-1166, 1979.

44. BAŽANT, Z. P., Response of Aging Linear Systems to Ergodic Random Input. Journal of Engineering Mechanics, 112, No. 3, 322-342., 1986.

45. ANDERSON, C. A., Numerical Creep Analysis of Structures, Creep and shrinkage in Concrete Structures, Chapt. 8, Ed. by Z. P. Bazant and F. H. Wittmann, John Wiley, New York, 259-303, 1982.

46. WHEAT, H. G., An Electrochemical Investigation of the Corrosion of Steel in Concrete. Ph.D. Dissertation, Univ. of Texas, Austin, 1985 (249pp.).

Modelling Thermal and Hygrometric Effects in Concrete

Modélisation des effets thermiques et hydriques dans les bétons

Modellierung der Wärme- und Feuchtwirkungen in Beton

Paul ACKER
Ingénieur ECP
LCPC
Paris, France

Jean-Michel PIAU
Ingénieur des PC
LCPC
Paris, France

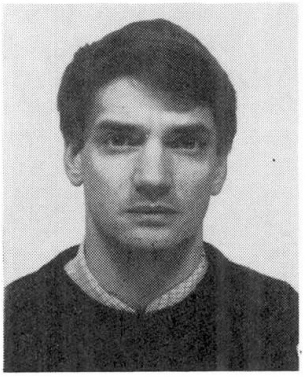

Isabelle RADOUANT
Ingénieur des TPE
LCPC
Paris, France

SUMMARY

The development of programs that are increasingly simple to handle and make possible numerical simulation of the phenomena of heat and moisture diffusion in concretes, together with an evaluation of the resulting mechanical effects, which are often large, provides a powerful tool for designers, in optimizing their choices, for those responsible for regulations, in improving standard practice, and for experts, in their diagnostic work. The experience acquired in these three areas is illustrated by examples of recent investigations and appraisals.

RÉSUMÉ

Le développement de logiciels, de plus en plus simples à manipuler, permettant la simulation numérique des phénomènes de diffusion de la chaleur et de l'humidité dans les bétons, ainsi que l'évaluation des effets mécaniques, souvent intenses, qui en résultent, constituent un outil puissant tant pour l'ingénieur concepteur dans l'optimisation de ses choix, que pour le responsable de la réglementation, dans l'amélioration des règles de l'art, et pour l'expert, dans sa démarche diagnostique. L'expérience acquise dans ces trois domaines est illustrée par divers exemples d'études et d'expertises récentes.

ZUSAMMENFASSUNG

Die Entwicklung von immer einfacher zu handhabenden Programmen zur numerischen Simuliering von Wärme- und Wasserverteilungsphänomenen in Beton und zur Ermittlung der daraus entstehenden, oft erheblichen mechanischen Auswirkungen liefert ein leistungsfähiges Hilfsmittel sowohl für den Planungsingenieur bei der Suche nach der optimalen Lösung, als auch für den Verfasser von Bestimmungen bei der Verbesserung von Bauregeln, sowie für den Experten bei der Erstellung seines Gutachtens. Die auf diesen drei Gebieten gesammelten Erfahrungen werden anhand verschiedener Beispiele von jüngeren Untersuchungen und Gutachten veranschaulicht.

1. THE IMPORTANCE OF THERMAL AND HYGROMETRIC EFFECTS IN CONCRETES

In analyzing the performance of concrete structures, three factors are generally considered separately :
- the material, defined by its mechanical properties (modulus, Poisson's ratio, creep law) ;
- the system of mechanical actions (dead load, distributed or concentrated live loads, imposed displacements, etc.) ;
- the ambient medium (climatic conditions, any corrosive agents).

In design rules, the ambient medium is taken into account either by parametering the laws of behaviour (hygrometry in the creep coefficient, for example) or by parametering the values of certain criteria (crack opening, for example).

While this approach is singularly effective in structural design (and can be used to develop satisfactory regulations), it has, nevertheless, two significant limitations. The first arises from the mechanical effects induced by temperature variations (whether during construction [1] or in service [2]) and/or by the natural drying of the concrete [3]. These effects are very large, and often lead to stresses substantially greater than those resulting from the the mechanical actions themselves. The second limitation arises because the mechanical properties of concrete evolve, and this evolution may be significantly altered by local temperature and humidity values [1][4]. The mechanical properties of the concrete are therefore not always uniform throughout the structure.

2. MODELLING OF THEIR MECHANICAL EFFECTS

As in the case of mechanical loads, temperature fields and humidity fields have both structural effects and local mechanical effects.

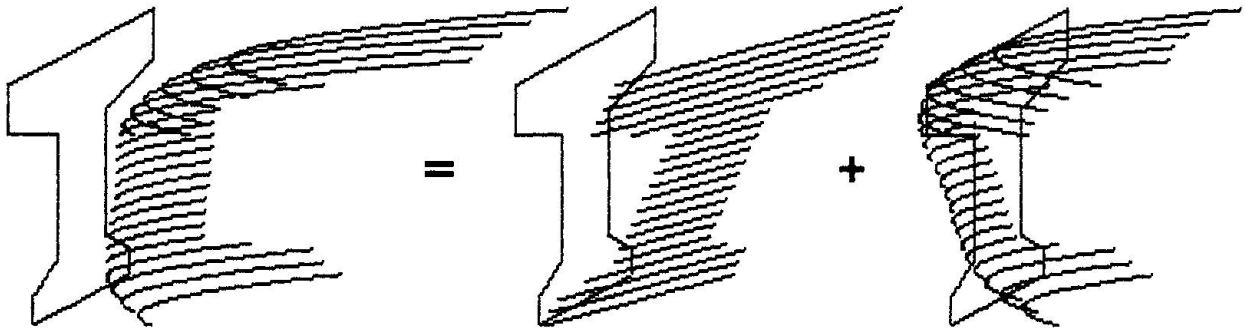

Fig.1 Breakdown of an imposed strain field (in beam theory)

Longitudinal total deformation imposed by a temperature or a moisture field T:	Equivalent plane field (= mean deformation + "effective gradient") defined by :	Self-balanced field in the section ("self-stresses") defined by :
$\varepsilon_z = \alpha.[T-T_0](x,y)$	$\varepsilon_\ell = A.x + B.y + C$	$\varepsilon_r = \varepsilon_z - \varepsilon_\ell$

Constants A, B, and C are obtained from :

$$\int_S \varepsilon_r.ds = 0 \quad ; \quad \int_S \varepsilon_r.x.ds = 0 \quad ; \quad \int_S \varepsilon_r.y.ds = 0$$

In this way, it can be shown [2] that, where beam theory applies, a given

imposed strain field can be regarded as the sum of two fields : a linear field and a self-balanced field. The former is, in each cross section S, a linear function of transverse coordinates x and y. It is obtained by equating its reduction elements (mean over the section and moments about the axes of inertia) with the true field. Its first component appears in form of a longitudinal deformation, generally free (expansion or contraction), the second component, called the "effective gradient", involves an imposed bending deformation, free only in an isostatic beam, where this first field produces no longitudinal stress. The difference between the first plane field and the true field, called the "self-stress" field, has only local effects (longitudinal stresses of which the integral over the section is null). Finally, the resultant longitudinal stresses are reduced by the free bending displacement. This does not hold of the transverse stresses, which result from the true field. This is one of the reasons why, depending on the static diagram of the structure, cracking of thermal origin may be strongly oriented in one direction or the other. This effect can also be quantified by a two-dimensional finite-element calculation (in addition to the plane strain and plane stress cases, the case of free bending must be allow for).
Obviously, this approach can be applied in a similar manner to the effects of drying, and casts new light on the delayed behaviour of concrete structures : shrinkage, as defined by regulations (i.e. as a uniform deformation) is only one of the three components that result from the dessiccation of concrete ; depending on the distribution of the water content in the cross section, there may also be (if the section is asymmetrical and/or dries asymmetrically) an imposed bending strain, free or restrained, and self-balanced stresses.

3. AID TO DIAGNOSTICS

For a certain number of problems (research on laws of behaviour, optimization of certain constructive arrangements, and especially the expert appraisal of pathological structures), it is essential to bear the following two remarks in mind :

1. — the mechanical properties of the material concrete are sometimes far from uniform, and a local value depends on the entire thermo-hygrometric history of the point in question and, to some extent (fatigue, creep recovery), on the entire history of mechanical stresses of the point.

2. — the stress condition at a point (and any cracking) may result not only from the usual mechanical actions (distributed and concentrated loads, imposed displacements) but also from stresses of thermal and/or hygrometric origin, in the form of imposed strain fields.

Such an approach is fully operational for surveys and analyses of the behaviour of structures in service. Its apparent complexity is no reason to take alarm, since, in such applications :

1. — the mechanical and physical properties of the concrete can be determined in situ by various experimental methods, mastered even more completely to the extent that the various causes of heterogeneity are known (elimination of the zones having a high hygrometric gradient, the depth of which can be estimated from the age of the structure, in the samples taken from the structure, for example).
2. — in view of the factors of safety applied to our engineering structures, the probability that damage results from the combined action of two independent causes is rather small : in most of the cases we have dealt with at the LCPC in recent years (about ten a year), the behaviour is or becomes pathological because a parameter, or an elementary mechanism, has not been taken into account

in the design, either through oversight, or because of a gap in the regulations, or because of incorrect prediction of or a change in the actual conditions of service of the structure.

This being the case, the analysis of thermal and hygrometric effects in concrete structures is in the context of the following approach :

1. — recording and examination of the apparent damage, in particular of its topological, geometrical (position, orientation, and spacing), and kinetic characteristics (age at onset, rate of evolution, any cycles), which is full of information ; as a general rule, this examination makes it possible to distinguish clearly between local effects and those related to the overall mechanical behaviour of the structure ; it also makes it possible to distinguish instantaneous and delayed causes, monotonic and cyclic causes ;

2. — analysis of the information to determine, exhaustively, the possible cause(s) ; this stage often yields feedback to point 1 ;

3. — quantitative analysis of each of the causes ; this analysis makes extensive use of numerical models, which make it possible, using the finite element method, to simulate both the processes of thermal or hygrometric diffusion and the resulting mechanical effects ; it then becomes acceptable, and sometimes even preferable, to ignore, idealize, or simplify all the other components, since the aim is to compare the order of magnitude of the calculated effect with that of the observed effects.

The aim of the examples given below is to show the effectiveness of this approach.

4. EXAMPLES OF EFFECTS OF THERMAL ORIGIN

The mechanical effects that result from the temperature fields that develop in a concrete part in the course of its manufacture, with or without accelerated curing, and numerical tools that may be used to deal with these problems have been described extensively elsewhere, with many examples of industrial applications [1][5].
These examples of applications clearly show that, except in the case of design problems, even a rough estimate of the physical and mechanical parameters of the material is more than adequate for dealing with such problems as :
- the choice of the best accelerated curing ;
- a search for and economic comparison of technical solutions to the problem of the cracking that appears during manufacture in parts that undergo accelerated curing or in massive parts ;
- optimization of the staging of concreting in large monolithic structures.
These technological problems of manufacture can generally be simulated by two-dimensional calculations (BITEX program). Thermal phenomena may also have consequences in the longer term, consequences that can be quantified using the same numerical tools, but which in some cases require three-dimensional calculation. This is why we have incorporated the computing module specific to the heat of hydration in the large modular code developed at the LCPC (CESAR system [8]), making it possible to go from the thermal calculations to calculations of their mechanical effects (directly, if the evolution of the mechanical properties of the material is neglected, as is acceptable for the technological objectives mentioned above).

5. EFFECTS OF HYGROMETRIC ORIGIN

The mechanical effects resulting from the natural drying of concrete may be

regarded as resulting from imposed strain fields, just as is routinely done, as we have seen, in thermo-elasticity. Such an approach has been fully described elsewhere and has proven its utility in interpreting the behaviour both of the material [3][6] and of structures [7].

5.1. Law of behaviour of material

By calculating the mechanical effects resulting from the true water-content fields in concrete parts, it has been shown that, in small parts, in spite of the surface cracking that always occurs, an apparent shrinkage is in fact found, as the result, after cracking, of residual stresses in the concrete. The scale effect, which is quite marked, can be explained very well thanks to numerical methods. Even drying creep, or at least most of it, is explained [3][6]. The numerical simulation of drying [9] and the calculation of the imposed strains pose no special problem ; the cracking behaviour of the concrete can be taken into account in a satisfactory manner by damage models [10] or, more recently, by a stochastic model [11]. Here, the contribution of numerical models will be to check out the laws of macroscopic behaviour (i.e. of the regulation type), which are difficult to validate experimentally (today, to predict the delayed behaviour of structures of which the running thickness is between 25 and 120-cm, creep laws obtained on specimens that are rarely more than 15-cm thick, in which the mechanisms are significantly different, are used !).

5.2. Behaviour of structures

With few exceptions, it is only in thin parts that dry symmetrically that the effects of drying can be reduced to only "shrinkage" as defined in regulations (i.e. in the form of a uniform deformation). When the thickness of concrete exceeds 80-cm (or 40-cm with a waterproofed side), there is practically no shrinkage, but only restrained deformations. In common structures, the effect of drying is reflected, depending on the thickness of the part, by a mean deformation (the "shrinkage" of the regulations), surface cracking, and, what is most often overlooked, an imposed moment. This imposed moment results from two effects :
- the first is due to the asymmetry of the part and of the boundary conditions (an effect of pavement surfacings on bridges has been observed) ; this is the "moment" component of the imposed field (cf. fig. 1) ;
- the second is due to the asymmetry of the cracking - on the compressed side, the concrete cracks less or not at all ; this effect has been observed in prestressed concrete parts [7], in zones where the stress of one of the two extreme fibres is close to zero ; it can be shown that this effect is large and is capable of explaining the variations in support reaction in redundant prestressed-concrete structures [7].
Here the solution is far less simple, since the nonlinearity introduced by the cracking makes it impossible to superimpose the various effects, or to quantify them separately : as soon as there is bending, cracking is asymmetrical and drying creep becomes meaningless. This is a structural effect, and it can be combined with the law of behaviour of the material only under certain highly restrictive conditions.

5.3 Example of survey

The most important consequence for the engineer is that, in thick parts (i.e., in the case of compact "bridge grade" concretes, over 50-cm thick), shrinkage, considered as overall deformation, is negligible, since drying affects only a very small depth of concrete. Under these conditions of hindered deformations, designing the reinforcements is no longer a question of size (a tendon that is not stretched does no work) but of positioning (the closer together the cracks, the smaller they will be) ; here, the constructive arrangements can be optimized

only by modelling the anchorage of a tendon in a concrete subjected to an imposed strain field.
We were recently led to deal with a problem of this type in order to understand (an essential preliminary to choosing the type of repair) the cracking of a series of motorway bridges. These reinforced-concrete bridges, with solid slabs (fig. 2) had parallel longitudinal cracks, quite open (1 to 2-mm), extending practically their full length. Because their positions were unrelated to those of the supports, we ruled out, from the start, any cause having to do with the mechanical functioning of the structure as a whole.

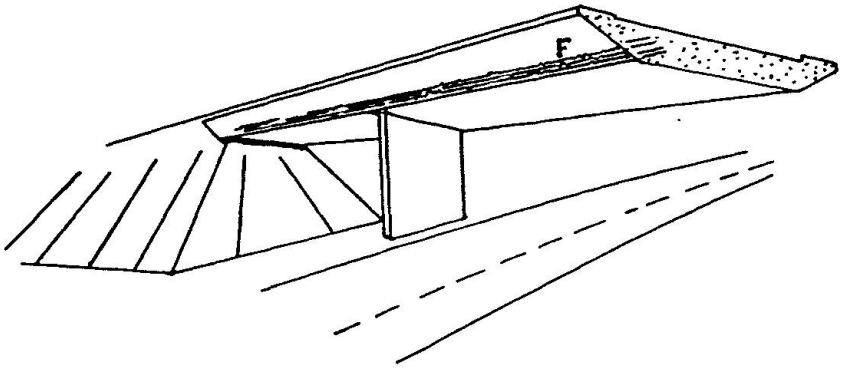

Fig.2 : Schematic drawing of half of one of the motorway bridges having, among other things, longitudinal cracks (F) parallel to 32-mm-dia. reinforcements not included in the working plans and not joined by a transverse tier. The thickness of concrete in the centre portion is 90-cm.

The cracks found were localized in the cantilever arms near each of the large reinforcements (dia. 32-mm) constituting the longitudinal reinforcement of this part of the deck. These reinforcements, not included in the working plans, were added at the last minute, but without the transverse reinforcements standard practice calls for. This body of information led us to hypothesize cracking caused by drying shrinkage. Numerical modelling of the finite-element type was used to quantify this hypothesis.

5.3.1. Hygrometric simulation

Cores taken from the structure were used to determine the distribution of water content versus depth. The water loss was about 5 % at the skin and less than 1 % at a depth of 8-cm. A numerical simulation of drying in the form of an exponential function of depth was judged to be an altogether satisfactory idealization of the phenomenon (fig.3).

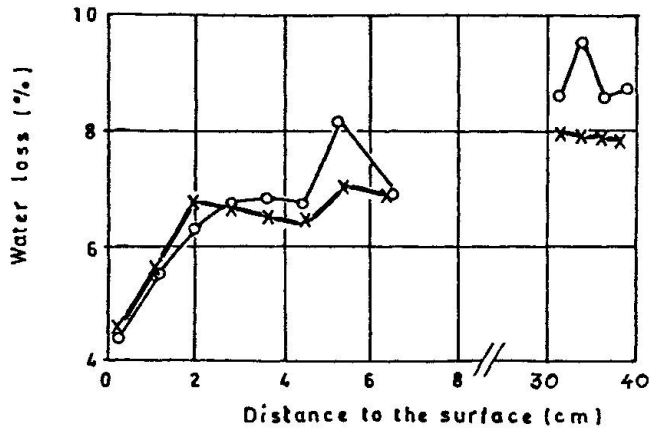

Fig.3 : Distribution of residual water content near the skin of the concrete, obtained by drying discs 6-mm thick taken from the structure, at 105°C. It can be seen that the depth of drying did not exceed 50-mm in spite of the age of the structure (11 years).

5.3.2. Description of computing model

Numerical modelling was carried out using the CESAR finite element computing

program [8]. We carried out a two-dimensional calculation in plane strain, for obvious reasons, and in linear elasticity, assuming, a priori, that the crack was open as far as the reinforcement. Given the symmetries of the structure and cracking pattern, the dimensions of the model used were considerably reduced (fig.4). In addition, we limited the depth of the model to 15-cm, since it seems reasonable to suppose that surface drying no longer affects the concrete at this depth.
Only the concrete portion was taken into account in the calculation. The concrete was here regarded as an isotropic material having a Young's modulus of 40,000 MPa and a Poisson's ratio of 0.17.
We used six-node triangles for the mesh, made denser in the zone around the reinforcement. The boundary conditions pose no special problem (cf.fig.4).
The only loading taken into account in this calculation was loading of the hygrometric type. We estimated the hygrometric contraction coefficient of this concrete at 10^{-3} per point of water loss as a percentage of total weight [12].

5.3.3. Calculation results

Figures 4 and 5 show, respectively, the deformation of the structure and the principal stresses.

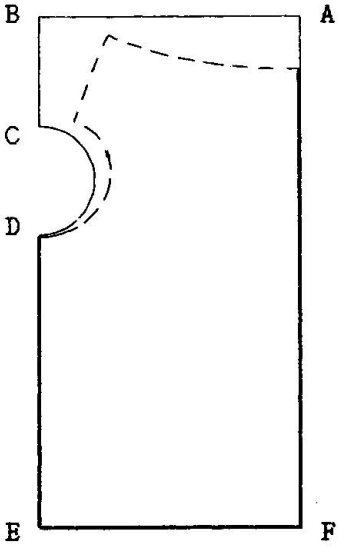

Fig.4 : Model used and its deformation, under an imposed strain field, determined from the measured water contents.
The boundary conditions are :
AB = 75-mm (half of distance between reinforcements : edge free
BC = 32-mm (coating) : edge free (crack)
CD = 32-mm (reinforcements) : circular edge free
DE = 86-mm : U = 0 (no crack)
EF = 75-mm : U = V = 0
FA = 150-mm : U = 0

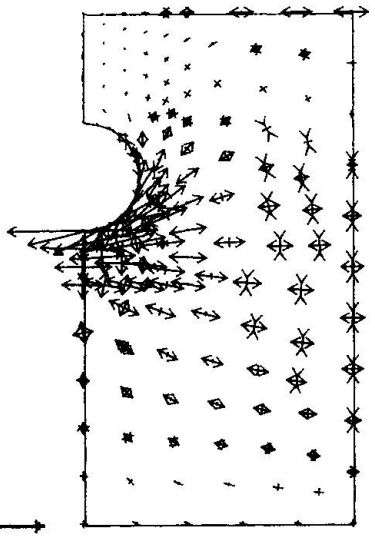

Fig.5 : Principal stresses →

Three remarks may be made in the light of the calculation results :

1. Because of the symmetries, the values of the horizontal displacements of the nodes on the edge of the crack are half the crack opening values. We accordingly obtained a crack opening of 0.75-mm at the surface and about 0.40-mm at the reinforcement.

2. The values of the principal tensile stresses at the nodes just below the reinforcement remain of the order of 100 MPa. We may conclude that the crack depth does extend beyond the reinforcement. Two other calculations were carried out, with the nodes free over an additional depth of 16 and 60-mm, respectively. The crack opening at the surface changed little, but substantial tensile stresses persisted in the vicinity of the interface with the reinforcement, suggesting the existence of radial cracks.

3. A first calculation carried out with friction-separation contact elements between the steel and the concrete showed that all of the nodes of these

elements separated when the same loading was applied. This justifies our decision not to model the steel or its action on the concrete in our linear calculation.

5.4 Discussion

From the water contents measured in situ, we were able to quantify the opening of the cracks at the 32-mm-dia. reinforcements at 0.75-mm. This agrees with the order of magnitude of the cracks found in the structures, and it may therefore be concluded that the cracks along these reinforcements are indeed caused essentially by drying shrinkage. If such cracks are not found elsewhere in the structure, it is doubtless because the longitudinal and transverse reinforcements are sufficient to ensure cracking that is more closely spaced and hence less marked.
After this validation, two other calculations was made, (i) with an other width of the mesh, in order to confirm that the cracks are more open at the extreme steels of this tier, and (ii) with an other hygral strain distribution, in order to explain why the cracks were not observed previously.
Finally, it was concluded that a passive (so cheeper) repairing will be sufficient to prevent an aggravation of the disorders.
It would be pointless to seek greater precision in the evaluation of the crack openings. However, the existence of very strong tensile stresses tangent to the steel-concrete interface shows that the use of radial contact elements in the vicinity of this interface would doubtless have allowed for a finer-scale analysis of the cracking mechanisms. However, this approach calls for a number of successive calculations simulating the course of the drying process.

REFERENCES

1. ACKER P., FOUCRIER C., MALIER Y., "Temperature-related mechanical effects in concrete elements and optimization of the manufacturing process". J.F. Young ed., ACI, 1986.
2. BEHR M., "Ponts en béton précontraint : effets des gradients thermiques". Compte rendu LCPC, 1981.
3. ACKER P., ABIAR G., MALIER Y., "Delayed behavior of concrete : model taking into account local humidity". Z.P. Bazant ed., RILEM, 1986.
4. TORRENTI J.M., "A constitutive model for concrete with the consideration of water content". In "Constitutive Laws for Engineering Materials", Desai C.S. ed., Elsevier, 1987.
5. ACKER P., "Effets thermiques dans les bétons en cours de fabrication et applications aux ouvrages d'art". Annales de l'ITBTP, Série Béton 235, n°442, février 1986.
6. WITTMANN F.H., ROELFSTRA P.E., "Total deformation of loaded drying concrete". Cement and Concrete Research, Vol.10, n°5, 1980.
7. ACKER P., DIRUY M., LAU M.Y., "Interprétation du comportement à long terme des ouvrages d'art en béton précontraint : rôle des migrations d'eau". Proc. RILEM Symposium, Budapest, 1984.
8. FEZANS G., HUMBERT P., PIAU J.M., RICHER S., "Notice d'utilisation du programme CESAR" et "CESAR Manuel théorique". LCPC ed., Paris, 1987.
9. MENSI R., ACKER P., ATTOLOU A., "Séchage du béton : analyse et modélisation". Materials and Structures, 1987.
10. MAZARS J., "A description of micro- and macro-scale damage of concrete structures". Eng. Fract. Mech., Vol.25, n° 5/6, 1986.
11. ROSSI P., RICHER S., "Stochastic modelling of concrete cracking". In "Constitutive Laws for Engineering Materials." Desai C.S. ed., Elsevier, 1987.
12. BUIL M. "Contribution à l'étude du retrait de la pâte de ciment durcissante". Rapport de Recherche n°92, LCPC ed., Paris, 1979.

Computer Codes for Material Science and Structural Engineering

Codes de calcul pour la science des matériaux et la construction

Programmeinheite für Werkstoffwissenschaften und Baustatik

Pieter E. ROELFSTRA
Civil Engineer
Swiss Fed. Inst. of Techn.
Lausanne, Switzerland

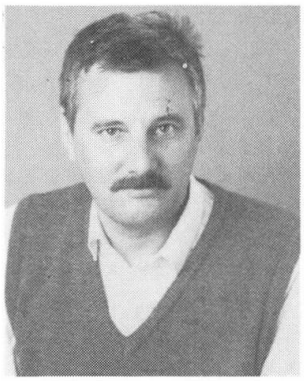

Pieter E. Roelfstra, born 1946, got his civil engineering degree at Delft University of Technology. For 12 years he was involved in structural engineering at the Ministry of Public Works. Actually, he is head of the Modelling and Numerical Analysis group of the Laboratory for Building Materials at the Swiss Federal Institute of Technology, Lausanne.

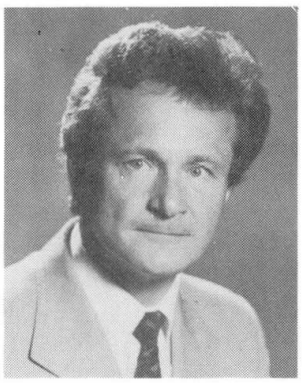

Folker H. Wittmann, born 1936, habilitated in Physics of Building Materials at Munich Institute of Technology. For 4 years he was professor for Building Materials at Delft University of Technology, The Netherlands. He is now professor and director of the Laboratory for Building Materials at the Swiss Federal Institute of Technology, Lausanne.

Folker H. WITTMANN
Professor
Swiss Fed. Inst. of Techn.
Lausanne, Switzerland

SUMMARY

A system of finite element modules has been developed to study and characterize the material behaviour of concrete and, at the same time, to provide realistic material laws for structural analysis. Some of the most important modules are briefly described. Several modules are combined for the prediction of the deflexions of a large span prestressed bridge during and after construction.

RÉSUMÉ

Un ensemble de logiciels, basés sur la méthode des éléments finis, a été développé pour étudier et caractériser le comportement du béton, et permettant en même temps de fournir des lois des matériaux réalistes utilisables dans les calculs de structure. Les programmes les plus importants sont brièvement décrits dans la présente contribution. Plusieurs modules ont été combinés pour prédire les flèches d'un pont-poutre précontraint de longue portée pendant et après la construction de celui-ci.

ZUSAMMENFASSUNG

Ein System von modularen Programmeinheiten wurde entwickelt, um einerseits das Verhalten des Betons zu studieren und zu charakterisieren und andererseits, um realistische Werkstoffgesetze für die Baustatik zu formulieren. Einige der wichtigsten Programmeinheiten werden kurz beschrieben. In einem Beispiel wird gezeigt, wie mehrere Programmeinheiten kombiniert werden können, um damit die Durchbiegungen einer vorgespannten Brücke im Bauzustand und nach Fertigstellung zu berechnen.

1. INTRODUCTION

Traditionally simplified material laws are used in structural engineering. Before the introduction of powerful computers there were no means to take the complex behaviour of a material such as concrete into consideration in an approximately realistic way. Nowadays the possibility exists to use more complicated material laws in computerized structural analysis. It has soon been realized that pure experimental studies cannot provide us with a better understanding of the materials behaviour. Numerical analysis and simulation of the different processes allows us to develop realistic material laws in a systematic way.

First it will be pointed out in this contribution in which way finite element analysis can be applied in materials science. Heat and moisture transfer are chosen as examples. Specific modules have been developed within a wider system called FEMMASSE to deal with these problems. For a more rigorous study of the behaviour of the composite material concrete the 3L-Approach has been developed [1-3]. As an example it will be explained how the obtained results can be used directly in a comprehensive numerical structural analysis of a prestressed concrete bridge.

Big computer are not available everywhere and their use is certainly not justified for structural analysis of simple structures under usual conditions. But even with a PC material laws more realistic than those given by normal codes can be used. One aim of building materials science today is to develop realistic but simple material laws to be used directly in structural analysis. In this way many of the contraversial points which can still be found in modern codes can be overcome. Numerical methods can be looked upon to be the major link between advanced materials research and structural analysis. At the end of this contribution this statement will be illustrated with an example.

2. DEVELOPMENT OF A SYSTEM OF SOFTWARE MODULES

2.1. The aim

When young concrete is exposed to an arbitrary climatic environment it has usually to be considered to be a drying and aging material. During hydration of cement heat of hydration is liberated in a concrete element. That means that during service life of most concrete structures pore humidity H, temperature T and degree of hydration α vary as function of time. In order to be able to determine point properties under these conditions the following three basic equations have to be solved :

$$C_H \dot{h} + p \dot{\alpha} = \text{div } \lambda_{HH} \text{ grad } H + \text{div } \lambda_{HT} \text{ grad } T \qquad (1)$$

$$C_T \dot{T} - q \dot{\alpha} = \text{div } \lambda_{TH} \text{ grad } H + \text{div } \lambda_{TT} \text{ grad } T \qquad (2)$$

$$\dot{\alpha} = f_1(\alpha)\, f_2(T)\, f_3(H) \qquad (3)$$

In these equations C_H and C_T stand for hygral and thermal capacity, p and q are material parameters which depend essentially on the type of cement, α is the degree of hydration, λ_{HH} and λ_{TT} are the hygral and thermal permeability coefficients whereas λ_{HT} and λ_{TH} are the cross coefficients; in equation (3) $f_1(\alpha)$ takes the influence of degree of hydration and the concrete composition into consideration, $f_2(T)$ stands for the well-known Arrhenius equation, and $f_3(H)$ finally describes the influence of pore humidity on rate of hydration. Further details of this set of differential equations can be found in Ref. [4].

Equations (1) to (3) are solved in order to obtain pore humidity, temperature and degree of hydration in any point of a given concrete element. These equations can be simplified if for instance the temperature distribution under sealed conditions or the moisture distribution under isothermal conditions is of interest.

The moisture and temperature distributions can be used directly. Furthermore these distributions can serve as a basis in rate-type constitutive equations. In this case the overall material behaviour is determined as the resultant of all point properties.

2.2. Brief description of some existing modules

A series of modules has been developed. Although they have primarily been produced for use in research projects and to solve practical problems some are at the same time used in teaching. An overview of the so far existing modules of FEMMASSE is given in Ref. [5]. Here only a brief description of the most important modules can be given :

- Heat/1
Time-dependent temperature distribution (2D) in a concrete element can be calculated. Heat of hydration as well as external heating can be taken into consideration. The influence of cooling pipes and formwork on the temperature gradient is predicted. For further details see Ref. [6].

- Moist/1
In using a humidity-dependent diffusion coefficient the time-dependent moisture distribution of a drying concrete element is calculated [7].

- Fracture/1
Based on the concept of the fictitious crack [8] crack propagation in notched bars, beams, CT-specimens, ring-beams and cubes can be simulated [9].

- Softfit/1
Tensile strain softening of a material is determined from the measured load-displacement diagram [10].

- CCB/1
It is possible to simulate different stages during the construction of a large span prestressed concrete bridge. Tendon paths of prestressing elements are calculated and stress losses due to friction and relaxation are determined. Inhomogeneous shrinkage and creep in the cross sections are taken into account. Time-dependent deformations and stresses during and after the construction are calculated. This module can also be used to determine the so-called excess heights of the shuttering necessary to compensate for subsequent time-dependent deflexions. This module is an extended version of an earlier published program [13].

- HMG/1
This module is developed for the analysis of non-stationary coupled flow of moisture and heat in 2D in a gravity field [12].

These modules can be used separately or they can be combined in a more comprehensive analysis. In the next paragraph two examples for the use of individual modules are given, and in paragraph 5 combination of modules is demonstrated in form of a practical application.

3. TWO EXAMPLES FOR THE APPLICATION OF FEMMASSE MODULES

3.1. Heat/1

This module together with the theoretical background is described in detail in Ref. [6]. Let us consider a cross section of a girder. The web of the girder is supposed to be casted two weeks before the deck. The deck plate is furthermore supposed to have a thickness of 150 mm and a 400 kg/m^3 of a rapid hardening cement is used.

For the sake of simplicity the temperature distribution 12 hours after placing the fresh concrete is shown exclusively in Fig. 1. Isotherms are shown by solid lines. The thermal conductivity of the hardened web is much higher than the one of the formwork of the deck plate therefore the maximum temperature of 45,4^{0}C is not obtained above the web.

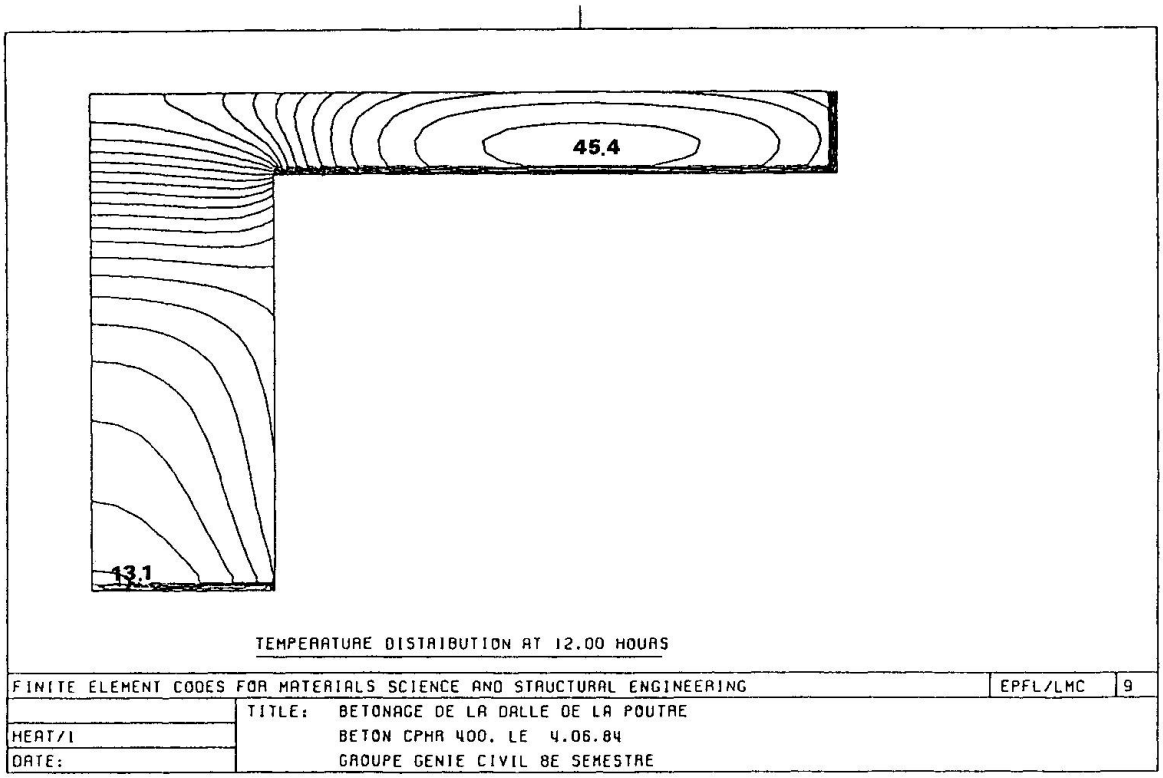

Fig. 1 Calculated temperature distribution 12 hours after concreting.

If we admit daily temperature changes due to solar radiation for instance we can introduce at the border a temperature-time relation for the top T_t and for the bottom T_b as follows (if t is counted in hours) :

$$T_t = 25 + 10 \sin (0.26\ t + 5.0) \quad (4)$$

$$T_b = 18 - 5 \sin (0.26\ t + 5.0) \quad (5)$$

The resulting temperature functions in points along an arbitrarely chosen cross section are shown in Fig. 2. It can be seen that the heating of the young concrete due to the heat of hydration fades away very quickly. Thus can be explained by the dimensions of the plate and the fact that a rapid hardening cement has been used.

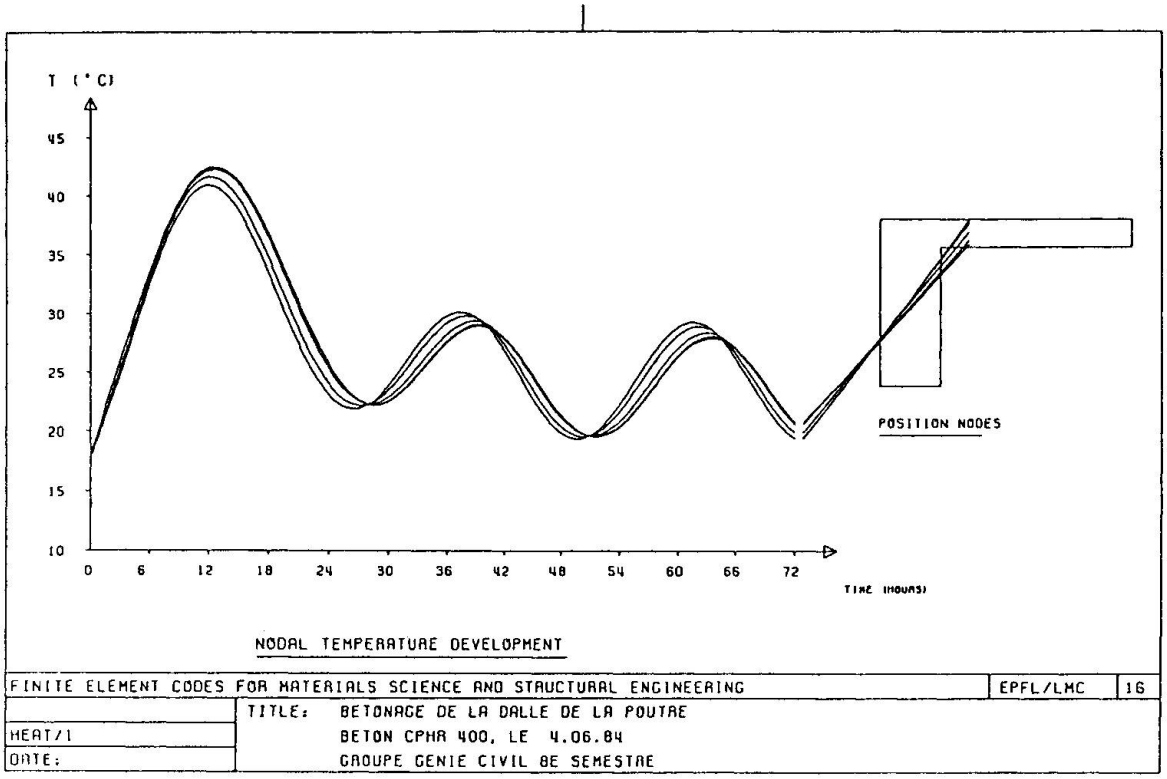

Fig. 2 Calculated development of nodal temperatures.

3.2. Moist/1

The drying of a cross section of a box girder bridge is chosen as an example to demonstrate the applicability of module Moist/1. A typical cross section is shown in Fig. 3. In this case it is assumed that the surface is covered with a moisture barrier. The relative humidity of the surrounding air varies in yearly cycles (if t is given in days) :

$$H = 70 + 10 \sin (0.02\ t) \qquad (6)$$

In the box the relative humidity remains higher for a long time and it does not vary as much as outside. For this reason a constant value of RH = 80 % has been chosen.

The moisture distribution calculated under these conditions is shown in Fig. 3 by means of isohygres (lines of equal pore humidity) for a drying time of 1000 days. It is obvious from this result that even after three years the construction is still far from hygral equilibrium.

The nodal moisture development along an arbitrarely chosen line in the cross section is shown in Fig. 4. The layer close to the outer surface follows after a drying time of little more than a year the reasonal humidity changes. At deeper layers the amplitude of the humidity-time function is changes and a phase shift is observed. The inner surface layer reaches hygral equilibrium after about two years, while the center part is still wet after three years.

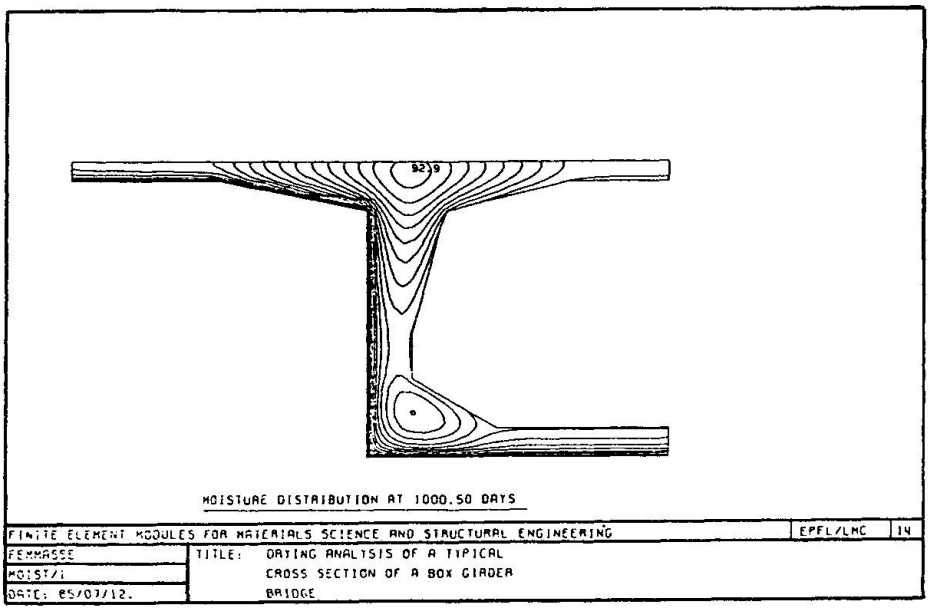

Fig. 3 Calculated moisture distribution 1000 days after demoulding.

4. APPLICATION OF MODULE CCB/1

4.1. Description of the problem

At this moment a bridge over the Rhone near Riddes (Valais, Switzerland) is in construction. The general situation, cross sections, longitudinal sections and side views of this bridge are shown in Fig. 5. The main span of 143 meters and the side spans each of 55 meters are erected by means of the cantilever method. A problem to solve was the prediction of the excess heights of the shuttering in every construction stage, needed to compensate the time-dependent deflexions. Therefore a very accurate prediction of the time-dependent behaviour is needed.

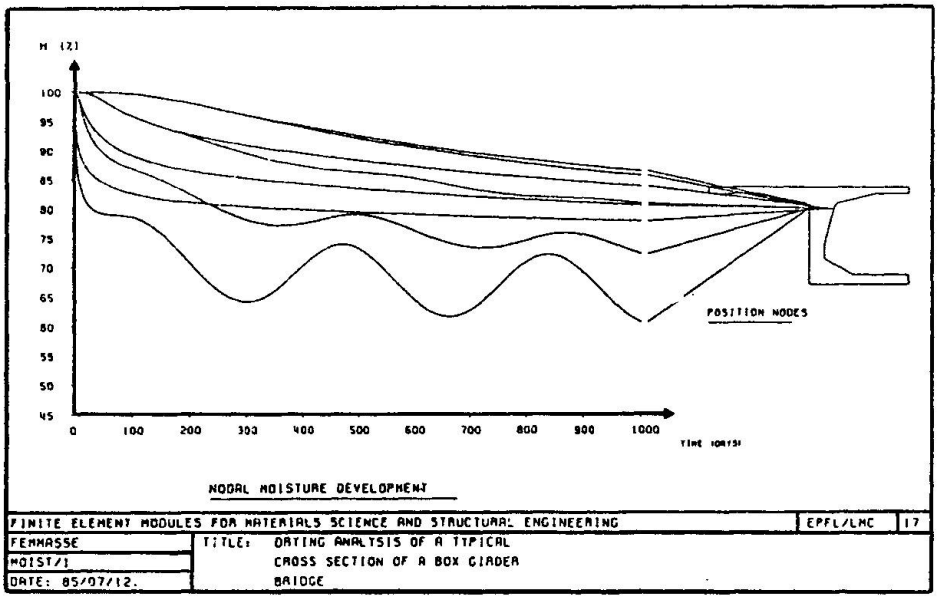

Fig. 4 Calculated development of nodal moisture.

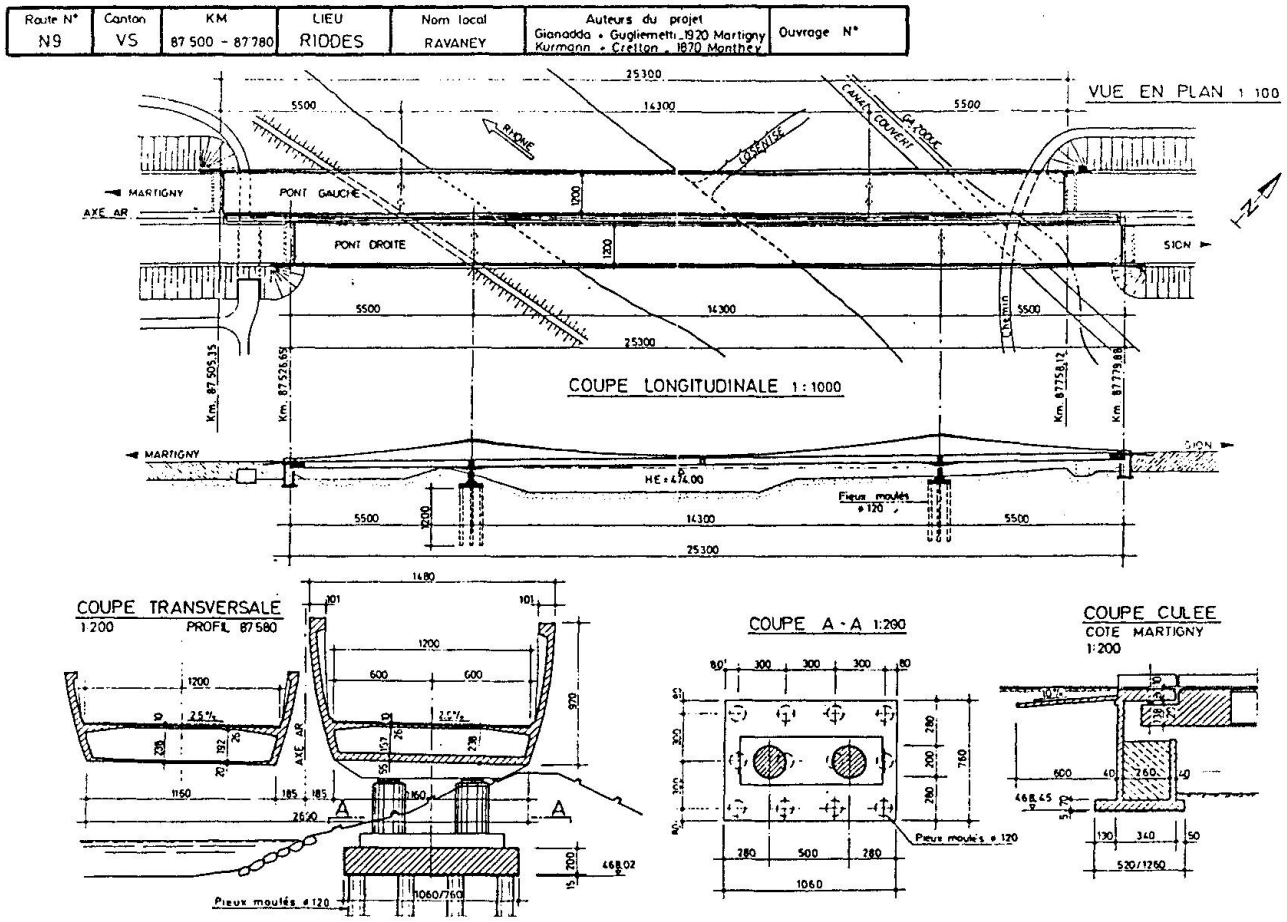

Fig. 5 General situation, cross sections and a longitudinal section of the bridge in construction near Riddes.

Update creep and shrinkage laws of CEB-FIP model code 1978 were implemented in an earlier version of module CCB/1 and the time-dependent behaviour of about 9 large span bridges have been predicted successfully [13]. This purely empirical approach may be sufficient for usual applications but from a materials science point of view it is unsatisfactory and more important it cannot be applied in a generalized way. Therefore, in the context of a research project, a more realistic analysis based on a point property approach was carried out at EPFL.

4.2. Analysis

The first step in the analysis was the determination of the moisture and temperature distributions as function of time in some characteristic cross sections of the bridge. The drying process was simulated with module Moist/1 and the calculated moisture distributions were stored on disc files. It was assumed that there were no temperature gradients in the structure and that the temperature of the bridge followed the temperature of the surrounding air. The creep deformations have been calculated with an aging Maxwell chain model as proposed by Bazant [14]. The calculated moisture distributions were used to determine the shrinkage and the so called effective time "t_e" in a number of points of the

cross sections. Creep and shrinkage experiments have been carried out on cylinders prepared with the concrete on the site to determine the materials parameters used in this analysis.

4.3. Results

All most all relevant results of module CCB/1 are given in a graphical form. In Fig. 6 details of one of the composite elements is shown. All practical and useful information is indicated in this computer plot and helps to check if the input data was correct. A calculated tendon path of the prestressing elements and the determined prestressing forces are shown in Fig. 7. In addition the elongation at both ends of the tendon as well as the slip length are indicated in this figure. A large computer plot is made of the side view together with all calculated deflexions of the bridge during and after completion of the construction. A detail of this computer plot is shown in Fig. 8. From the data of the desired alignement at a given time and the calculated deflexions of the bridge the excess heights of the shuttering in every construction stage is determined. Some results of this analysis are shown in Fig. 9. In Fig. 10 the evolution of the stresses in the uppermost and lowermost fibre of an element during and after completion of the construction is plotted.

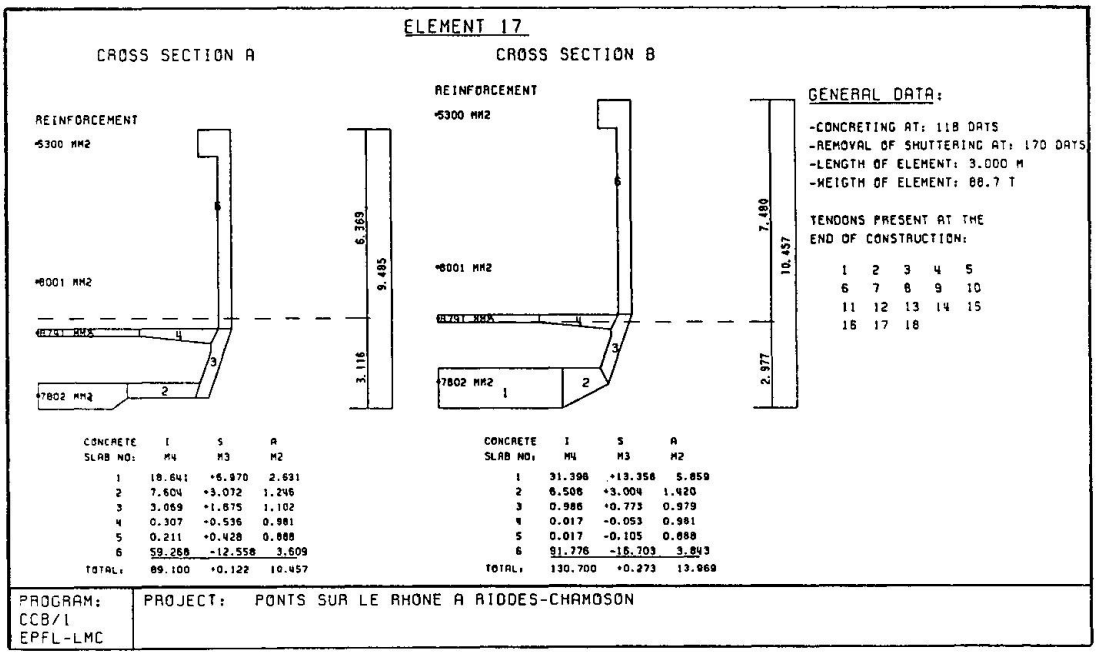

Fig. 6 General information of a composite element in order to check on input data errors.

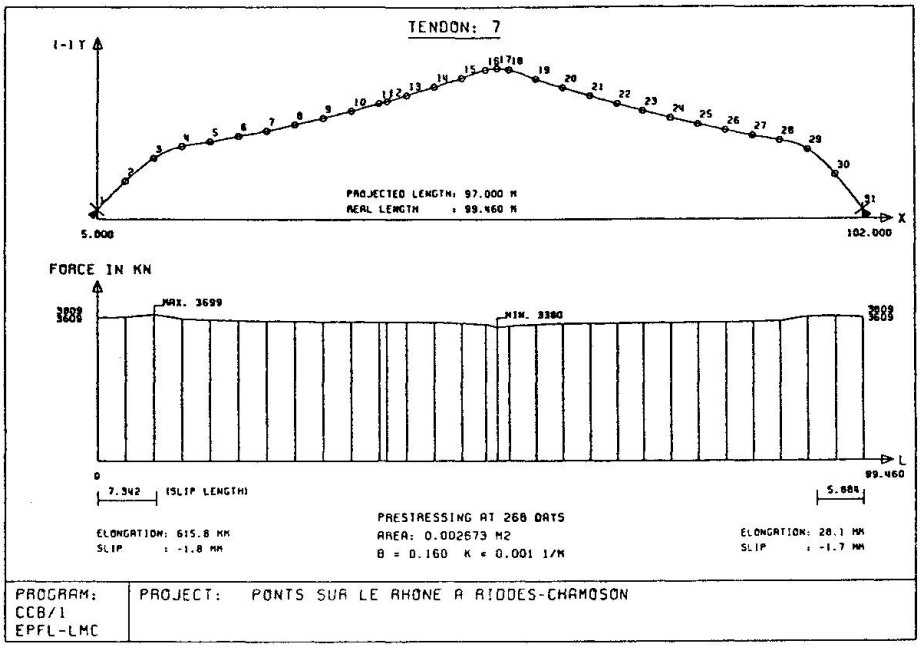

Fig. 7 Tendon layout, calculated prestressing forces, and elongations of the tendon.

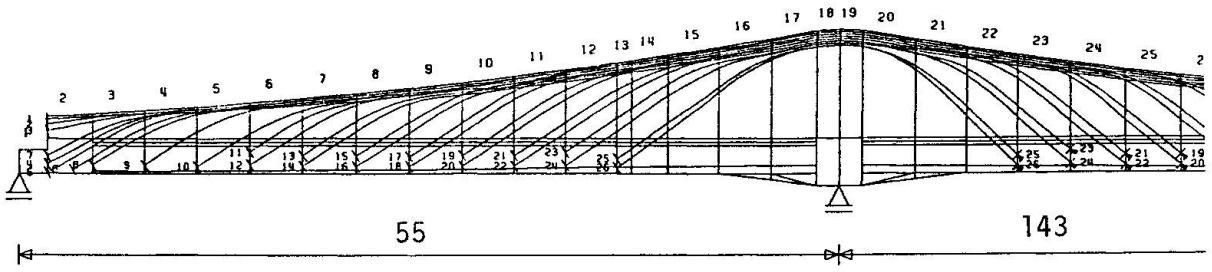

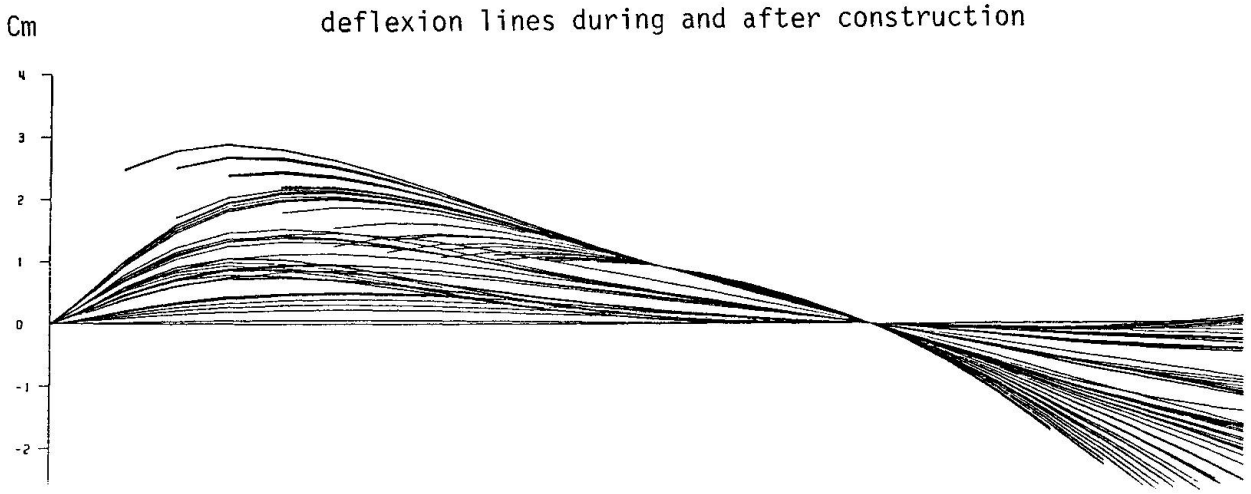

Fig. 8 Detail of a larger computer plot concerning the geometry, tendon layout and calculated deflexion lines.

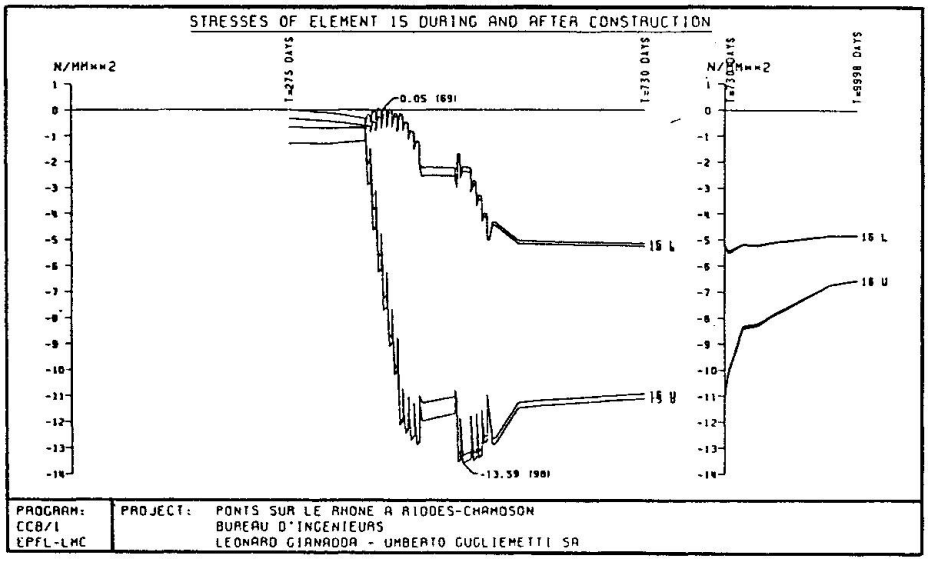

Fig. 9 Calculated evolution of the stresses in the upper and lowermost fibre of a composite element.

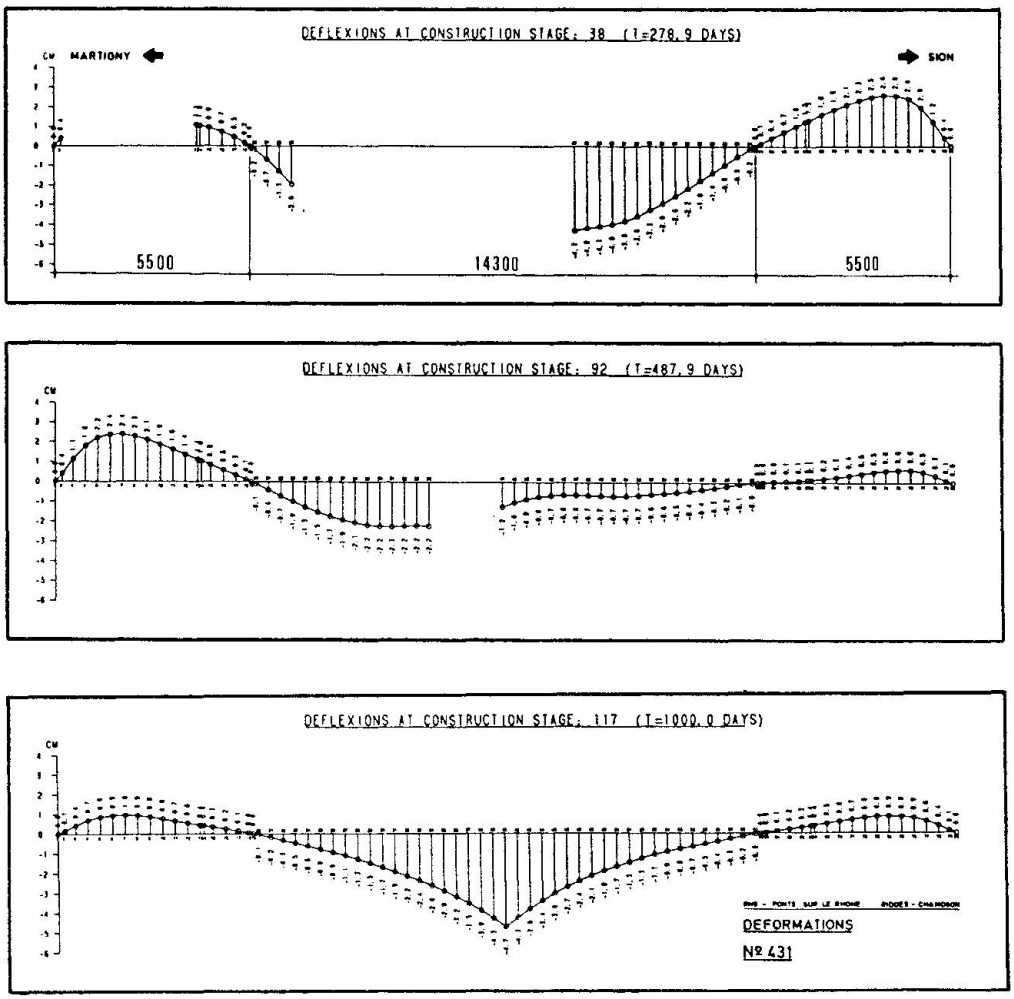

Fig. 10 Calculated deflexion lines of the bridge at different construction stages, from which excess heights of the shuttering can be determined.

At this moment the construction of the main span is half way but it is still too early to draw final conclusions on the comparison between the predicted and measured deformations. So far, however, the observed differences were very small. Conclusions of the final comparison will be published elsewhere.

5. REALISTIC SIMULATION OF DRYING SHRINKAGE WITH A PC

From what is presented in the preceeding paragraphs one might get the impression that realistic materials laws can be introduced in structural analysis with the help of very powerful computers only. We will demonstrate here, however, that this also can be realized approximately but with sufficient accuracy for many practical situations with a small PC.

The example we choose is the analysis of the drying process of a cross section of the before mentioned bridge at Riddes, in order to determine an effective axial and rotation shrinkage strain. The cross section and its devision in subsections is shown in Fig. 11. It was assumed that the drying process could be described by a uniaxial nonlinear diffusion equation. A relatively small computer code has been developed on a PC which can solve this uniaxial (and also axi-symmetric) nonlinear diffusion equation with variable boundary conditions. The parameters of the nonlinear diffusion equation were determined from shrinkage measurements performed on cylinders with a diameter of 160 mm stored at a constant temperature of 18^0C and a constant RH of 65 %. The dependence of the diffusion coefficient on the relative humidity was described by a mathematical expression proposed by Bazant and Najjar [15]. This function originally has been determined by data fitting. More recently a physical explanation has been given and thus a basis for more general applications [16]. The influence of temperature on the diffusion coefficient was, for the expected conditions (relatively small variations), supposed to be linear.

The nonlinear diffusion equation and the boundary conditions used for subsection 5 are shown in Fig. 12. The temperature and relative humidity of the surrounding air as function of time are based on meteorological observations in situ. In Fig. 13 measured shrinkage values of concrete cylinders are compared with the calculated shrinkage curve. This function is considered to be the standard shrinkage of the type of concrete used. The calculated shrinkage based on this predetermined material law is shown in Fig. 13 as function of time of all subsections. As can be seen in Fig. 13 the shrinkage curve of subsection 4 intersects the shrinkage curves of subsection 2 and 5. This is caused by the effect of paving with asphalt on the top of subsection 4, which is taken into account in the analysis.

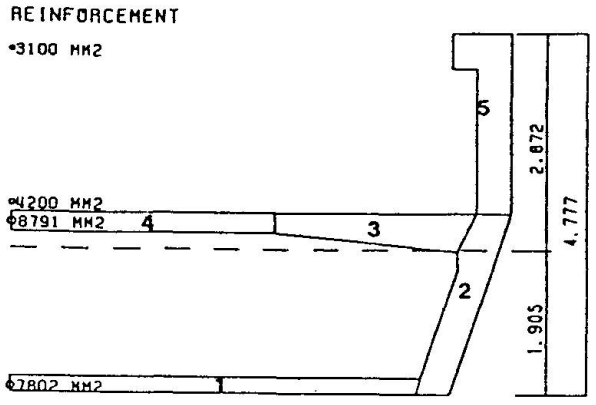

Fig. 11 Division of a cross section in elements.

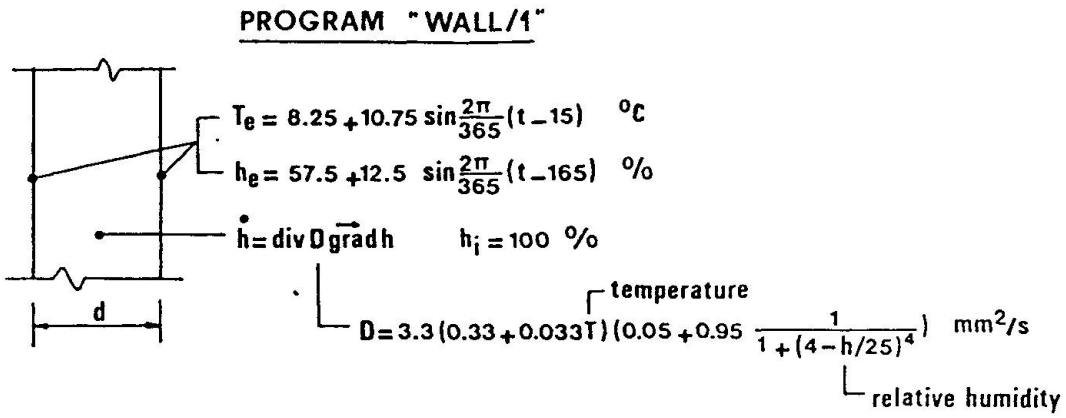

Fig. 12 Diffusion equation and boundary conditions used in the drying analysis of element 5 of the cross section.

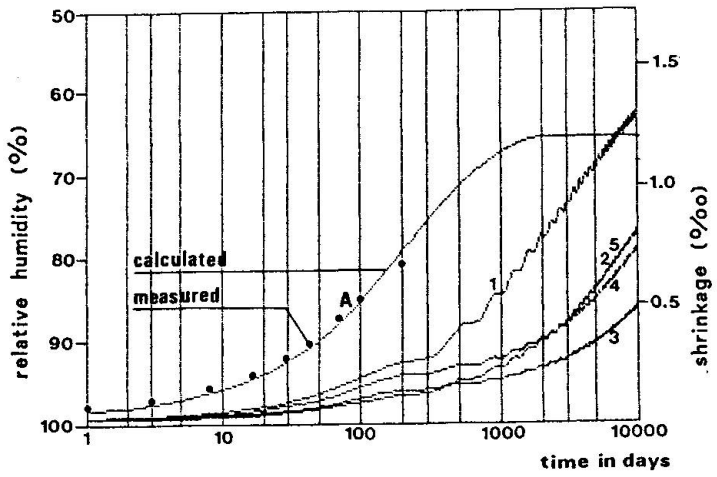

Fig. 13 Calculated evolution of the average relative humidity in the different elements of the cross section.

ACKNOWLEDGEMENT

We would like to thank consulting engineers Gianadda & Guglielmetti (Martigny, Valais, Switzerland) for their steady interest in this work and for their collaboration.

REFERENCES

1. WITTMANN F.H., Creep and Shrinkage Mechanisms, in Z.P. Bazant and F.H. Wittmann (eds), Creep and Shrinkage in Concrete Structures, John Wiley & Sons Ltd (1982) Chapter 6.

2. WITTMANN F.H., Structure of Concrete and Crack Formation, in K.P. Herrmann and L.H. Larsson (eds), Fracture of Non-Metallic Materials, ECSC, EEC, EAEC, Brussels and Luxembourg (1987) pp. 309-340.

3. ROELFSTRA P.E., Numerical Analysis and Simulation of Crack Formation in Composite Materials such as Concrete, in K.P. Herrmann and L.H. Larsson (eds), Fracture of Non-Metallic Materials, ECSC, EEC, EAEC, Brussels and Luxembourg (1987) pp. 359-384.

4. ROELFSTRA P.E., Numerical Concrete, Ph.D. Thesis, Swiss Federal Institute of Technology, Lausanne (to be published 1987).

5. WITTMANN F.H., Summary Report on Research Activities, EPFL, Laboratory for Building Materials, Switzerland (1986).

6. with theoretical backgrounds applications, EPFL, Laboratory for Building Materials, Switzerland (1985).

7. ROELFSTRA P.E. and KAMP C., MOIST/1, Manual with theoretical backgrounds and applications, EPFL, Laboratory for Building Materials, Switzerland (1985).

8. HILLERBORG A., A Model for Fracture Analysis, Report TVBM-305, Lund Institute of Technology, Division of Building Materials, Sweden (1978).

9. ROELFSTRA P.E. and SADOUKI H., FRACTURE/1, Manual with theoretical backgrounds and applications, EPFL, Laboratory fo Building Materials, Switzerland (1986).

10. ROELFSTRA P.E., SOFTFIT/1, Manual with theoretical backgrounds and applications, EPFL, Laboratory for Building Materials, Switzerland (1986).

11. ROELFSTRA P.E., CCB/1, Manual with theoretical backgrounds and applications, EPFL, Laboratory for Building Materials, Switzerland (1986).

12. KAMP C., HMG/1, Manual with theoretical backgrounds and applications, EPFL, Laboratory for Building Materials, Switzerland (1986).

13. ROELFSTRA P.E., Computerized Structural Analysis applied to Large Span Bridge, in F.H. Wittmann (ed), Fundamental Research on Creep and Shrinkage of Concrete, Martinus Nijhoff Publishers, The Hague/Boston/London (1982) pp. 353-367.

14. BAZANT Z.P., Mathematical Models for Creep and Shrinkage of Concrete, in Z.P. Bazant and F.H. Wittmann (eds), Creep and Shrinkage of Concrete Structures, John Wiley & Sons Ltd (1982) Chapter 7.

15. BAZANT Z.P. and NAJJAR L.J., Nonlinear Water Diffusion in Nonsaturated Concrete, Materials and Structures, RILEM, Paris, pp. 3-20.

16. KAMP C., ROELFSTRA P.E. and WITTMANN F.H., Aspects of Moisture Flow in HCP and Concrete, Contribution to this conference.

Leere Seite
Blank page
Page vide

Energy Dissipation Analysis for Creep in Heated Concrete

Analyse de la dissipation d'énergie par fluage dans les bétons chauffés

Analyse der Energiedissipation für Kriechen in erwärmtem Beton

Khaldoun ZEITOUNI
Civil Eng. Dept.
King's College London
London, U.K.

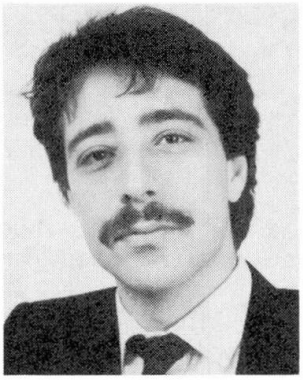

Khaldoun Zeitouni obtained his B.Sc (Eng) degree in civil engineering in 1983 and since that time has been researching into the time- and temperature-dependent behaviour of concrete structures undergoing creep; with a particular interest in their mathematical description. This work will lead to a Ph.D. thesis.

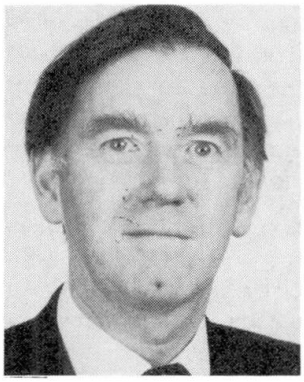

As a member of the academic staff of King's College George England obtained his B.Sc (Eng) in 1975; became Reader in Engineering Mechanics and now holds a personal Chair as Professor of Mechanics and Structures. His consultancy activities centre around structural problems involving time dependency.

George ENGLAND
Civil and Struc. Eng.
King's College London
London, U.K.

SUMMARY

The paper highlights the need for creep analyses of non-uniformly heated concrete structures. The energy dissipation rate from the structure as a whole uniquely defines a given problem, and is used to establish fundamental theorems relating to the nature of the energy-dissipation-rate/time curve for a structure and to derive a variational technique based on power concepts to evaluate the time-dependent stresses. One outcome of the work is the identification of a simple direct approach to the calculation of the limiting (in time) steady-state stresses. An illustrative example is presented.

RÉSUMÉ

L'article montre le besoin d'analyse de fluage sur des structures en béton chauffées de manière non-uniforme. Le taux de dissipation d'énergie de la structure dans sa totalité, qui définit à lui seul et entièrement un problème donné, est utilisé pour l'établissement de théorèmes fondamentaux liés à la nature des courbes du taux de la dissipation d'énergie dans le temps pour une structure; il en découle une technique de formulation variable basée sur des concepts de puissance pour évaluer les contraintes en fonction du temps. Un résultat des travaux est l'identification de la simple approche directe pour le calcul des contraintes de l'état constant limité dans le temps. Un exemple d'application est présenté.

ZUSAMMENFASSUNG

Dieses Referat wirft ein Licht auf die Notwendigkeit von Kriech-Analysen der ungleichmässig geheizten Betonstrukturen. Die Rate der Energiedissipation der Konstruktion als Ganzes beschreibt einzig und allein ein bestimmtes Problem und wird benutzt, um fundamentale Theoreme festzustellen, die mit der Art der Kurve der Energiedissipationsrate/Zeit einer Konstruktion zusammenhängen, und um eine Variations-Methode abzuleiten, die auf Kraftkonzeptionen basiert, um die zeitbedingten Belastungen auszuwerten. Eines der Ergebnisse dieser Arbeit ist die Identifikation eines einfachen direkten Ansatzes zur Berechnung der zeitlich limitierenden Belastungen. Ein illustratives Beispiel wird vorgelegt.

1. INTRODUCTION

Creep in concrete structures causes displacements to change with time and stresses to undergo redistribution whenever non-homogeneous properties are present. Because creep is strongly temperature dependent non-uniformly heated structures often exhibit major redistribution of internal stresses - during time-invariant mechanical loading - and with attendant changes to external supporting reactions.

Understanding the behaviour of heated concrete structures is of importance to the Engineer, and he must be provided with design rules which allow him to predict structural performance from specified conditions of loading, temperature, etc.

In order to develop sound analytical and design procedures it is essential to understand the basic principles which govern the way in which a structure will perform during creep. The first part of this paper therefore addresses some philosophical aspects of structural performance in a mathematical context. These lead to a useful predictive analysis for the time-varying stresses which is based on a power variational formulation. The analysis is then recognised in the context that,

> **"The total Virtual Power of a structure or body that is undergoing creep, is zero when the strain rates (and support displacement rates) are at all times compatible, and the structure/body is subjected to an equilibrium variation to the internal stresses (and support reactions)".**

A three-dimensional analysis is then formulated and some observations relating to its predictive capacity are made and compared with experimental performance for justification. In the last section a simple example is presented for a once redundant pin-jointed structure, to illustrate the solution technique.

Reference also is made to other uses of the theory in two- and three-dimensional finite element analysis.

2. THEORETICAL DEVELOPMENT

The derivation of the Virtual Power equation of section 4, Eq.(23), is assisted here by the adoption of a specific constitutive creep law in which the strain rates, $d\varepsilon/dt$, are related to the current stresses, σ, and stress rates, $d\sigma/dt$, only. Eq(1) is the one-dimensional relationship which is suitable for representing the temperature-dependent flow component of creep for concrete.

$$\frac{d\varepsilon}{dt} = \frac{1}{E}\frac{d\sigma}{dt} + \sigma\phi(T)\frac{dc}{dt} \qquad (1)$$

In this equation c represents a normalised creep strain, with respect to stress, σ, and a temperature function, $\phi(T)$. Rearrangement of Eq.(1) gives,

$$\frac{d\varepsilon}{dc} = \frac{1}{E}\frac{d\sigma}{dc} + \sigma\phi(T) \qquad (2)$$

Comparison of Eqs.(1) and (2) reveals a simple time transformation such that Eq.(2) represents a linear Maxwell law for which the normal viscosity, η, is replaced by the reciprocal of $\phi(T)$ and time is replaced by the normalised creep parameter itself, c. This parameter is a psuedo-time variable in the analysis which follows, and all 'dotted' terms relate to differentiations with respect to pseudo-time, c. In the engineering problem conversion to real time, t, is effected at the end of the analysis by reference to the c-t curve for the appropriate material. Eq.(2) may now be rewritten,

$$\dot{\varepsilon} = \frac{\dot{\sigma}}{E} + \sigma\phi(T) \qquad (3)$$

In the creeping material subjected to external mechanical loading the work balance equation takes the form,

$$\dot{W} = \dot{D} + \dot{U} \tag{4}$$

where $\dot{W}$ is the rate of working of the external loads

$\dot{D}$ is the rate at which energy is dissipated in creep

$\dot{U}$ is the rate of change of internal strain energy

Hence $U = \frac{1}{2}\int \{\sigma\}^T \{\varepsilon_e\} dv$ (5)

$$\dot{D} = \int \{\sigma\}^T \{\dot{\varepsilon}_c\} dv \tag{6}$$

where $\{\sigma\}$ and $\{\varepsilon_e\}$ are the conventional six component elastic stress and strain vectors and $\{\dot{\varepsilon}_c\}$ (derived from experimental creep data) have the form,

$$\{\dot{\varepsilon}_c\} = \begin{Bmatrix} \dot{\varepsilon}_{c,x} \\ \dot{\varepsilon}_{c,y} \\ \dot{\varepsilon}_{c,z} \\ \dot{\varepsilon}_{c,xy} \\ \dot{\varepsilon}_{c,yz} \\ \dot{\varepsilon}_{c,zx} \end{Bmatrix} = \phi(T) \begin{bmatrix} 1 & -\nu_c & -\nu_c & 0 & 0 & 0 \\ -\nu_c & 1 & -\nu_c & 0 & 0 & 0 \\ -\nu_c & -\nu_c & 1 & 0 & 0 & 0 \\ 0 & 0 & 0 & 2(1+\nu_c) & 0 & 0 \\ 0 & 0 & 0 & 0 & 2(1+\nu_c) & 0 \\ 0 & 0 & 0 & 0 & 0 & 2(1+\nu_c) \end{bmatrix} \begin{Bmatrix} \sigma_x \\ \sigma_y \\ \sigma_z \\ \sigma_{xy} \\ \sigma_{yz} \\ \sigma_{zx} \end{Bmatrix} \tag{7}$$

Also $\{\varepsilon_e\}$ are related to the stresses in a similar manner to Eq.(7), after ν_c is replaced by ν_e the elastic Poisson's ratio, and $1/\phi(T)$ is replaced by the elastic modulus, E.

Eq.(5) now has the form,

$$U = \frac{1}{2}\int \frac{1}{E}\{\sigma\}^T [V_e]\{\sigma\} dv \tag{8}$$

and $$\dot{U} = \int \frac{1}{E}\{\sigma\}^T [V_e]\{\dot{\sigma}\} dv \tag{9}$$

Also $$\dot{D} = \int \phi(T)\{\sigma\}^T [V_c]\{\sigma\} dv \tag{10}$$

Experiments reveal that $\nu_e \doteq \nu_c$; hence writing $[V_e] = [V_c] = [V]$ the external work rates are,

$$\begin{aligned} \dot{W} &= \int \frac{1}{E}\{\sigma\}^T [V]\{\dot{\sigma}\} dv + \int \phi(T)\{\sigma\}^T [V]\{\sigma\} dv \\ &= \int \{\sigma\}^T \left(\frac{d}{E} + \phi(T)\right)[V]\{\sigma\} dv \end{aligned} \tag{11}$$

where $d = d(\ )/dc$

Because $\dot{W} = \int \{\sigma\}^T \{\dot{\varepsilon}\} dv$ (12)

it follows that the three-dimensional stress/total strain relationship is,

$$\{\dot{\varepsilon}\} = \left(\frac{d}{E} + \phi(T)\right)[V]\{\sigma\} \tag{13}$$

Observations of Eq.(9) and (10) suggest that if a steady state of stress exists then $\dot{U} \to 0$ and $\dot{D}$ tends to a constant positive value at large times. The nature of these time-dependent variations of $\dot{U}$ and $\dot{D}$ however are not revealed; though numerical computations have for some time indicated that the variation of $\dot{D}$ with time (pseudo-time) is a monotonically declining function which approaches asymptotically a minimum value[1].

A formal proof of this behaviour is now given and used to derive the variational equations from which a solution for the time-varying stresses is obtained.

From Eqs.(6) and (10) the incremental change in $\dot{D}$, $\Delta\dot{D}$, over a time interval, Δ_c is,

$$\dot{D} + \Delta\dot{D} = \int\{\sigma+\Delta\sigma\}^T[V]\{\sigma+\Delta\sigma\}\phi(T)dv$$

but $\Delta\dot{D} = \dot{D}(c+\Delta c) - \dot{D}(c)$, hence,

$$\Delta\dot{D} = \int\{(\{\sigma\}^T[V] + \{\Delta\sigma\}^T[V])(\{\sigma\} + \{\Delta\sigma\}) - \{\sigma\}^T[V]\{\sigma\}\}\phi(T)dv$$

Ignoring second order terms in $\Delta\sigma$ leads to,

$$\Delta\dot{D} = \int\{\{\Delta\sigma\}^T[V]\{\sigma\} + \{\sigma\}^T[V]\{\Delta\sigma\}\}\phi(T)dv \tag{14}$$

From Eq.(13)

$$\{\dot{\varepsilon}\} = (\frac{d}{E} + \phi(T))[V]\{\sigma\}$$

Multiplying both sides by $[V]^{-1}$ gives,

$$[V]^{-1}\{\dot{\varepsilon}\} = (\frac{d}{E} + \phi(T))\{\sigma\}$$

$$\therefore \quad [V]^{-1}\{\dot{\varepsilon}\} = \frac{1}{E}\{\dot{\sigma}\} + \phi(T)\{\sigma\} \tag{15}$$

$$\text{or} \quad \phi(T)\{\sigma\} = [V]^{-1}\{\dot{\varepsilon}\} - \frac{1}{E}\{\dot{\sigma}\} \tag{16}$$

Substituting $\phi(T)\{\sigma\}$ from Eq.(16) into Eq.(14) yields,

$$\Delta\dot{D} = \int(\{\Delta\sigma\}^T[V]\{[V]^{-1}\{\dot{\varepsilon}\} - \frac{1}{E}\{\dot{\sigma}\}\} + \{[V]^{-1}\{\dot{\varepsilon}\} - \frac{1}{E}\{\dot{\sigma}\}\}^T[V]\{\Delta\sigma\})dv$$

Noting that

$$[[V]^{-1}]^T = [V]^{-1}$$

$$\Delta\dot{D} = \int(\{\Delta\sigma\}^T\{\dot{\varepsilon}\} - \frac{1}{E}\{\Delta\sigma\}^T[V]\{\dot{\sigma}\} + \{\dot{\varepsilon}\}^T\{\Delta\sigma\} - \frac{1}{E}\{\dot{\sigma}\}^T[V]\{\Delta\sigma\})dv$$

The first and third terms of this equation vanish by reason of $\{\dot{\varepsilon}\}$ being compatible and $\{\Delta\sigma\}$ being an equilibrium set of stresses; hence,

$$\Delta\dot{D} = -\int\frac{1}{E}(\{\Delta\sigma\}^T[V]\{\dot{\sigma}\} + \{\dot{\sigma}\}^T[V]\{\Delta\sigma\})dv$$

Dividing through by $\Delta c>0$ and taking the limit as $\Delta c\to 0$,

$$\frac{d\dot{D}}{dc} = -\int\frac{1}{E}(\{\dot{\sigma}\}^T[V]\{\dot{\sigma}\} + \{\dot{\sigma}\}^T[V]\{\dot{\sigma}\})dv$$

$$= -2\int\frac{1}{E}\{\dot{\sigma}\}^T[V]\{\dot{\sigma}\}dv \tag{17}$$

The scalar quantity under the integral sign can only be positive if the matrix [V] is positive definite. For a compressible material, $\nu<\frac{1}{2}$, the eigenvalues of [V] are all positive; hence [V] is positive definite. It then follows that the slope of the $\dot{D}$ curve is always negative, Eq.(17). This statement is necessary but not sufficient to define the monotonic behaviour of the $\dot{D}$ curve. Additionally it is necessary to establish a positive curvature of the curve at all times. Thus by differentiating Eq.(17) with respect to pseudo-time, c, gives,

$$\frac{d^2\dot{D}}{dc^2} = -2\int\frac{1}{E}(\{\ddot{\sigma}\}^T[V]\{\dot{\sigma}\} + \{\dot{\sigma}\}^T[V]\{\ddot{\sigma}\})dv \qquad (18)$$

From Eq.(15)

$$[V]^{-1}\{\ddot{\varepsilon}\} = \frac{1}{E}\{\ddot{\sigma}\} + \phi(T)\{\dot{\sigma}\}$$

Substituting this into Eq.(18) gives,

$$\frac{d^2\dot{D}}{dc^2} = -2\int(\{\ddot{\varepsilon}\}^T[V]^{-1}\{\dot{\sigma}\} - \phi(T)\{\dot{\sigma}\}^T[V]\{\dot{\sigma}\} + \{\dot{\sigma}\}^T[V][V]^{-1}\{\ddot{\varepsilon}\} - \phi(T)\{\dot{\sigma}\}^T[V]\{\dot{\sigma}\})dv$$

The first and third terms of this equation vanish because of compatibility and equilibrium. Hence the equation reduces to,

$$\frac{d^2\dot{D}}{dc^2} = 4\int\phi(T)\{\dot{\sigma}\}^T[V]\{\dot{\sigma}\}dv \geq 0 \qquad (19)$$

Thus Eqs. (17) and (19) together, do establish that the $\dot{D}$ curve is of a monotonically declining shape leading to a steady-state value at infinite time.

3. STRUCTURAL PERFORMANCE

The theory of the previous section was based on the belief that the initial stresses change during creep and tend to limiting or steady-state values at large times. This hypothesis has been tested in a number of experiments and the findings are given in this section.

Imposed support displacements in statically indeterminate structures cause immediate changes to the internal moments and stresses, and to external supporting reactions. It has been long recognised that when these displacements are sustained creep tends to return the structure to the original stress, moment and force state, when the mechanical loading is sustained and the material behaviour of the structure is homogeneous. In this case the steady state is identical with the initial elastic state.

In structures heated non-uniformly and with sustained temperature gradients, the steady state is distinct from the initial elastic state [2,3]. Prestress, when it exists, acts simply as a component of the mechanically applied loading on the structure and therefore influences the steady-state solution.

The existence of a steady state in a structure is often masked because the creep of concrete as a material exhibits a declining rate with increasing time under stress. This masking feature was overcome in experiments carried out at King's College in which selective support displacements were imposed at appropriate times to cause the structure to approach its steady state alternately from below and above [4]. Figure 1 illustrates the behaviour as observed and provides conclusive evidence of the existence of a preferred or steady state.

The theory of Section 2 indicates that during any period of sustained loading and temperature the rate at which energy is dissipated during creep is always decreasing and tending to a minimum value in the steady state. Figure 2 (upper curve) shows the typical $\dot{D}/c$ behaviour. This implies that whenever a change of state is imposed on the structure, e.g. by a change of loading or temperature, or by the imposition of displacements,

(a) there will exist a new limiting value of $\dot{D}_{SS}$ defined by the new conditions of load and/or temperature,

and (b) the current value of $\dot{D}$ will be such that $\dot{D} \geq \dot{D}_{SS}$. Figure 3 illustrates this behaviour.

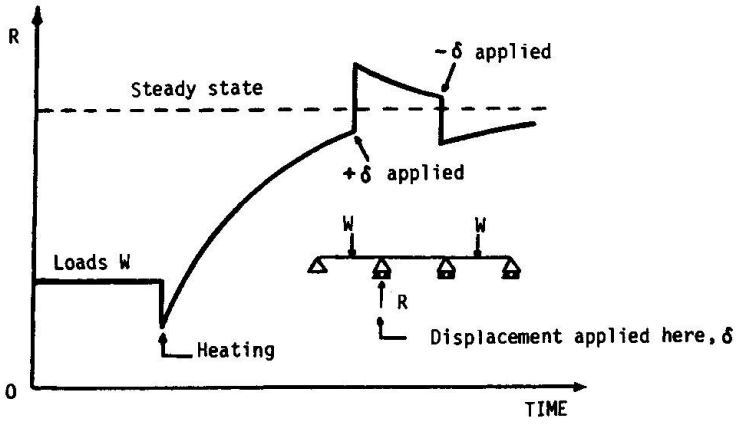

Fig. 1. Influence of creep, temperature and imposed displacement on beam reaction, R.

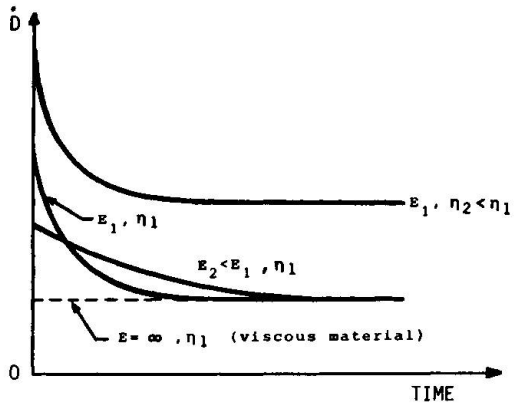

Fig. 2. Dependence of Energy Dissipation Rate on elastic and viscous parameters of Maxwell model. Note: for concrete, $\eta = 1/\phi(T)$.

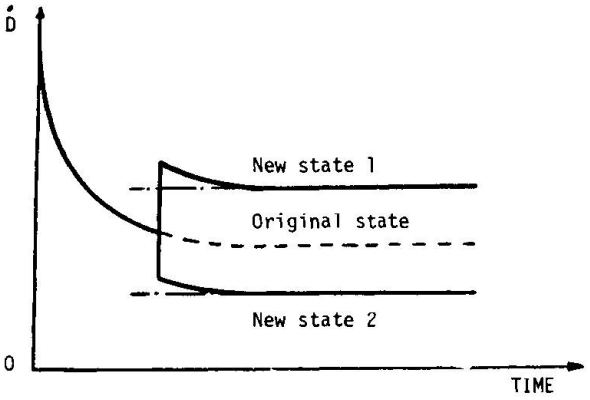

Fig. 3. Changes in Energy Dissipation Rate due to changes of state.

Problems associated with cyclic temperature changes represent another class for which the 'state' is changing repeatedly, and hence $\dot{D} \gg \dot{D}_{SS}$ always, Figure 4. Such problems may be formulated in terms of a single parameter, the **average weighted energy dissipation rate** over a complete temperature cycle, $\dot{D}_{av}$. For this representation the $\dot{D}_{av}$ curve is again of monotonic shape tending to a non-zero steady-state value*. Eqs.(17) and (19) then have counterparts for which $\dot{D}$ is replaced by $\dot{D}_{av}$.

Figure 4 illustrates also that although the average energy dissipation rate declines montonically with time, and the dissipation rate during any constant temperature period has a similar form; on a cycle-by-cycle basis the energy dissipation rate in the lower temperature state, T_1, is seen paradoxically to rise as the steady state* is approached.

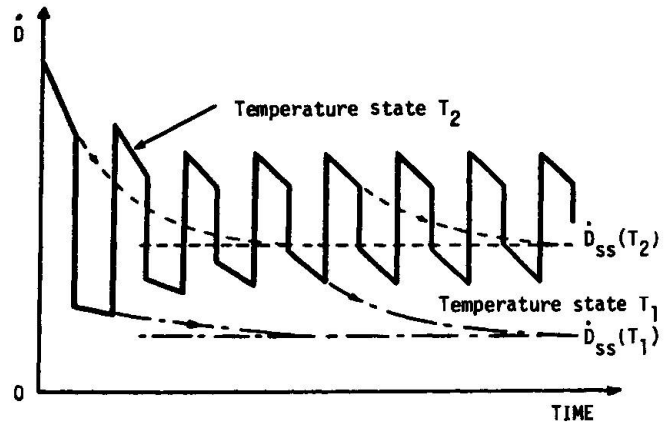

Fig. 4. Energy Dissipation Rate - Time behaviour under cyclically changing temperature states.

4. TIME-DEPENDENT STRESS ANALYSIS

The theory of Section 2 is used here to develop an analysis procedure for the determination of the time-varying stresses during sustained loading and temperature conditions. For the continuum problem it is approximate but may be exact for problems containing a finite number of redundancies.

Equating the right hand side of Eq.(17) to Eq.(10) after differentiation leads to:

$$\int \phi(T)\{\sigma\}^T[V]\{\dot{\sigma}\}dv = -\int \frac{1}{E}\{\dot{\sigma}\}^T[V]\{\dot{\sigma}\}dv \tag{20}$$

i.e.
$$\int \left(\phi(T) + \frac{d}{E}\right)\{\sigma\}^T[V]\{\dot{\sigma}\}dv = 0 \tag{21}$$

Employing Eq.(13) then reduces this equation to the statement,

$$\int \{\dot{\varepsilon}\}^T\{\dot{\sigma}\}dv = 0 \tag{22}$$

Expressing $\{\dot{\sigma}\}$ as $\{\frac{d\sigma}{dc}\} \div \{\frac{\delta\sigma}{\delta c}\}$ allows Eq. (22) to be written,

$$\int \{\dot{\varepsilon}\}^T\{\delta\sigma\}dv = 0 \quad \text{for } \delta c \neq 0 \tag{23}$$

Eq.(23) is valid in a more general sense than the specific derivation might suggest. It represents the same Virtual Power statement as given in Section 1 for the case of no imposed boundary displacement rates. The requirements of Eq.(23) are therefore:

---

*This state is not a true steady state but is simply a repeating cyclic state.

(a) $\{\dot{\varepsilon}\}$ represent a set of compatible internal strain rates.
(b) $\{\delta\sigma\}$ represent any set of equilibrium stresses and not necessarily those relating to the actual changes over the time interval δc.

4.1 Solution procedure

Equilibrium at any time is chosen to be represented by the following state of stress,

$$\{\sigma\} = \{\sigma_0\} + a_1\{\sigma_1\} + \ldots\ldots + a_n\{\sigma_n\} \tag{24}$$

in which $\{\sigma_0\}$ is any set of stresses satisfying equilibrium of the boundary loading. $\{\sigma_1\}$ to $\{\sigma_n\}$ are sets of internal self-equilibrating stresses, and a_1 to a_n are time-dependent weighting parameters.

It may be observed from the form of Eq.(24) that $\{\delta\sigma\}$ of Eq.(23) take the form,

$$\{\delta\sigma\}_i = \frac{\partial}{\partial a_i}\{\sigma\} = \{\sigma_i\} \tag{25}$$

The stress solution is now confined to the determination of the n values of a_i. Eq.(23) is used to generate n independent equations from which the a_i parameters may be evaluated.

Eq.(24) may be expressed as,

$$\{\sigma\} = \{\sigma_0\} + [J]\{a\} \tag{26}$$

where $[J] = [\{\delta\sigma\}_1 \ldots\ldots \{\delta\sigma\}_n]$

Employing Eq.(13), with the inclusion of $\{\sigma\}$ as defined in Eq.(26), $\{\dot{\varepsilon}\}^T$ of Eq.(23) is defined in terms of the stress components (viz. Eq.(24) representation) and weighting parameters, a_i. The introduction of $\{\delta\sigma\}$ into Eq.(23) then leads to a set of first order differential equations in time from which a_i may be evaluated. Thus, Eq.(23) becomes,

$$0 = \int\left(\frac{1}{E}[J]^T[V][J]\{\dot{a}\} + \phi(T)[J]^T[V][J]\{a\} + \phi(T)[J]^T[V]\{\sigma_0\}\right)dv$$

This reduces to the following set of equations.

$$[A]\{\dot{a}\} + [B]\{a\} + [C] = 0 \tag{28}$$

The general terms of the matrices in Eq.(28) are,

$$\begin{aligned} A_{r,s} &= \int\frac{1}{E}\{\sigma_s\}^T[V]\{\sigma_r\}dv \\ B_{r,s} &= \int\phi(T)\{\sigma_s\}^T[V]\{\sigma_r\}dv \\ C_r &= \int\phi(T)\{\sigma_0\}^T[V]\{\sigma_r\}dv \end{aligned} \tag{29}$$

5. ILLUSTRATIVE EXAMPLE

5.1 Statement of the Problem

The inset diagram of Figure 5 shows a symmetrical pin-jointed structure of three members (each of length, L, and the same cross-sectional area, A) supporting a single concentrated load, W, acting in the line of the central member. The outer members, inclined at angle θ to the horizontal, are at temperatures, $T_1<T_2$. It is assumed that the elastic modulus, E, is uniform throughout and that the Maxwell creep law of Eq.(2) is applicable; with $\phi(T) = T$.

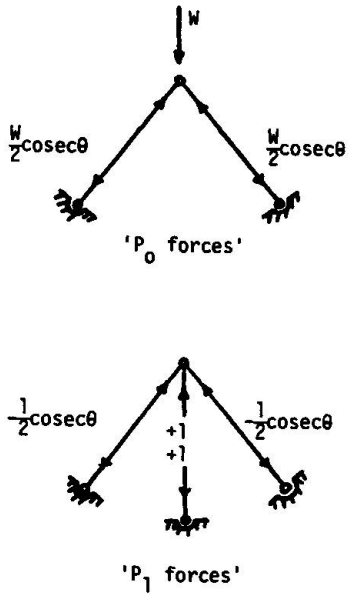

Fig. 5. Loadings on statically determinate released structure.

5.2 Solution Procedure

The equivalent one-dimensional statement to Eq.(23) is,

$$\int \dot{\varepsilon}\delta\sigma dv = 0$$

which becomes for a set of pin-jointed members, subjected to axial forces only,

$$\sum_{\text{members}} \dot{\varepsilon}\delta\sigma AL = 0 \tag{30}$$

For the once redundant problem the state of stress is represented everywhere by the expression,

$$\sigma = \sigma_0 + a_1\sigma_1 \tag{31}$$

where σ_0 and σ_1 are defined by the stresses created by the actual loading and a unit internal force applied separately to a statically determinate released structure as detailed in Figure 5.

For the pin-jointed structure Eq.(30) reduces to the form,

$$\sum\left(\frac{\dot{P}}{AE} + \frac{PT}{A}\right)\frac{\delta P}{A}AL = 0 \tag{32}$$

where the summation is taken over all the members, and $P = \sigma A$, etc. Further substitution leads to,

$$\sum\left\{\frac{\dot{a}_1 P_1}{AE} + (P_0 + a_1 P_1)\frac{T}{A}\right\}P_1 L = 0$$

or

$$\dot{a}_1 \sum \frac{P_1^2 L}{AE} + a_1 \sum \frac{P_1^2 TL}{A} + \sum \frac{P_0 P_1 LT}{A} = 0 \tag{33}$$

Eq.(33) is then written,

$$A^*\dot{a}_1 + B^*a_1 + C^* = 0 \qquad (34)$$

where, $A^* = \frac{1}{E}(1+2\sin^2\theta)$

$B^* = T_1 + 2T_2\sin^2\theta$

$C^* = -WT_1$

The solution of Eq.(34) for a_1 is,

$$a_1 = e^{-B^*c/A^*}G^* - C^*/B^*$$

Here, the constant, G*, is obtained from the initial condition at t=0, i.e. from the elastic solution; and the product -C*/B* represents the steady-state solution to which the creep solution tends at large times. Figure 6 shows the way in which the member stresses (and forces) change during creep for this non-uniform temperature problem.

Eq.(23) has also been used successfully in three-dimensional analysis in a prestressed concrete nuclear reactor containment vessel [5].

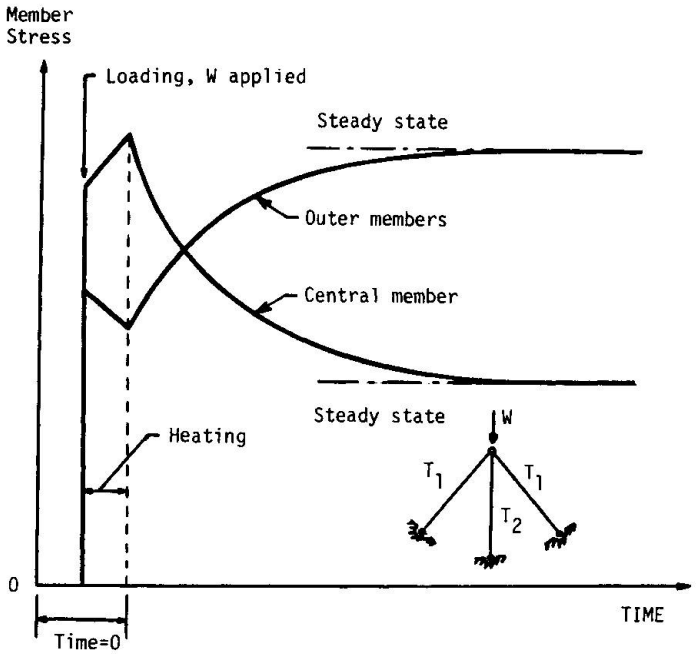

Fig. 6. Variation of member stresses with time in heated pin-jointed structure

6. CONCLUDING REMARKS

Section 2 has established a formal proof that the energy dissipation rate during creep (for the structure as a whole)† is a monotonically declining quantity leading to a minimum value in the steady state.

The theoretical existence of a steady state for which stresses become time-invariant but strains continue to change is in accord with experimental findings.

A general theory derived from energy dissipation concepts is presented in Section 4 for the evaluation of time-dependent stresses under sustained loads and temperatures during non-homogeneous creep.

†Non-homogeneous creep where the isotropic behaviour is Maxwell.

An application of the theory to a simple example has demonstrated the capabilities of the procedures and the nature of the creep problem in concrete at non-uniform temperatures.

REFERENCES

1. ENGLAND G.L., Time-dependent stresses in creep-elastic materials. JBCSA, Royal Aeronautical Society, London, U.K., March 1968.

2. ROSS A.D., ENGLAND G.L., and SUAN R.H., Prestressed concrete beams under a sustained temperature crossfall. Magazine of Concrete Research, Vol.17, N72, September 1965.

3. KRISHNAMOORTHY S., ENGLAND G.L., and YU C.W., The behaviour of prestressed concrete portal frames as influenced by creep and temperature. Magazine of Concrete Research, Vol.23, N74, March 1971.

4. LABIB G.A., Short and long-term behaviour of plain and prestressed concrete subjected to temperature gradients and thermal cycling. PhD thesis, University of London, 1980.

5. ENGLAND G.L., SMITH I.G., and MACLEOD J.S., Application of a cost-effective 3-D stress analysis program for creep and temperature to a prestressed concrete nuclear containment. Proc. of the conference on Structural Analysis and Design of Nuclear Power Plants, Porto Alegre, Brazil, 1984.

Leere Seite
Blank page
Page vide

Simulation and Evaluation of Deterioration of Reinforced Concrete Structures

Simulation et évaluation de la détérioration des structures en béton armé

Simulation und Auswertung der Schädigung von Stahlbetonkonstruktionen

Hiroshi SAKURAI
Lecturer Concrete Eng.
Kitami Inst. of Techn.
Kitami, Japan

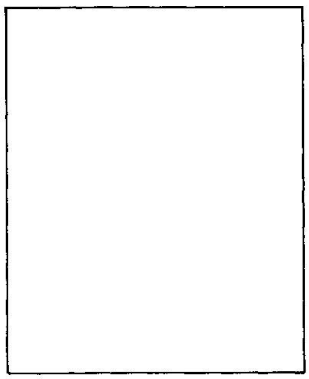

Hiroshi Sakurai is a lecturer in concrete engineering at the Developmental Engineering Dept., Faculty of Engineering, Kitami Institute of Technology. He is a member of the Japan Society of Civil Engineers and a member of the Japan Concrete Institute.

Toshihiko AOKI
Engineer
Taisei Corp.
Yokohama, Japan

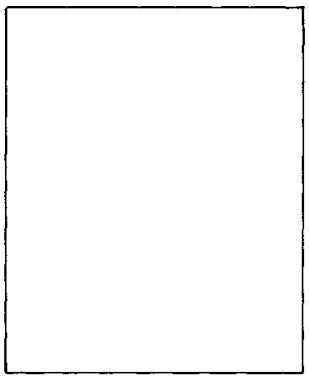

Toshihiko Aoki is an engineer in the Osaka Branch of Taisei Corporation. He is a member of the Japan Society of Civil Engineering.

Kazuhiro MOMOZAKI
Senior Res. Eng.
Taisei Corp.
Yokohama, Japan

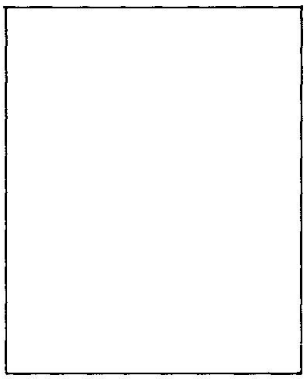

Kazuhiro Momozaki is a senior research engineer at the Technical Research Institute of Taisei Corporation.

Aketo SUZUKI
Chief Res. Eng.
Taisei Corp.
Yokohama, Japan

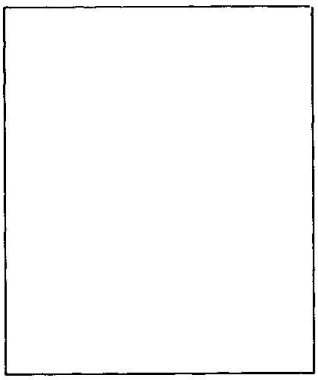

Aketo Suzuki is a Doctor of Engineering and chief research engineer of the Technical Research Institute of Taisei Corporation. He is a member of the Japan Society of Civil Engineering.

SUMMARY

The purpose of this study is to evaluate the deterioration of reinforced concrete structures at the planning and design stages. This paper examines the basis for quantifying the durability of structures. In addition, reinforced concrete structure (kaleidoscopic change) deterioration predictions were analyzed.

RÉSUMÉ

Le but de cette étude est d'évaluer la détérioration des structures en béton armé dans la phase du projet. L'article examine les bases permettant d'évaluer la durabilité des structures. Des prévisions sont faites pour l'évaluation de la détérioration des structures en béton armé.

ZUSAMMENFASSUNG

Das Ziel dieser Studie ist es, die Schädigung von Stahlbetonkonstruktionen im Planungs- und Entwurfsstadium zu bewerten. Der Beitrag befasst sich mit möglichen quantitativen Erfassungsmethoden.

1. INTRODUCTION

Recently, calculation of life cycle cost and quantifying of service life for concrete structures have been of concern, and establishment of rational and objective techniques for quantifying the durability of new structures at planning are in demand. The technique for quantifying durability of concrete structures are distinguished between evaluating the degree of health for existing structures and the techniques of quantifying for planning structures by purpose. This paper examines the basis of quantifying for structures at planning at the design stage and the prediction of concrete deterioration change in time by analyzing and choosing of concrete durability data. One of the latest studies are the projects of synthetic developing techniques of the Building Research Institute of the Ministry of Construction. Some of the purposes are development of synthetic techniques for research and improvement of durability, and preparing of criterion for judgment of structures. At the present, the techniques for judging the degree of deterioration of existing structures for maintenance and the technical skill has been given in the project. On the other hand, the test method or construction materials and quantifying durability and the prediction of service life are given at ASTM E-632. The development of the technique of quantifying for planning structures at the design stage would be an advance.

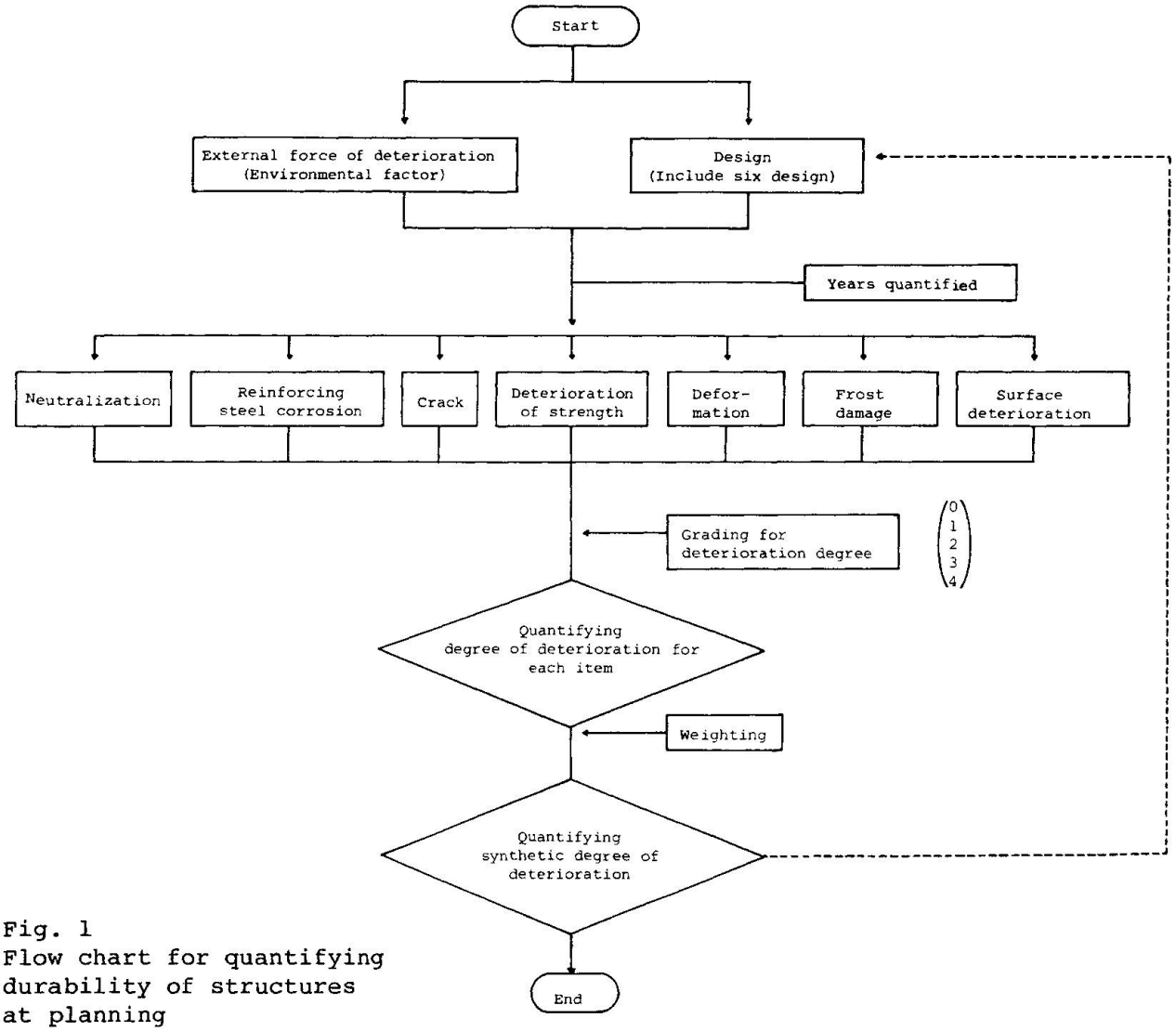

Fig. 1
Flow chart for quantifying durability of structures at planning

2. INVESTIGATION OF TECHNIQUE FOR QUANTIFYING DURABILITY

2.1 Investigation of Flow for Quantifying Durability of Structure at Planning

The Flow chart for quantifying durability of structures at planning is shown in Fig. 1. In this flow chart, the initial data of temperature, humidity, the distance from the sea, the result of water analysis and so on, which are external forces of degradation of external factors, and environmental factors around the structure, are imputted. The strength of concrete, its stress, the strength of its reinforcing steel, mix proportion of concrete (w/c, type of cement, water amount, content of air, material and so on), which are the value of design and inner factors, are imputted too. Further, years of quantifying are imputted. Next, the degree of deterioration for year for each item are calculated, graded, and weighted with capability demanded in each item. Lastly, the synthetic degree of deterioration are quantified with calculation results.

2.2 Choice of Items for Quantifying Durability

Seven items for quantifying civil structures were chosen which are neutralization, reinforcing steel corrosion, crack, deterioration of strength deformation, frost damage and surface deterioration. The definition of these are shown in Table 1. The reason why surface deterioration is chosen is that good siting and adequate cover of reinforcing steel are demanded for bridges and so on in civil structures. However, the deterioration phenomenon of each item's quantified durability are regarded as independent against their dependence of each other.

2.3 Choice of Deterioration Indicator

In choosing a deterioration indicator, the possibility of quantifying deterioration change in time and much existing data supported with enough experiments are to be taken into account. As the indicator, neutralization depth, ratio of corrosion, change rate in relative dynamic modulus of elasticity and average depth of damage are selected for each item to be quantified, as shown in Table 2.

Table 1. Definition of deterioration for each item quantified

Item of quantifying	Definition
a Neutralization	Deterioration due to declining alkalinity of concrete with carbonic acid gas in air and sodium carbonate in water (pH < 10)
b Reinforcing steel corrosion	Deterioration due to corroding reinforcing steel by oxidation and deoxidation with neutralization of concrete around it, water from cracks and corrosion (cl^- , SO_4^{2-})
c Crack	Deterioration due to growing macro and scopic failure of concrete by over permi stress (major stress over tensile strength) of concrete
d Deterioration of strength	Deterioration due to decreasing strength of concrete with material, environment in service, thermal action and chemical action
e Deflection	Deterioration due to deflecting horizontal members by structural external force action and dry shrinkage (excepting short term load)
f Frost damage	Deterioration due to decreasing strength properties of concrete by freezing and thawing water in concrete
g Surface deterioration	Deterioration lossing concrete surface by scaling and popout

Table 2(a) Deterioration indicator, factor, calculation and grading for each item quantified

Quantifying Item	Selected Indicator		Factor (1): valuable)		Calculation of Deterioration Indicator (durability) at Lapse of Year	Grading
	Indicator	Phenomenon	External Factor	Inner Factor		
a. Neutralization	Depth of neutralization X (mm)	① Neutralization	[t: Service life (year)]	W/C: Water cement ratio (%) R: Type of cement Type of AE agent Type of aggregate	W/C≧60%: $x=10x\sqrt{\frac{R^2(0.01W/C-0.25)^2}{0.3(1.15\cdot0.01W/C)}t}$ W/C<60%: $x=10x\sqrt{\frac{R^2(0.046W/C-1.76)^2}{7.2}t}$ 4)	1: 20≦X<40 2: 40≦X<80 3: 80≦X<100 4: 100≦X X: Depth of neutralization / Depth of cover %
b. Reinforcing steel corrosion	Ratio of corrosion surface P (%)	① Corrosion of penetrating chloride	[t: Service life (year)] L: Distance from sea (m) Co: Amount of chloride from sea (wt%)	Dc: Diffusivities of concrete (cm^2) D: Depth of cover (mm) UC: Unit weight of cement (kg/m^3) W/C: Water cement ratio (%) γ: Index of workability: γ=1	Co=0.48-0.07ln L (Pacific side) Co=0.45-0.06ln L (Japan sea side) $C=Co\left(1-erf\frac{D/10}{2\sqrt{Dc\cdot t\cdot3.1536x10^7}}\right)$ 5) $erfx=\int_0^1 cxp(-\mu^2)d\mu$ m·0.094t+0.245-0.029D 6) $P=\gamma\frac{2000}{UC}\cdot\frac{C}{2}\cdot(0.01W/C-0.3)\cdot10^n$ 7)	0: P<10 1: 10≦P<20 2: 20≦P<30 3: 30≦P<50 4: 50≦P
		② Corrosion of neutralization		D: Depth of cover (mm) X: Depth of neutralization (mm)	P=(1-φ(d-X/0.41X))x100 8) where; φ(a): Normal distribution function	
		③ Corrosion of crack		D: Depth of cover (mm) Wmax.: Maximum width of crack (mm)	$Wmean=\frac{Wmax+0.03}{1.91}$ 9) where; Wmean: Average width of crack $P=0.167(Wmean/D^2x10^6-20)$ 10)	
c. Crack	Maximum width of crack (mm)	① Crack of steel stress		fs: Stress of reinforcing steel (kgf/cm^2) D: Depth of cover (mm) β: Note 1) A: Note 2)	$Wmax=0.0108\ \beta\cdot fs\sqrt[3]{D/10xA}\ x\ 10^{-3}$ 11)	0: Wmax<0.05 1: 0.05≦Wmax<0.2 2: 0.2 ≦Wmax<0.3 3: 0.3 ≦Wmax<0.5 4: 0.5 ≦Wmax
		② Crack of dry and temperature shrinkage	TC: Change of temperature (°C)	b: (m) h: (m) NH: fct: (kgf/cm) fb: (kgf/cm) φ: (m) cs: te: Show in Table 4	$Wmax=\frac{2b\cdot h\cdot fct}{\pi\cdot NH\cdot\phi\cdot1b}(\varepsilon cs+\varepsilon te-100x10^{-6})x1000$ 12)	
		③ Crack of alkali silica reaction		RG: Content of reactionable aggregate (%) Ru: Amount of Na^2O in aggregate by cement (%)	The expansion (EX) is estimated by RG and RU 13)	

Table 2(b)

Quantifying Item	Selected Indicator		Factor (1): valuable		Calculation of Deterioration Indicator (durability) at Lapse of Year	Grading
	Indicator	Phenomenon	External Factor	Inner Factor		
d. Deterioration of strength	Notes 2) Ratio of compressive strength SN(%)	① Deterioration of penetrating sulfate	[t: Service life (year)]	W/C: Water/cement ratio	Linear Regression of experimental data 14) W/C=55% H_2SO_4: 0.3%, SN=-40.15t+100 H_2SO_4: 2.0%, SN=-233.6t+100 H_2SO_4: 5.0%, SN=-244.55t+100	0: 95<SN 1: 90<SN≦95 2: 80<SN≦90 3: 70<SN≦80 4: SN≦70
		② Deterioration of frost damage	[t: Service life (year)] M: Cycles of freeze-thaw a year	W/C: Water/cement ratio AE or NonAE: Whether the there is AE agent	DN of f① is converted to by the equation $SN=\frac{DN-25}{0.75}$ AE W/C=40% SN=-0.04 N·t+100 15) W/C=50% SN=-0.07 N·t+100 W/C=55% SN=-0.11 N·t+100 W/C=60% SN=-0.12 N·t+100 NonAE W/C=40% SN=-0.49 N·t+100 16) W/C=60% SN=-0.69 N·t+100	
		③ Deterioration of alkali silica reaction aggregate		RG: Content of reactionable aggregate RU: Amount of Na_2O in aggregate (%)	SN(f(EX)) is estimated with the expansion EX of c③ 17)	
e. Deformation	Strain ε (%)	① Deformation of creep strain	σ: Stress of concrete loading (kgf/cm^2)	Ec: Youngs modulus φ: Coefficient of creep	$\varepsilon=\frac{\sigma}{Ec}\cdot\phi$ (outdoor φ=2.0) 18)	0: ε< 420 1: 420≦ε< 670 2: 670≦ε<1033 3: 1033≦ε<2290 4: 2290≦ε
		② Deformation of dry and temperature	Tc: Change of temperature (°C)	Uc: Unit weight of cement W/C: Water cement ratio	εcs=0.00148W/C+0.000301UC-0.131 εte=10x10^{-6}xIC 19)	
f. Frost damage	Change rate in relative dynamic modulus of elasticity DN (%)	① Frost damage	[t: Service life (year)] N: Cycles of freeze-thaw a year	W/C: Water cement ratio (%) AE or NonAE: Whether there is AE agent	Linear Regression of experimental data 15) AE W/C=40% DN=-0.028N·t+100 W/C=50% DN=-0.053N·t+100 W/C=55% DN=-0.080N·t+100 W/C=60% DN=-0.085N·t+100 NonAE W/C=40% DN=-0.36 N·t+100 W/C=60% DN=-0.51 N·t+100	0: 96<DN 1: 93<DN≦96 2: 85<DN≦93 3: 78<DN≦85 4: DN≦78
g. Surface deterioration	Average depth of damage H(mm)	① Surface deterioration of frost damage	[t: Service life (year)] N: Cycles of freeze-thaw year W: Coefficient of supplying seawater	W/C: Water cement ratio (%) α: Coefficient of type of cement and curing condition fc: Compressive strength of concrete K: Construction	$H=W\cdot\alpha(N(\frac{W/C}{55})^3-(0.001195k^2\cdot fc^2)(\frac{W/C}{55})^3)$ 20) W=0.5 where; α=0.0129 21)	0: H<1 1: 1≦H<2 2: 2≦H<3 3: 3≦H<4 4: 4≦H

Note 1) β: The ratio of distance from axial of neuturality to center of reinforcing steel to distance from axial of neuturality to tensile side in the case of beam 1.2

A: The area of tensile side concrete of symmetry with steel number of reinforcing steel

Note 2) Superpose the development strength at the age {SN=-55.32+16.60ln(365t)} {DN=-41.49+12.45ln(365t)}

2.4 Quantifying Change of Deterioration in Time by Deterioration Indicator

In the case that the deterioration indicators are varied by plural deterioration phenomenon, the progress of deterioration is distinguished by the assumptions which are shown in Table 3. The equation and data to quantify the change of indicator in time correspond to the deterioration phenomenon distinguished. In the case that the progress of deterioration is not described with an equation in general, the data was analyzed and adjusted by regression analysis statistically. The increase of the indicator of each deterioration phenomenon are calculated by the equation and they are added by the relation as shown in Table 3. The indicators of each quantifying item are made with the sum. However, crack and deformation are assumed that they occur at the early stage because the setting up of the condition to calculate the occurrence and the change in time are complex.

Table 3. Relation between quantifying item (deterioration indicator) and deterioration phenomenon

Item	Deterioration Phenomenon												
	Neutralization	Reinforcing Steel Corrosion	Crack	Deterioration of Strength	Deformation	Frost Damage	Surface Deterioration	Dry Shrinkage and Thermal Shrinkage	Alkali-Aggregate Damage	Strain of Creep	Diffusion of Chloride	Crack of Steel Stress	Diffusion of Sulfate
Neutralization (Neutralization depth: mm)	●												
Reinforcing steel corrosion (Ratio of corrosion surface: %)	■	○	■					△	△		●	△	
Crack (Width of crack: mm)			○					●	●			●	
Deterioration of strength (Ratio of compressive strength: %)				○		■			●				●
Deformation (Strain: %)					○			●		●			
Frost damage (Change rate in relative dynamic modulus of elasticity: %)						●							
Surface deterioration (Average depth of damage: mm)						■	○						

Table 3 Note 1) ●: Deterioration phenomenon which vary deterioration indicator and are converted to the indicator.
○: Deterioration phenomenon which subordinate other deterioration phenomenon and are not converted to deterioration indicator.
■: Deterioration phenomenon which subordinate other quantifying item and are converted to deterioration indicator.
△: Deterioration phenomenon which are subordinated the Case (3) and are not converted to deterioration indicator.

2.5 Investigation of Grading for Degree of Deterioration

The maximum values of the varying indicators are assumed. They are divided with proportion and so on, and made to grade from 0 to 4. The grading is shown in Table 2.

2.6 Calculation of Synthetic Degree of Deterioration

The synthetic degree of deterioration are calculated by equation (1). The number of items quantifying are seven.

$$\text{SYNTHETIC DEGREE OF DETERIORATION} = \sqrt[2]{\sum_{i=1}^{7} \left(Ai^2 \cdot \frac{\alpha i}{100}\right)} \quad \cdots\cdots\cdots\cdots (1)$$

Where Ai is the average degree of deterioration and αi is weight of deterioration at the each item ($\sum_{i=1}^{7} \alpha\, i=100$).

3. APPLICABLE INVESTIGATION FOR EXISTING STRUCTURES

The external forces of deterioration of existing structures, the value of design and the number of years at the investigation were inputted and calculated. The results were compared to the actual deterioration, and those applicable for existing structures were examined. The conditions of the existing structure, which was a wharf, and shown in Table 4 were inputted. The change in time of the item quantifying were calculated and shown in Fig. 2 from 1 to 7 , but the calculation was done without considering crack because cracks occurred at the early stage and was maintained at the beginning. The rate of the depth of neutralization and the corrosion of reinforcing steel of the actual data were very much faster than the calculation showed. The reason seemed to be the effect of crack which occurred at an early stage. The structural safety and fire proof capability were assumed to be the capability of the structures, and the weight of capability were assumed to be shown in Table 5. The synthetic degree of deterioration was calculated and shown in Fig. 2.

Table 4. Data of actual structures for examination

Factor		Mark: Parameter (unit)	Actual Structure	
			Wharf(A)	Wharf(B)
External factor	External factor of deterioration	t: Service life (year)	18	24
		L: Distance from sea (m)	1	1
		Co: Amount of chloride from sea (Wt%)	1.3	0.33
		Ic: Change of temperature (°C)	30.3	33.3
		S: Concentration of sulfate of water contacted surface (Wt%)		
		M: Cycles of freeze-thaw a year	5	5
		W: Coefficient of supplying seawater	0.5	0.5
Inner factor	Design	D: Depth of cover (mm)	75	50
		fs: Stress of reinforcing steel (kgf/cm^2)	816	1,400
		α: Stress of concrete (kgf/cm^2)	17.4	50.0
		β: Note 1	1.2	1.2
		A: Note 2 (cm)	260	62.5
		b: Width of the section (m)	0.80	0.50
		h: Depth of the member (m)	1.30	0.60
		WH: Number of steel members	4	4
		ϕ: Diameter of the steel (m)	0.029	0.019
	Material	fc: Compressive strength of concrete (kgf/cm^2)	271	344
		fct: Tensile strength of concrete (kgf/cm^2)	* 27.1	* 34.4
		fb: Average bond strength of concrete and steel (kgf/cm^2)	* 54.0	* 68.9

Factor		Mark: Parameter (unit)	Actual Structure	
			Wharf(A)	Wharf(B)
Inner factor	Material	Ec: Youngs modulus (kgf/cm^2)	2.58×10^5	3.29×10^5
		ϕ: Coefficient of creep	2.0	2.0
		W/C: Water cement ratio (%)	49.1	62.0
		Uc: Unit weight of cement (kg/m^2)	320	282
		Uw: Unit weight of water (kg/m^2)	157	174
		Type of cement R: Type of AE agent Type of aggregate	0.6	0.6
		Ru: Amount of Na_2O in aggregate by cement (%)		
		RG: Content of reactionable aggregate (%)		
		AE or Non AE: Whether there is AE agent	AE	AE
		Dc: Diffusivities of concrete (cm^2)	1.6×10^{-8}	0.44×10^{-8}
	Construction	α: Coefficient of type of cement and curing condition	0.0129	0.0129
		K: Ratio of decreasing surface strength		
		γ: Index of workability: γ=1	1.0	1.0
Result of investigation		x: Depth of neutralization (mm)	19.0	15.1
		p: Corrosion surface	70	65
		Crack etc.	Loss of cover	Loss of cover

Note (1) β: The ratio of distance from axial of neuturality to center of reinforcing steel to distance from axial of neuturality to tensile side in the case of beam 1.2

Note (2) A: The area of tensile side concrete of symmetry with steel number of reinforcing steel

Table 5. Assumption of weight for capability demanded in each item quantified

Capability of structure	Structure safety	Fire proof capability	Factor of weight ( )
Weight of capability	80%	20%	
Neutralization	4%	7%	5%
Reinforcing steel corrosion	58%	20%	50%
Crack	8%	20%	10%
Deterioration of strength	20%	20%	20%
Deformation	4%	7%	5%
Frost damage	3%	13%	5%
Surface deterioration	3%	13%	5%
Total	100%	100%	100%

Fig. 2. Example of calculation for actual structure

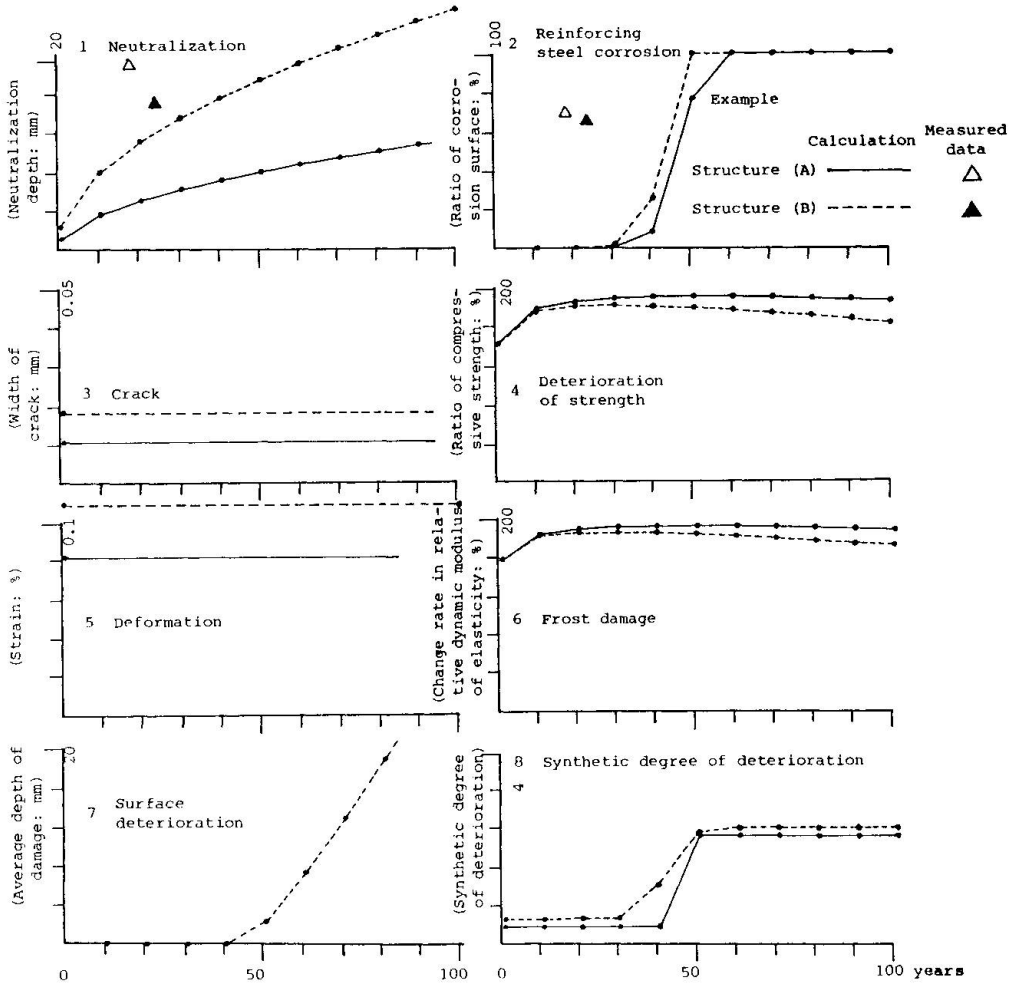

4. FUTURE PROBLEMS

For developing the technique for quantifying durability of reinforced concrete structures, the following studies are needed for further application of the technique.

1) The mechanisms and the factors of deterioration must be understood and readjusted. F.T.A. (Fault Tree Analysis) and so on must be put into practice.
2) The measuring and understanding of the rate of damage occurrence, and the grading must be studied.
3) The capability and the weight of capability must be examined using many cases of deterioration in existing structures and items of quantified deterioration should be weighted to each of them.
4) Many detailed experiments combined with accelerated tests and exposed tests of items quantifying deterioration must be put into practice.
5) The pursuit of investigation into existing structures which are calculated with synthetic degrees of deterioration, must be put in practice for many years.

Thus what is demanded now is a systematic study for the development of the technique for quantifying durability of reinforced concrete structures.

REFERENCES

1) Building Research Institute: Development in maintenance of existing structure and improvement of durability of new building, report of committee of Ministry of Building, 1984
2) Building Research Institute: Report of the second department of Building Research Institute at spring lecture, 1985
3) ANSI/ASTM: "Standard Recommended Practice for Developing Short Term Accelerate Tests"
4) K. Kishitani: "Durability of Reinforced Concrete", Kajima Shuppankai
5) K. Kashino: "Investigation of effect of chloride from sea for building", The third edition of ARAKA, 1985
6) H. Nagano: "Application of Diffusion Theory for Chloride Penetration into Concrete Located at Splashing Zone", JCI 7th Conference, 1985
7) K. Takewaka, "Estimation of Steel Corrosion in Concrete Structure by Autoclave Process", JCI 4th Conference, 1982
8) Y. Tomozawa: "The problem in neutralization", Seko No. 229, 1985
9) M. Yachida: "Research for Cracks of Concrete Bridges and Corrosion of Reinforcement", JCI 6th Conference, 1984
10) H. Kamiyama: "Crack of Concrete and Corrosion of Steel", CAJ REVIEW of The 31 GENERAL MEETING, 1977
11) ACI 224 Committee: "ACI standard of structural design (ACI 318-77)", ACI, 1977
12) BSI: BS5337 "The Structural use of concrete for retaining aqueous liquids", 1976
13) The Society of Material Science Japan: "Symposium about Alkali-Silica Reaction, 1985
14) H. Ikenaga: "The deterioration of concrete soaked in water which are different kind and concentration of acid and chloride", 1976
15) K. Ayuta: "The Effect of Aggregate in durability of freeze and thaw", Hokkaido branch of JSCE Conference, 1976
16) S. Ito: "New edition of Concrete Engineering", Morikita Shuppan
17) H. Yamashita: "Basic Experiment of reaction aggregate (NO. 1)", JSCE Conference
18) JSCE: "Specification of Reinforced Concrete", 1980
19) JCI: "Point of Concrete technique'82", JCI, 1982
20) H. SAKURAI: "Progress Degree of Scaling on Concrete Surface", Hokkaido branch of JSCE Conference, 1980
21) H. SAKURAI: "Some Experiments of Progress Degree of Scaling on Concrete Surface", JSCE Conference, 1980

Aspects of Moisture Flow in Hardened Cement Paste and Concrete

Transport de masse dans la pâte de ciment durcie et dans le béton

Feuchtigkeitsdiffusion in erhärtetem Zementstein und in Beton

Cornelis L. KAMP
Struct. Engineer
Swiss Fed. Inst. of Techn.
Lausanne, Switzerland

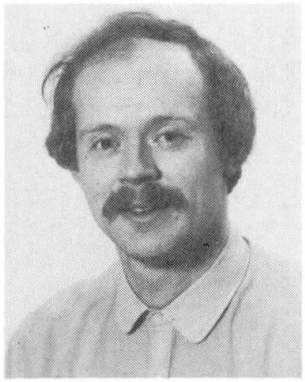

Cornelis L. Kamp, born 1955, got his civil engineering degree at Delft University of Technology, with honours, in 1981. He worked for several years as a structural engineer at DHV engineering consultants, Amersfoort, and joined the Laboratory for Building Materials at the Swiss Federal Institute of Technology, Lausanne, in 1984.

Pieter E. ROELFSTRA
Civil Engineer
Swiss Fed. Inst. of Techn.
Lausanne, Switzerland

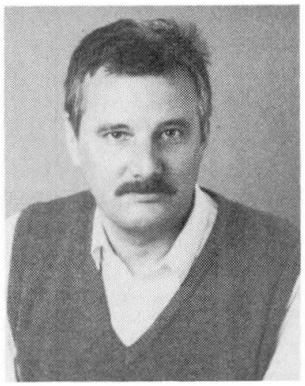

Pieter E. Roelfstra, born 1946, got his civil engineering degree at Delft University of Technology. For 12 years he was involved in structural engineering at the Ministry of Public Works. Actually he is head of the group Modelling and Numerical Analysis of the Laboratory for Building Materials at the Swiss Federal Institute of Technology, Lausanne.

Folker H. WITTMANN
Professor
Swiss Fed. Inst. of Techn.
Lausanne, Switzerland

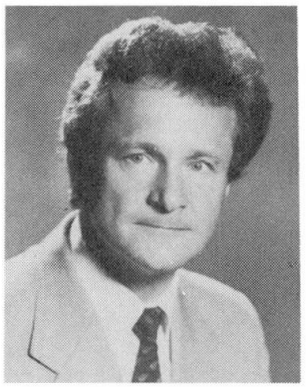

Folker H. Wittmann, born 1936, habilitated in Physics of Building Materials at Munich Institute of Technology. For 4 years he was professor for Building Materials at Delft University of Technology, The Netherlands. He is now professor and director of the Laboratory for Building Materials at the Swiss Federal Institute of Technology, Lausanne.

SUMMARY
Different mechanisms of moisture flow in porous media are outlined. Several models are developed and discussed. On the basis of these models it is possible to explain a number of effects commonly observed on drying hardened cement paste and concrete. Numerical methods are applied to test the models quantitatively.

RÉSUMÉ
On discute les différents mécanismes de transport de masse dans les milieux poreux. Des modèles de la structure poreuse de la pâte de ciment durcie sont proposés. Ces modèles permettent d'expliquer les phénomènes habituellement observés lors du séchage de la pâte de ciment durcie et du béton. Des prédictions quantitatives sont obtenues avec des méthodes numériques.

ZUSAMMENFASSUNG
Unterschiedliche Transportmechanismen der Feuchtigkeitsdiffusion in porösen Werkstoffen werden betrachtet. Mehrere Modelle werden entwickelt und diskutiert. Mit Hilfe dieser Modelle ist es möglich, eine Reihe von Erscheinungen, die man gewöhnlich bei trocknendem Zementstein und Beton beobachtet, zu erklären. Mit numerischen Methoden gelingt es über die Modelle zu quantitativen Aussagen zu kommen.

1. INTRODUCTION

HCP (hardened cement paste) has a large internal specific surface and therefore all properties are strongly influenced by moisture content. In addition it is well-known that moisture diffusion is a very slow process. That means that time-dependent moisture gradients exist for a long time in concrete elements. Creep, shrinkage, and crack formation depend essentially on the moisture distribution in a specimen and the stresses created by moisture gradients.

Moisture fields are generally calculated with the diffusion equation :

$$C(H)\,\frac{\partial H}{\partial t} - \nabla \cdot \lambda(H)\nabla H = Q \qquad (1)$$

where : $C(H)$ = moisture capacity, $\lambda(H)$ = permeability coefficient, H = moisture potential, and Q = moisture source.

A convenient choice for the moisture potential is relative humidity; other quantities are sometimes preferred, e.g. suction height. Thermodynamics solely requires that the quantity chosen is uniquely related to the energy of the pore water per unit mass.

The functions $C(H)$ and $\lambda(H)$ are normally determined by experiments. They are defined with the following equations :

$$C(H) = du/dH \qquad (2)$$

$$J = -\lambda\,\nabla H \qquad (3)$$

where : J = total water flux, u = water content.

It has to be mentioned, however, that these functions are very difficult to be determined experimentally. These functions depend both on the porous system and on the environmental conditions i.e. the relative humidity and temperature. If one would try to study all those influences in detail it would mean an enormous series of time-consuming experiments. This fact justifies a more thorough analysis of the problem.

2. PHYSICAL ASPECTS OF STORAGE AND FLOW OF MOISTURE

Only a brief review of the main points will be given here. The reader is referred to /7/ for a more thorough discussion.

Porous media can retain liquid water at relative humidities below 100%. Two mechanisms prevent evaporation of the pore water : physical adsorption and capillary condensation.

Physical adsorption is generally viewed as a piling up of molecules on a plane surface, in the presence of attractive forces in the neighborhood of the surface of an adsorbent. Several quantitative treatments have been proposed; the one developed by Brunauer, Emmett and Teller /3/ is the most frequently used.

Direct measurement of physical adsorption is only possible below 40% RH in HCP; above this value capillary condensation falsifies the measurements. An indirect approach is possible, which requires the following steps :

a. Measurement of the specific surface area in the low-humidity region with the BET-method.

b. Measurement of the physical adsorption on a similar solid in which capillary condensation does not occur.

c. Correction of the results obtained under b) for the different surface areas.

Figure 1 shows results obtained by Badmann /1/ for adsorption on unhydrated cement. These results are probably reliable below some 80% RH; above this value, the cement begins to hydrate noticeably.

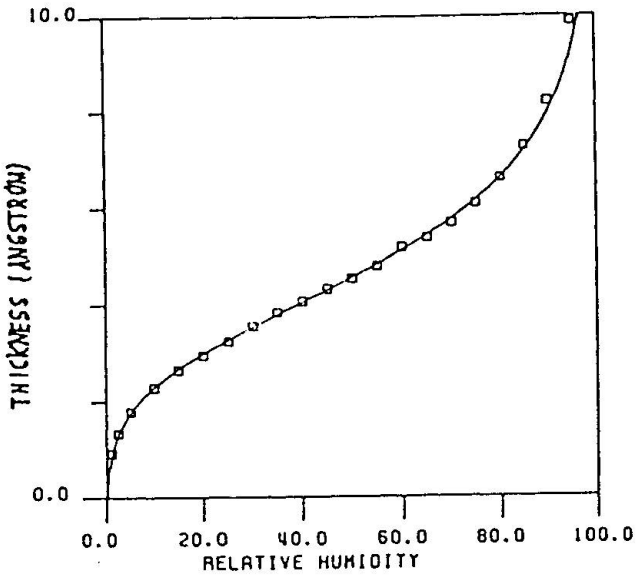

Fig. 1 Physical adsorption on unhydrated cement /1/.

Measured specific surface areas of HCP range from 100 to 250 m^2/g; other adsorbates such as N_2 yield only some 20% of this value. This suggests the presence of a "hidden" porosity in the solid material which is accessible to water, but not to nitrogen. The same explanation was proposed by Diamond /4/ for the strikingly different pore-size distributions determined by mercury-porosimetry and vapour adsorption. It might also explain why specific surface areas calculated from pore-size distributions are generally lower than BET-areas determined from the water-vapour sorption isotherm. The second mechanism, capillary condensation was explained by Kelvin, who showed the vapour pressure above a curved liquid surface to be related to surface curvature and surface energy by the following equation :

$$P \simeq P^S \exp(-\frac{\sigma V K}{RT}) \qquad (4)$$

where : P = vapour pressure, P^S = saturated vapour pressure, σ = surface energy, V = molar volume of liquid, K = total surface curvature, R = universal gas constant, and T = absolute temperature.

Application of equation (4) to a porous medium requires the introduction of a

pore model, which permits to relate the curvature K to the pore radius r. The most frequent choice is that of a cylindrical pore with a spherical liquid surface, leading to :

$$K = 2/(r-t) \tag{5}$$

where t is the thickness of the physically adsorbed layer. Note that it is more correct to use only half of the curvature given by equ. (5) in case of adsorption.

Introduction of the corresponding values for water in equations (4) and (5) shows that at 90% RH all pores with radii smaller than 10 nm are filled with liquid water; at 40% RH the critical pore radius has dropped to 1.2 nm.

Several mechanisms contribute to the flow of moisture, owing to the presence of several phases : liquid, vapour, and adsorbate.

Liquid flow is sufficiently slow to be purely laminar. Not even convective effects caused by the continuously varying cross section need to be taken into account. The following equation for the permeability coefficient λ^L can be derived for a porous medium :

$$\lambda^L = \frac{eRT}{36\nu vH} \frac{\langle r^4 \rangle_f}{\langle r^2 \rangle_a} \tag{6}$$

where : e = porosity, ν = kinematic viscosity, v = molar volume of the liquid, $\langle\ \rangle_f$ = average to be taken over the pores filled with liquid, $\langle\ \rangle_a$ = average over all pores, and r = pore radius.

Equation (6) is subject to the limitation that the pore-size distribution be uniform in space. In that case, there is a sufficient number of paths around obstacles such as wide pores which contain only vapour. The correction for the somewhat longer flow path in this case is fully accounted for in equ. (6) (see Matheron /8/).

Vapour flow in HCP is not diffusive as is generally assumed. The pore diameters in HCP are small in comparison with the mean free path of water vapour in air, so that molecule-wall interactions dominate molecule-molecule interaction. This type of gas transport is commonly termed "Knudsen diffusion", although the word diffusion is quite misleading. The permeability coefficient for vapour transport λ^V for a porous medium is given by the following equation :

$$\lambda^V = \frac{4}{27} \frac{e\, p^S\, M\bar{c}}{RT} \frac{\langle (r-t)^3 \rangle_e}{\langle r^2 \rangle_a} \tag{7}$$

where : M = molar mass, $\bar{c}$ = average thermal velocity, and $\langle\ \rangle_e$ = average to be taken over "empty" pores, i.e. pores not filled by capillary condensate.

The third mechanism flow of the adsorbed layer, will not be considered in this paper. At this time there is not enough reliable information on this phenomenon. There are indications that the mechanism is only of secondary importance in HCP; the heat of adsorption of some 75 kJ/mole corresponds to a surface diffusivity of only $\pm\ 10^{-8}$ cm^2/s. Radjy /9/ showed that flow of the adsorbed layer is negligible under these circumstances. Further support can be found in the generally observed decrease of the permeability between 0 and 40 % RH; if surface flow would have a major contribution an increase in this interval would have to be expected.

3. A MODEL FOR MOISTURE FLOW IN HCP

Figure 2 shows a model which was developed to represent the porous structure of

HCP. The main feature of the model is the assumption that HCP is not a homogeneous porous system, but it is composed of different pore systems. The finest pores are the gel pores within the hydration products. They have been determined to be within a narrow band situated around 4 nm. In the microstructure of HCP these clusters are separated by coarser pores. It is supposed that the second and coarser pore system is centered around an average value of 20 nm. The exact meaning of this bi-porous system will be discussed in comparison with microstructural data elsewhere.

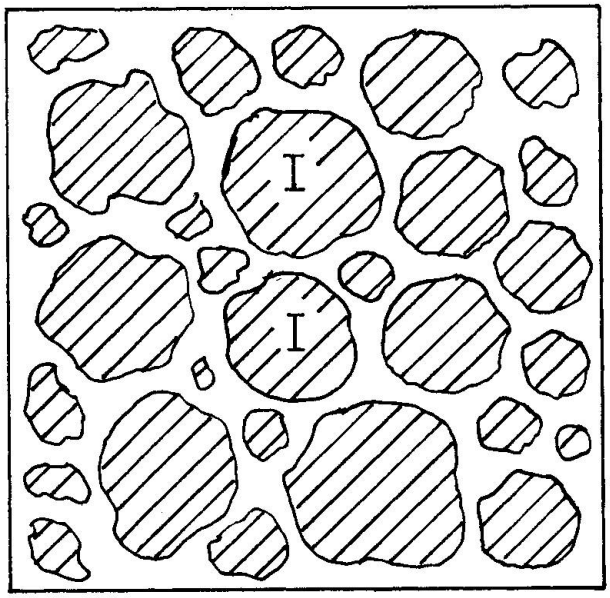

Fig. 2 Model microstructure of HCP.

The permeability coefficient of HCP is much lower than the values predicted by equ. (6) for liquid flow, even when a reasonable increase of viscosity in the narrow pores is alowed for. The model explains this by the interruption of the liquid flow paths. Vapour flow only is possible in the inter-cluster space, unless the porous system is fully saturated.

The model explains the sharp increase of the permeability coefficient at about 80% RH by capillary condensation and ensuing liquid flow inside the clusters (regions I, fig. 2). At low humidities these regions are obstacles; their small pores permit only a small amount of vapour flow. Capillary condensation at high relative humidity, however, frees the way for low-resistance liquid flow; thus all regions with high resistance are systematically converted into regions with low resistance.

Remark that the model is quite insensitive to the precise flow resistance in regions I; these regions act either as obstacles (low RH) or as short circuits (high RH) for the vapour flow through the porous material. The flow mechanisms in the inter-cluster space are much better known; the water in these large pores behaves "normally", and flow of the adsorbed surface layer is definitely negligible. The global flow is dominated by the transport through the intercluster space and the mechanisms within the clusters only modify this transport phenomenon.

As an illustration of the model we calculated the moisture capacity and permeability coefficient of HCP on the basis of the following data :

- Volume concentrations: finely porous material (clusters) 61%, intercluster space 39%.
- Total porosity: 28%, of which 72% is the finely porous material, and 28% is the coarser one.

The pore size distribution of this model material is shown in Figure 3.

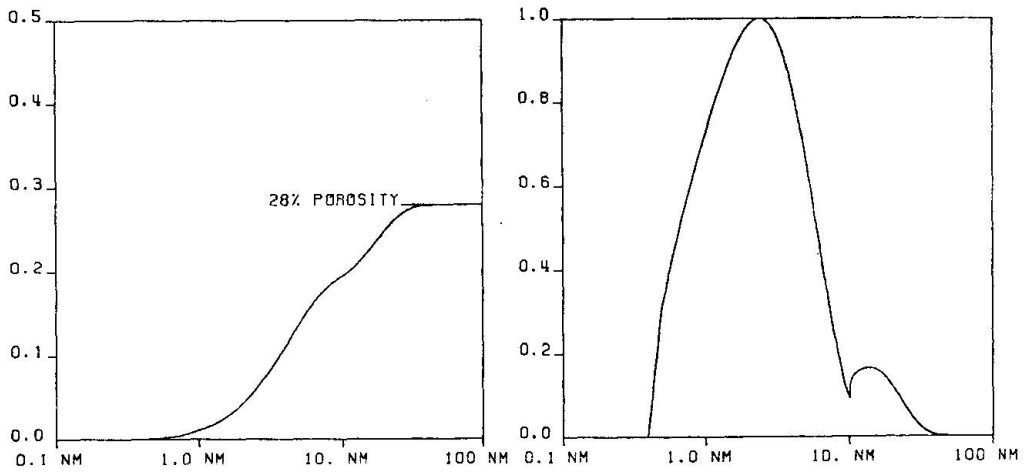

Fig. 3 Cumulative and differential pore size distribution.

Note that this distribution has been generated in a computer by simulating two Weibull distribution functions for the bi-porous model material. By changing the structural parameters, different pore size distributions can be obtained. Permeabilites, capacities, and sorption isotherms were calculated for this model material in a 2D random pore network. For the calculation of the permeability coefficient we generated the random structure shown in Figure 4 (circles represent clusters of hydration products). This structure can be analysed with the software developed for "numerical concrete" /10/ after proper modifications.

The calculated permeability coefficient is shown in Figure 5.

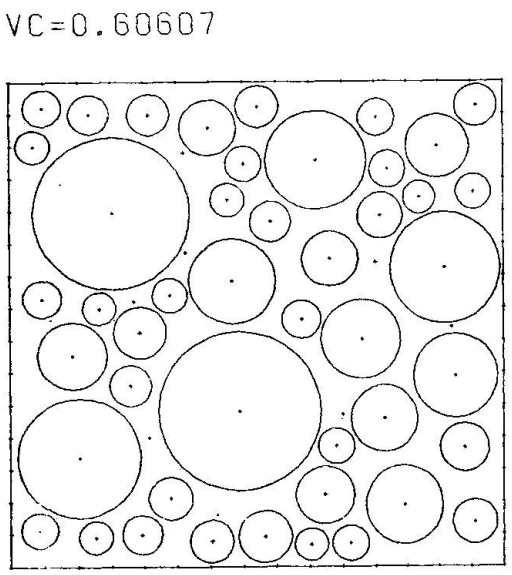

Fig. 4 Numerical model of microstructure.

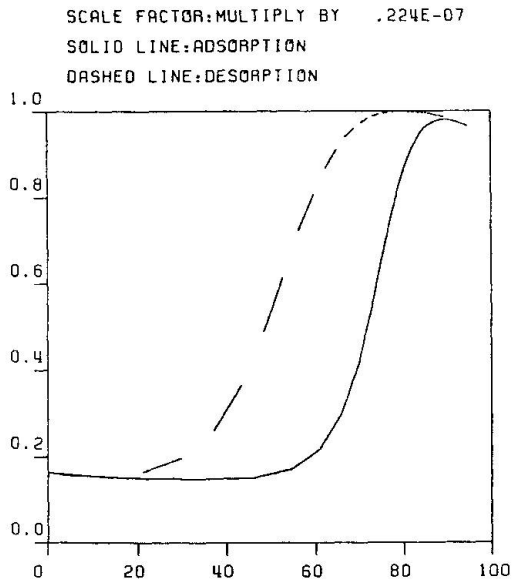

Fig. 5 Permeability coefficient.

The precise numerical values depend strongly on the chosen pore-size distribution of course. The maximum value is somewhat high as compared with experimental values. Better agreement could be reached in modifying the pore size distribution. This is not our aim, however, at the moment. The general validity of the model has been shown. The same applies for the strong increase of the permeability which lies usually around 70% for desorption. The calculated sorption isotherm and moisture capacity are shown in Figures 6 and 7.

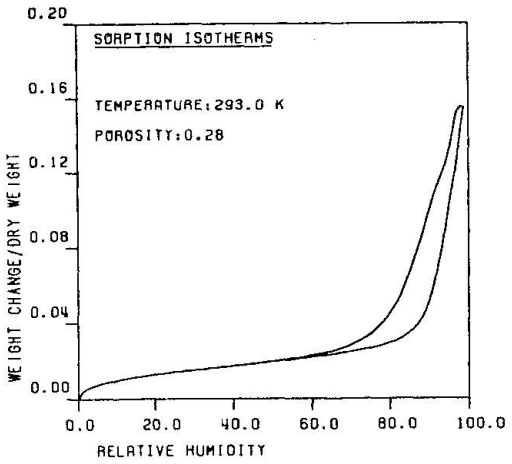

Fig. 6 Calculated sorption isotherm.

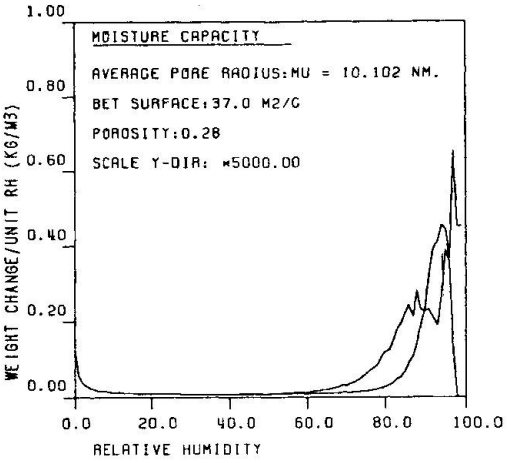

Fig. 7 Moisture capacity.

The calculated isotherms differ markedly from experimental results (see e.g. the curves published by Hundt /6/, Figure 8). Particularly desorption isotherms are much less convex at room temperature. This may be partly due to the so-called ink-bottle effect / 5 /; Figure 9 shows an isotherm in which this effect is taken into account. Surprisingly the calculated curves correspond much more closely to those measured at 70°; this cannot be explained on thermodynamical grounds, nor by the coarsening of cement gel, which is rather limited at this temperature.

In accordance with equation (1), the high capacity around 80% RH strongly delays drying; the phenomenon is analogous to the effect of phase changes in heat transfer problems. As a consequence, drying is predicted to be more rapid at, say, 70% RH than at 80% RH, which is in contradiction with experimental observation. Clearly, more research is necessary before a satisfactory description of the desorption isotherm is possible.

4. TRANSPORT PHENOMENA IN CONCRETE

The functions C(H) and λ(H) discussed in the previous chapter were used to simulate the drying of concrete with the methods of numerical concrete /10/ and /11/. The addition of aggregates has several consequences. The most obvious one is a reduction of permeability and moisture capacity. A second effect is the

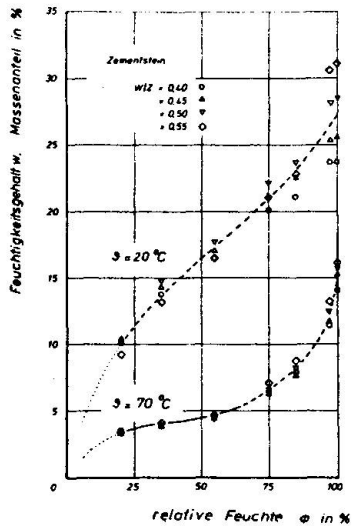

Fig. 8 Measured desorption isotherms /6/.

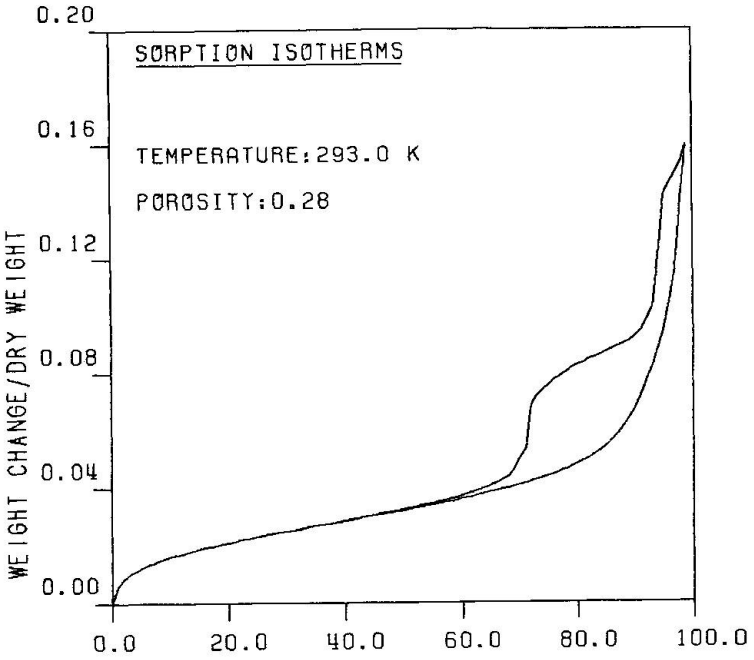

Fig. 9 Sorption isotherm, ink-bottle effects included.

introduction of highly process interfaces between matrix and aggregates, which facilitates flow at high humidities. Finally, voids are introduced in the material during mixing. The water contained in these voids and interfaces must flow away through the dense matrix before a true equilibrium state has been reached. As the quantities of excess water are usually not well known this must falsify the determination of diffusion coefficients from weight loss curves.

Theoretical aspects of the analysis are discussed in the invited lecture of Wittmann and Roelfstra /12/ for this conference.

Bazant /2/ found a relation for the humidity dependence of the diffusion coefficient by pure data fitting. In the present paper an attempt is made to explain the physical background of this relation. In this way it will be possible to formulate generally valid material laws. These laws can be used in a numerical analysis to predict moisture movement in real concrete structures such as large span bridges, large industrial floors, and prestressed concrete pressure vessels.

For the sake of the numerical analysis, all extra porosity of the matrix was lumped in the interfaces around the large aggregates. Figure 10 shows the weight loss curve obtained with the following data :

- Volume concentration of the big aggregates: 43%
- Total water content in interfacial regions (including voids in the matrix) at 100% RH: 1800 kg/m^3 relative to the interfacial volume.
- Permeability of the interfaces: $0.8 \cdot 10^{-5}$ kg/m/s.
- Thickness of the interfaces: 50μ.
- Zero capacity and permeability of the interfaces below 98% RH.

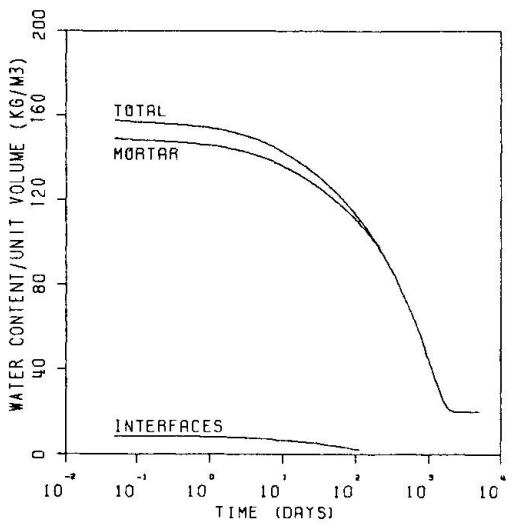

Fig. 10 Weight loss curve of concrete, drying from 100% to 50% RH.

The sharp kink in the curve is due to the convex form of the simulated desorption isotherm mentioned above which is usually not observed experimentally. With a refined model this can be overcome.

5. CONCLUSIONS

1. A bi-porous model material has been developed in order to describe the influence of moisture content on permeability coefficient and moisture capacity. This model can be adjusted to describe different transport mechanisms in HCP and concrete realistically.
2. The influence of temperature on moisture diffusion is predicted.
3. Based on this concept material parameters for diffusion in different types of concrete and under arbitrary climatic conditions can be indicated and used in computerized structural analysis.

ACKNOWLEDGEMENT

Financial support of the Swiss National Fund for scientific research under grant Nr. 2.845-0.85 is gratefully acknowledged.

REFERENCES

1. BADMANN, R., STOCKHAUSEN, N., SETZER, M., The statistical thickness and the chemical potential of adsorbed water films, Journal of Colloid and Interface Science, Vol. 82, No. 2, August 1981, pp. 534-542.

2. BAZANT, Z.P. NAJJAR, L.P., Drying of concrete as a nonlinear problem. Cement and Concrete Research, Vol. 1, pp. 461-473 (1971).

3. BRUNAUER, S., EMMETT, P.H., TELLER, E., Journal of the American Chemical Society, 60, 309 (1938).

4. DIAMOND, S., Cement and Concrete Research, Vol. 1, pp. 531-545 (1971).

5. GREGG, S.J., SING, K.S.W., Adsorption, surface area and porosity, Academic Press, London, 1982 (2nd edition).

6. HUNDT, J., KANTELBERG, H., Sorptionsuntersuchungen an Zementstein, Zementmörtel und Beton, Deutscher Ausschuss für Stahlbeton, Heft 297.

7. KAMP, C.L. WITTMANN, F.H., The mechanisms of moisture flow through porous materials, Second International Colloquium "Materials Science and Restoration", September 1986, Technische Akademie Esslingen.

8. MATHERON, G., Eléments pour une théorie des milieux poreux, Masson et Cie., Paris, 1967.

9. RADJY, F., Moisture transport in microporous substances, Journal of Materials Science, 9 (1974) 744-752.

10. ROELFSTRA, P.E., Numerical concrete, PhD Thesis, EPF Lausanne, 1987.

11. ROELFSTRA, P.E., SADOUKI, H., WITTMANN, F.H., Le béton numérique, Matériaux et Constructions, 107 (1985) pp. 327-335.

12. WITTMANN, F.H., ROELFSTRA, P.E., Applications of numerical concrete to the study of transient phenomena in concrete.

Simulation of the Mechanical Behaviour of Young Concrete

Simulation du comportement mécanique de béton jeune

Simulation des mechanischen Verhaltens von jungem Beton

Peter A.J. van den BOGERT
Delft Univ. of Techn.
Delft, The Netherlands

René de BORST
TNO-IBBC
Delft, The Netherlands

Pier NAUTA
TNO-IBBC
Delft, The Netherlands

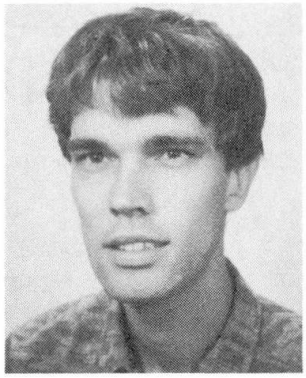

Peter A.J. van den Bogert, born 1961, got his civil engineering degree at Delft University of Technology in february 1987. He is presently employed at Delft University to develop numerical tools for the prediction of the mechanical behaviour of rubberlike solids.

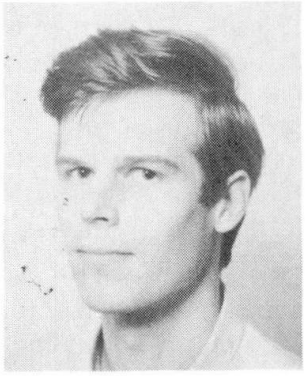

René de Borst, born 1958, earned his Ir. degree in civil engineering in 1982 and his Dr. degree in 1986, both from Delft University of Technology. He has been a member of the DIANA group of the TNO Institute for Building Materials and Structures since 1982.

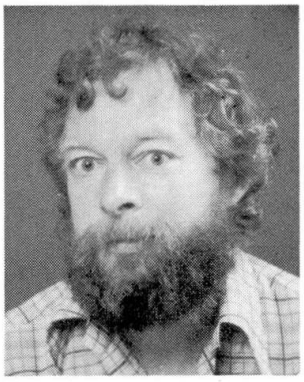

Pier Nauta, born 1947, earned his Ing. diploma in 1969 from HTS at Leeuwarden. He has been a member of the DIANA group of the TNO Institute for Building Materials and Structures since 1979.

SUMMARY

A model for the simulation of the time-dependent mechanical behaviour of concrete at an early age is outlined. Next, an efficient algorithm is derived for this model. The model is verified with experimental data. To demonstrate the applicability of the model, the stress is calculated as a function of time for an axisymmetric structure.

RÉSUMÉ

Un modèle pour la simulation du comportement mécanique du béton en fonction de l'âge est présenté pour un béton jeune. Un algorithme efficace est dérivé de ce modèle. Le modèle est vérifié à l'aide de données expérimentales. Afin de montrer la valeur du modèle, la contrainte est calculée comme une fonction du temps pour une structure axisymétrique.

ZUSAMMENFASSUNG

Ein Modell zur Simulation der zeitabhängigen Eigenschaften von jungem Beton wird beschrieben. Danach wird ein leistungsfähiger Rechenalgorithmus abgeleitet. Das Modell wird an Versuchsresultaten verifiziert. Die Anwendung wird an einem symmetrischen Betonbauteil demonstriert.

1. INTRODUCTION

The material properties in a hardening cement paste develop gradually during the hydratation process in which cement forms a compound with water. This chemical process produces heat and a consequence thereof we observe an increase in temperature in the structure. Stresses are introduced when thermal volume changes are prohibited. This happens especially in concrete members with a great volume compared with the surface.

In hardening cement paste we first observe an increase in temperature owing to the generated hydratation energy. Thereafter, a "cooling process" takes place during which crack formation is often observed. The temperature increase in the first period results in compressive stresses because the thermal expansion is suppressed by the surrounding concrete. These stresses, however, will not be significant since the stiffness of the young concrete is still low. The decrease in temperature in the second phase will cause higher tensile stresses because of the greater maturity and as a consequence thereof, the higher value for Young's modulus.

Basically, the hardening of the cement paste is a coupled thermomechanical problem. Because of the weak coupling in the present case, we can suffice by solving the separate problems of heat conduction and stress development. In the first part the temperature field and a so-called degree of maturity are calculated as a function of time taking account of the heat production by the cement paste [7,8]. Thereafter, the temperature field and the degree of maturity are used as input for the calculation of the stresses in the hardening cement paste.

In this paper a creep model is employed which has the form of a double power law (e.g., also [1]). The power law is developed in a Taylor series to make the model suitable for implementation in numerical programs. Experimental measurements are used to derive parameters for the model [6]. The model and the derived material parameters are subsequently employed in a finite element analysis of a cover element for a breakwater. Attention is also paid to the communication between the heat conduction analysis and the mechanical problem.

2. HEAT PRODUCTION IN HARDENING CEMENT PASTE

The hydratation process can be characterized by different parameters (e.g., [4,7,8]). In this paper Reinhardt [7,8] will be followed, and the degree of maturity $r(t)$ is employed, which is defined as the quotient of the accumulated heat production $Q(t)$ at time t and the total heat production at infinity Q_∞:

$$r(t) = \frac{Q(t)}{Q_\infty} \tag{1}$$

The actual heat production q $[J/m^3s]$ at time t is calculated using [8]:

$$q = q_{max}\, f(r) = a\, e^{-b/T} f(r) \tag{2}$$

with a and b material constants, T the absolute temperature $[K]$ and $f(r)$ the heat production characteristic. $f(r)$ is a function of the degree of maturity and must be determined experimentally.

Next, an evolution formula for Young's modulus can be developed based upon the known temperature $T(t)$ and the degree of maturity $r(t)$. In this paper, the expression proposed by Reinhardt, Blaauwendraad and Jongedijk [8] is utilized:

$$E(t) = E_0 \int_0^{r(t)} \left\{\frac{T}{273}\right\}^7 \left\{1 - \exp\left[\frac{-\beta\,(t-\tau)}{(T/273)^6}\right]\right\} dr(t). \tag{3}$$

In eq. (3), τ is the time at which the increment dr is added, E_0 is the initial value of Young's modulus, which depends on the amount of cement, and β is a "delay" factor. In the example which will be discussed in a subsequent section, the values E_0=20000N/mm^2 and β=0.075 have been employed.

3. VISCO-ELASTIC MODEL

The creep behavior of young concrete will be described with a visco-elastic model. As point of departure the creep formulation

$$\varepsilon_{ij}(t) = C_{ijkl} \int_0^t \frac{1}{E(\tau)} J(t-\tau)\, \dot{\sigma}_{kl}(\tau)\, d\tau, \tag{4}$$

is used. In eq. (4), $\dot{\sigma}_{kl}(\tau)$ is the the stress rate tensor, $E(\tau)$ is Young's modulus at $t=\tau$, $J(t-\tau)$ is a dimensionless function which describes the creep behavior and the summation convention is employed for repeated subscripts. The compliance term $1/E(\tau)$ is usually combined with $J(t-\tau)$ in a creep function, but this convention is not followed here because of the important role of the time dependent Young's modulus. Furthermore, the fourth-order tensor C_{ijkl} is defined by:

$$C_{ijkl} = \tfrac{1}{2}(1+\nu)[\delta_{ik}\delta_{jl} + \delta_{il}\delta_{jk}] - \nu\delta_{ij}\delta_{kl} \tag{5}$$

with ν Poisson's ratio, which is assumed to be independent of the degree of maturity.

The function $J(t-\tau)$ has been assumed to have the following form [1,4]:

$$J(t-\tau) = 1 + \alpha\, \tau^{-d}\, (t-\tau)^p \tag{6}$$

with α, p and d material constants. The factor τ^{-d} represents the influence of the time of the application of the load on the creep behavior, while $(t-\tau)^p$ constitutes the load duration.

For $d=0$ and $p=1$ the power law of eq. (6) degenerates to the same mechanical model as a single Maxwell unit. This case as well as other integer values of p are interesting since analytical solutions can then be obtained, which permits verification of the numerical algorithm to be discussed in the next section.

4. NUMERICAL ALGORITHMS

When we define $J_c(t-\tau)=\alpha\tau^{-d}(t-\tau)^p$ and substitute eq. (6), we can rewrite eq. (4) as

$$\varepsilon_{ij}(t) = C_{ijkl} \int_0^t \frac{1}{E(\tau)} (1+J_c(t-\tau))\, \dot{\sigma}_{kl}(\tau)\, d\tau, \tag{7}$$

Differentiating eq. (7), using Leibniz' rule, assuming that $J_c(0)$ vanishes, and rearranging gives:

$$\dot{\sigma}_{ij}(t) = D_{ijkl} E(t) \dot{\varepsilon}_{kl}(t) - \int_0^t J'_c(t-\tau)\, \dot{\sigma}_{ij}(\tau)\, d\tau \tag{8}$$

In eq. (8), $J'_c(t-\tau)$ is the first derivative of J_c with respect to $(t-\tau)$. When assume that $\dot{\sigma}_{ij}(t)\Delta t = \Delta\sigma_{ij}(t)$, with Δt the time step, and define $\Delta\varepsilon_{kl}(t)$ in a similar fashion, we get for time increment n:

$$\Delta\sigma_{ij}(t) = D_{ijkl}\, E(t) \Delta\varepsilon_{kl}(t) - \Delta t \left[\sum_{q=0}^{n-1} J'_c(t-\tau_q)\, \Delta\sigma_{ij}(\tau_q) \right] \tag{9}$$

so that the stress increment $\Delta\sigma_{ij}(t)$ from t to $t+\Delta t$ can be calculated from the strain increment $\Delta\varepsilon_{ij}(t)$ of the current time step and the stress increments $\Delta\sigma_{ij}(\tau_q)$ of all previous time steps. The product of an additional strain increment $\Delta\varepsilon_{ij}(t)$ and the actual Young's modulus $E(t)$ increases the current stress, while the second term in eq. (9) describes the relaxation process. The disadvantages of algorithm (9) are the fact that the entire load history of each material point needs to be stored and that the computational times explode as the period increases which has to be analyzed. Even for modern computer equipment this is an impossible requirement if realistic engineering structures have to be analyzed.

To derive an algorithm which is more suitable for use in numerical programs, $J'_c(t-\tau)$ is developed in a Taylor series at time $t=t_0$ [5]. Alternatively, $J'_c(t-\tau)$ can be developed in a Dirichlet series (e.g., [1,3]). Indeed, long time periods can be described better using a Dirichlet

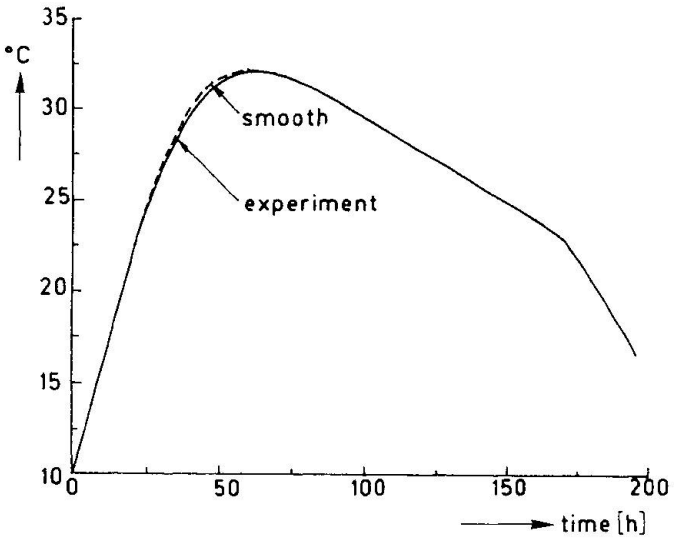

Fig. 1. Temperature functions from [6] and smooth input.

series, but for short time periods which are of interest in this study, a Taylor series is probably quite accurate. Developing $J'_c(t-\tau)$ at $t=t_0$ gives

$$J'_c(t-\tau) = J'_c(t_0) + J''_c(t_0)(t-\tau-t_0) + \frac{1}{2!}J'''_c(t_0)(t-\tau-t_0)^2 + \frac{1}{3!}J_c^{IV}(t_0)(t-\tau-t_0)^3 + \cdots \quad (10)$$

When we substitute $J_c(t-\tau)=\alpha\tau^{-d}(t-\tau)^p$, eq. (10) can be rewritten as

$$J'_c(t-\tau) = \alpha\, p\, \tau^{-d}\left[a_0 + a_1(t-\tau-t_0) + a_2(t-\tau-t_0)^2 + a_3(t-\tau-t_0)^3 + \cdots\right] \quad (11)$$

a_0, a_1 etc. are functions of the power p and of t_0. Collecting terms with the same power of τ yields:

$$J'_c(t-\tau) = \alpha\, p\, \tau^{-d} \sum_{r=0}^{m} h_r(t,t_0)\tau^r \quad (12)$$

with m the number of series used in the Taylor expansion. When $m=3$, $h_0(t,t_0)$ is defined by

$$h_0(t,t_0) = a_0 + a_1(t-t_0) + a_2(t-t_0)^2 + a_3(t-t_0)^3 \quad (13)$$

and $h_1(t,t_0)$, $h_2(t,t_0)$ are defined in a similar way. In principle, there is no restriction on the value of m, but significant gains in accuracy are usually not made by using more than five terms. Eq. (12) can be substituted in eq. (9), whereupon we get after rearranging:

$$\Delta\sigma_{ij}(t) = D_{ijkl}\, E(t)\Delta\varepsilon_{kl}(t) - \Delta t \sum_{r=0}^{m} \alpha p h_r(t,t_0)\left[\sum_{q=0}^{n-1} \tau_q^{-d}\,\tau_q^r\,\Delta\sigma_{ij}(\tau_q)\right] \quad (14)$$

Expression (14) has the desired properties, since the actual time t no longer appears in the sum over $n-1$ time steps. Every time a load step is executed the sum $\tau_q^{-d}\tau_q^r\Delta\sigma_{ij}(\tau_q)$ can be updated. In this way only m values need to be stored for each material point, and the calculation time will not grow with an increasing number of time steps.

As stated before, an analytical solution can be obtained for $d=0$ and for integer values of p. It appeared [2] that for small time steps the numerical algorithm yielded a solution which could hardly be distinguished from the analytical solution. An analytical solution could also be constructed for the case of $d=0$ and $p=\frac{1}{2}$. However, the agreement between the numerical solution and the analytical solution, which involves an error-function [2], was not as good as in the cases with the integer values for p, especially in the first hours of the simulation. This is not surprising, since a Taylor series already consists of polynomials. The error in the first hours can be

made smaller by taking a smaller value for t_0, but the consequence of doing so is that the Taylor series cannot capture the creep function accurately at later stages of the simulation. In the examples shown in this paper t_0 has been elected in the middle of the simulation period [2].

5. PARAMETER DETERMINATION

The application of the power law model to the prediction of the creep and relaxation behavior of hardening cement paste, needs realistic values of the parameters α, d and p. A direct use of values which are found in the literature is rather difficult, for similar parameters are often used in a slightly different form [1,4]. In this study the values for d range from 0.30 to 0.40, while the range for p is from 0.25 to 0.35. The specific values depend on the hardening conditions (humidity, temperature etc.) and the amount and type of cement. The shrinkage caused by drying of the hardening cement paste is not taken into account in this calculations. Incorporation of this phenomenon would result in different values of α, d and p.

Van Heyningen and Boon [6] have measured the development of the temperature, the stiffness and the stresses in concrete cubes in a laboratory environment. In Fig. 1 two temperature functions are plotted as a function of time, with the dashed line a smooth approximation. A smooth approximation of the measured time-temperature curve is used since a slight disturbance in the temperature results in a pronounced variation in the stress. The smooth temperature curve of Fig. 1 is subsequently used to determine Young's modulus with aid of eq. (3) and is compared with experimental data in Fig. 2.

The calculation of the stresses is performed on one element with a coefficient of thermal expansion of $11\times10^{-6}m/mK$ and a step size $\Delta t=1$h. is used. Figs. 3 and 4 show the development of the stress in the first 7 days for different combinations of the parameters. Unfortunately, different

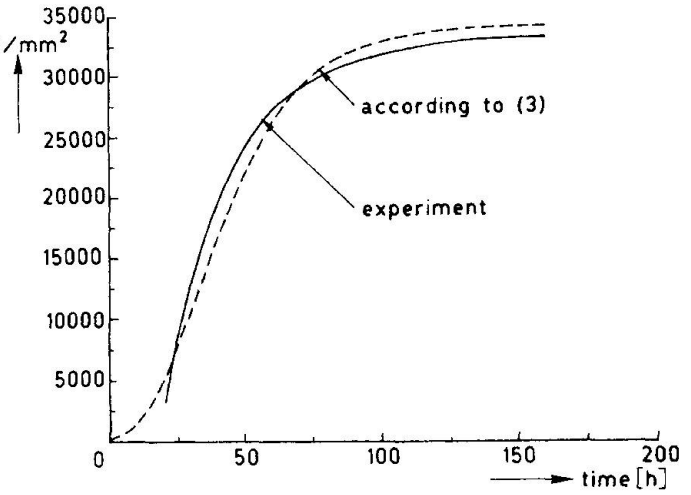

Fig. 2. Development of the stiffness $E(t)$ according to [6] and eq. (3).

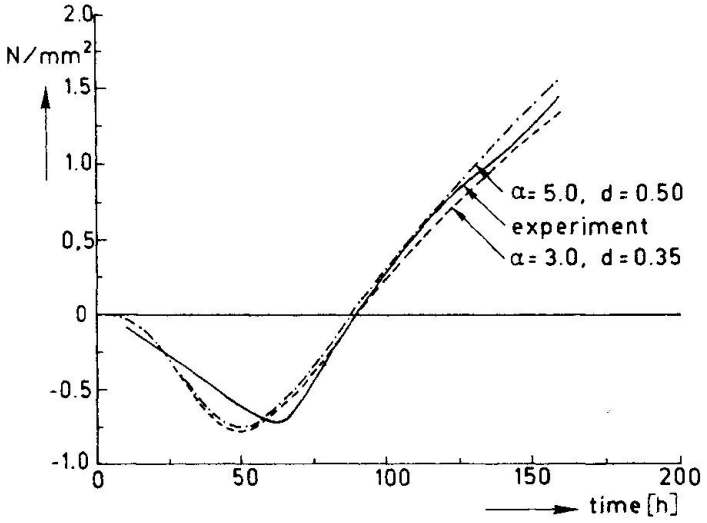

Fig. 3. Calculated stresses with $p=0.30$, $t_0=80$h., $\Delta t=1.0$h.

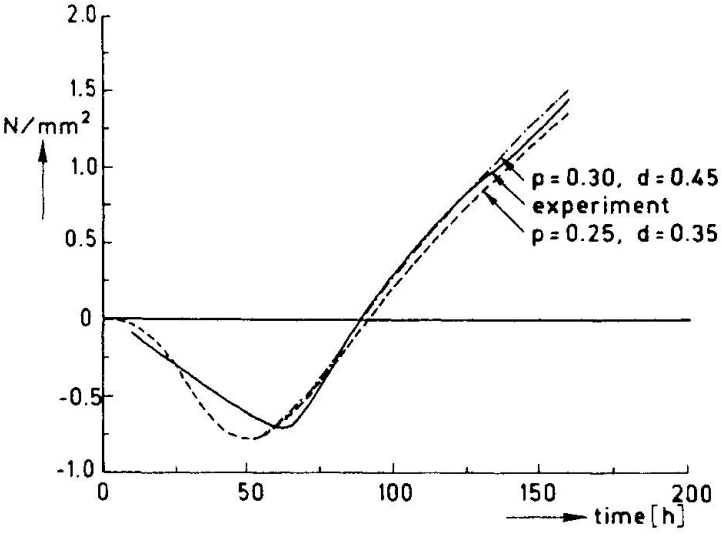

Fig. 4. Calculated stresses with $\alpha=4.0$, $t_0=80$h., $\Delta t=1.0$h.

combinations of α, d and p result in nearly the same stress history. In particular, the influence of the parameters on the peak stress is virtually the same. An increase of α yields a smaller peak stress, but the same effect can be established by increasing p or decreasing d. Moreover, an increase of α or p and a decrease of d all cause the same shift of the peak stress to a later time. To improve the stress simulation in the early hours and to control the time at which the peak stress occurs, it is necessary to extend the power law model with an additional function. When the possibility of crack formation is the primary goal of the analysis, the inaccuracies in the first 2 days are less important, since crack formation usually takes place during the cooling process. It is finally noted that the range of parameter values which is employed here, reasonably compares with values quoted by other investigators [1,4], especially d and p.

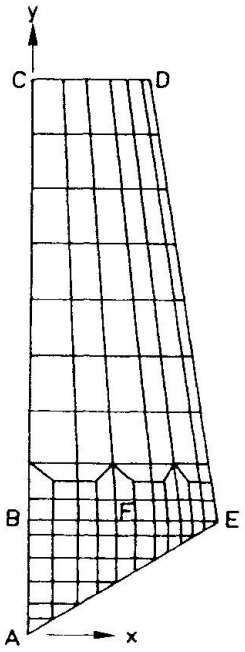

Fig. 5. Element mesh of one leg of a tetrapod.

6. STRESS CALCULATION IN A TETRAPOD

An example is now presented. It involves the calculation of the stresses during the hardening process in a tetrapod, which is used as a cover element for a breakwater. The element mesh is shown in Fig. 5. The boundary conditions of the heat conduction are a prescribed temperature of 15 $^{\circ}C$ along the edges CD and DE, while along the axis of axi-symmetry AC and edge AE no heat flow is permitted. For sake of simplicity the day-night cycle of the temperature has not been modeled.

The resulting time-temperature and time versus the degree of maturity curves are plotted respectively in Fig. 6 and Fig. 7 for some characteristic points in the tetrapod. The temperature as well as the degree of maturity are subsequently stored in a tabular form, whereby the time increments have been chosen smaller in the first 24 hours than afterwards.

Based upon the temperature and the degree of maturity as a function of time, the evolution of Young's modulus can be calculated using eq. (3). This results in the curves of Fig. 8, which give the development of Young's modulus in the corners of the tetrapod. A typical value for Young's modulus is in the order of 35000 N/mm^2. Fig. 8, however, shows a value of more than 55000 N/mm^2 near point A. This high value is caused by the fact that eq. (3) is rather sensitive for high temperatures, whereby it is noted that the temperature is again a function of the degree of maturity.

The fact that scalar variables (temperature) as well as vectorial quantities (displacements) enter the calculation has some consequences for the degree of interpolation and for the finite element discretization. Use of quadrilateral four-noded elements in a heat conduction analysis for instance results in a bilinear temperature distribution. When the result of the heat conduction analysis is subsequently used in the stress analysis, a linear temperature distribution also results in a linear thermal strain distribution. This strain distribution can only be described by a second-order displacement field, which necessitates the use of a quadratic element for the stress analysis. More general, we need an element for the stress analysis with an interpolation polynomial which is one order higher than the interpolation polynomial used in the heat conduction problem.

A related issue is the choice of the element mesh. The heat conduction problem and the stress analysis usually impose different requirements on the spatial discretization. If different meshes are employed for each analysis, the temperatures and the degrees of maturity which result

from the first calculation, must be interpolated to give nodal values in the mesh to be used in the stress analysis. Since the temperatures are primary variables in the heat conduction analysis, this interpolation is straightforward and results in a unique value of the temperature in each node of the mesh for the stress analysis. The calculation of the degree of maturity in the nodes of the new mesh is more complicated, for the degree of maturity is calculated in the integration points during the heat conduction analysis. To obtain a value for the degree of maturity in the nodes, the values in the integration points are extrapolated. This method gives a non-unique value of the degree of maturity in each node. If the same element mesh is used again for the stress analysis, this is not a major problem, since the interpolation to the (possibly new) integration points can be carried out using the old extrapolated nodal values of that particular element. When different meshes are employed in both analyses, it may be more correct to directly interpolate the degree of maturity in the new integration point from the integration points of the heat conduction analysis.

A third issue is the calculation of Young's modulus. This quantity must be known in the integration points of mesh for the stress analysis. To this end the temperature and the degree of maturity must be interpolated from the nodes to the integration points. Thereafter, Young's modulus can be computed as a function of time with aid of eq. (3).

Figs. 9, 10 and 11 show the development of the principal stresses in some points of the cross section BE in the course of time. In these figures σ_1 is the principal stress which is oriented approximately parallel to the x-axis, and σ_2 is the principal stress which is oriented approximately parallel to the y-axis.

7. CONCLUDING REMARKS

The development of a power law model in a Taylor series is an efficient way to simulate the creep behavior of concrete at early ages. A good simulation of the

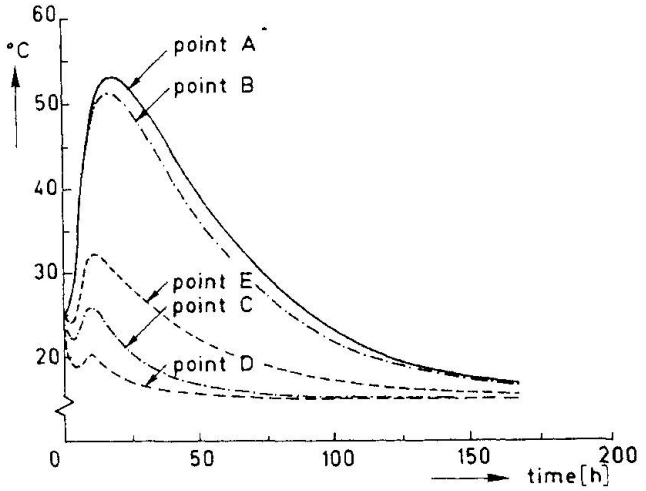

Fig. 6. Temperature as a function of time in the corners of the tetrapod.

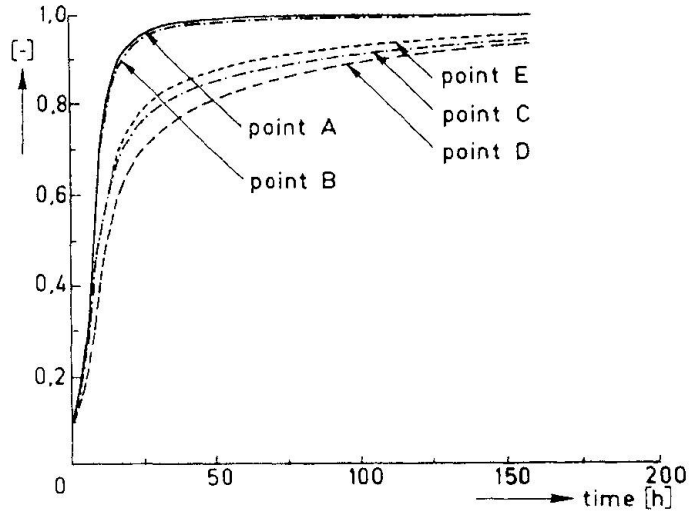

Fig. 7. Development of the maturity $r(t)$ in the corners of the tetrapod.

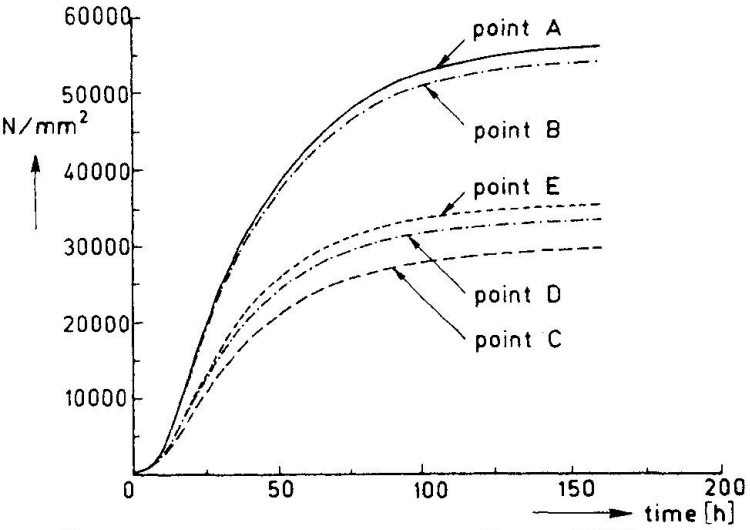

Fig. 8. Development of the stiffness $E(t)$ in the corners of the tetrapod.

stress development in a young concrete member can be made with the power law model after the first two days, while an additional function is needed for a better prediction in the initial phase. A good qualitative agreement between model prediction and experimental data could be achieved for some sets of the parameters α, p and d.

Special attention has to be paid to the communication between the heat conduction analysis and the stress analysis. When both calculations are carried out with the same element mesh, a good compromise must be found to describe flow and peak stresses in a proper way.

In regions with high temperatures the applied empirical model for the determination of Young's modulus results in unrealistic high values. This may be caused by the fact that the employed empirical functional for the determination of Young's modulus is rather sensitive for high temperatures.

ACKNOWLEDGEMENTS

This paper is largely a result of the first author's graduation work, which was carried out under supervision of Professors J. Blaauwendraad and H.W. Reinhardt of Delft University of Technology. The examples have been calculated with the DIANA finite element program of the TNO Institute for Building Materials and Structures. Financial support of the section Bouwspeurwerk of Rijkswaterstaat is gratefully acknowledged.

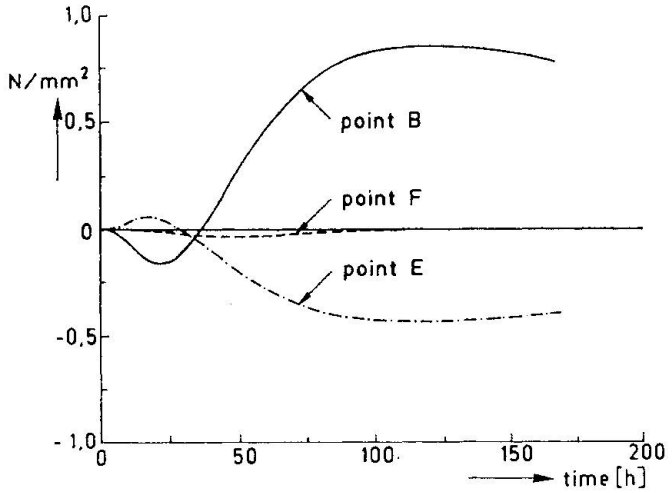

Fig. 9. Stress development σ_1 in some points in cross section BE

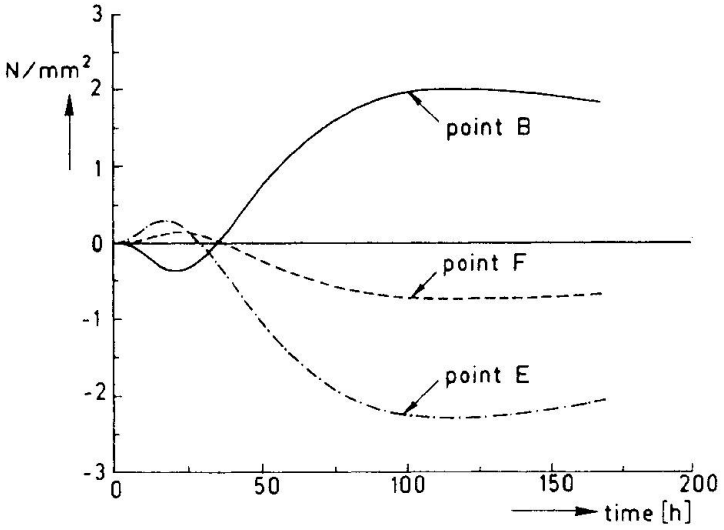

Fig. 10. Stress development σ_2 in some points in cross section BE

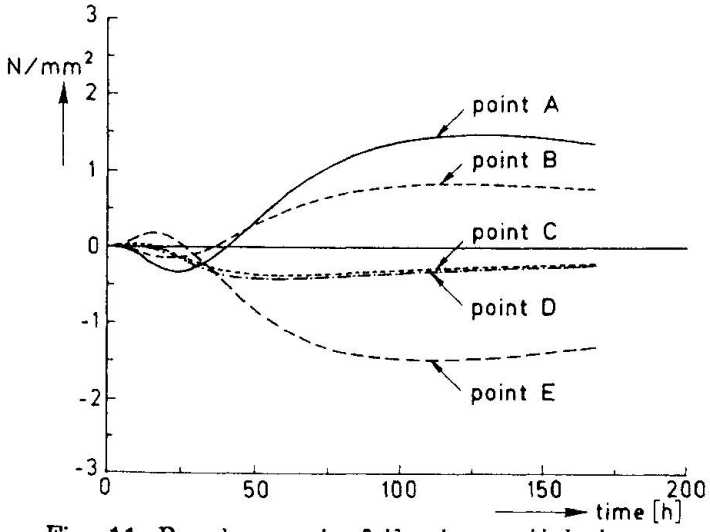

Fig. 11. Development of the tangential stress σ_t near the corners

REFERENCES

[1] BAZANT, Z.P. & OSMAN, E., Double power law for basic creep of concrete. RILEM Materials and Structures 9, 1976, pp. 3-11.

[2] BOGERT, P.A.J. VAN DEN, Numerieke simulatie van het kruipgedrag van jong verhardend beton, Model evaluatie (in Dutch). Report BI-86-45, IBBC-TNO, Delft, 1986.

[3] BORST, R. DE & BERG, P. VAN DEN, Analysis of creep and cracking in concrete members. Preprints RILEM Symp. on Creep and Shrinkage of Concrete: Mathematical Modeling (ed. Z.P. Bažant), Northwestern University, Evanston, Ill., 1986, pp. 527-538.

[4] BREUGEL, K. VAN, Relaxation of young concrete. Report 5-80-D8, Delft University of Technology, Faculty of Civil Engineering, Delft, 1980

[5] DIJK, H.H.G., Kruip en relaxatie van jong verhardend beton (in Dutch). BSW Report 84-05, Rijkswaterstaat Bouwspeurwerk, Utrecht, 1984.

[6] HEYNINGEN, B. VAN & BOON, J., Onderzoek naar het gedrag van jong beton ten behoeve van de tunnel te Vlake (in Dutch). Report B-73-214, IBBC-TNO, Delft, 1973.

[7] REINHARDT, H.W., On the hydratation of cements. Report 5-79-1, Delft University of Technology, Faculty of Civil Engineering, Delft, 1979

[8] REINHARDT, H.W., BLAAUWENDRAAD, J., JONGEDIJK, J., Temperature development in concrete structures taking account of state dependent properties. International Conference on Concrete at Early Ages, Paris, 1982.

Leere Seite
Blank page
Page vide